

**SPATIALLY RESOLVED AND POLARIZATION RESOLVED
ELECTROLUMINESCENCE OF 1.3 μm
InGaAsP SEMICONDUCTOR DIODE LASERS**

By

FRANK HUDSON PETERS, B.ENG.

A Thesis

Submitted to the School of Graduate Studies

in Partial Fulfilment of the Requirements

for the Degree

Doctor of Philosophy

McMaster University

(c) Copyright by Frank Hudson Peters, September 1991

DOCTOR OF PHILOSOPHY (1991)
UNIVERSITY
(Engineering Physics)

McMASTER
Hamilton, Ontario

**TITLE: Spatially Resolved and Polarization Resolved Electroluminescence of
1.3 μm InGaAsP Semiconductor Diode Lasers**

**AUTHOR: Frank Hudson Peters, B.ENG. (Technical University of
Nova Scotia)**

SUPERVISOR: Professor D. T. Cassidy

NUMBER OF PAGES: xi, 116

SPATIALLY AND POLARIZATION RESOLVED EL
OF DIODE LASERS

Abstract

A technique for obtaining maps of the spatially-resolved and polarization-resolved electroluminescence of 1.3 μm semiconductor diode lasers has been developed. It reveals information about the strain, scattering and absorption which exist in the active region of lasers. These data has been correlated with the spectral output of the lasers, and models have been developed which explain the correlation.

Acknowledgments

I would like to thank my supervisor Dr. Cassidy for his insight, guidance, time and support. I would like to thank God, my parents, and my wife Jo for being a refuge and a source of encouragement. Finally, I am grateful to the National Sciences and Engineering Research Council of Canada for their financial support.

Table of Contents

	page
Chapter 1. Introduction	1
Chapter 2. Method and Apparatus	4
2.1 Introduction	4
2.2 Sample Preparation	6
2.3 Apparatus	11
2.4 Results	18
2.5 Summary	27
Chapter 3 Strain and Scattering	28
3.1 Introduction	28
3.2 Strain Measurements	30
3.3 Effective Scattering Measurements	34
3.4 Scattering and the Spectral Properties	38
3.5 Summary	41
Chapter 4 Single Scattering Model	43
4.1 Introduction	43
4.2 Laser Model with Scattering Centre	45
4.3 Results	52
4.4 Summary	63
Chapter 5 Spontaneous Emission and Scattering	66
5.1 Introduction	66
5.2 Spontaneous Emission	67
5.3 Experimental Method	75
5.4 Summary	81
Chapter 6 Multiple Scattering and Absorption Model	83
6.1 Introduction	83
6.2 Numerical Fabry Perot Matrix Model	84
6.3 Spectral Output of Lasers with Multiple Scattering	87
6.4 Negative Spectral Tuning	89
6.5 Summary	100

Chapter 7 Conclusion	101
7.1 Introduction	101
7.2 Recommended Additional Research	101
7.3 Summary	103
Appendix Circuit Diagrams	105
References	112

List of Figures

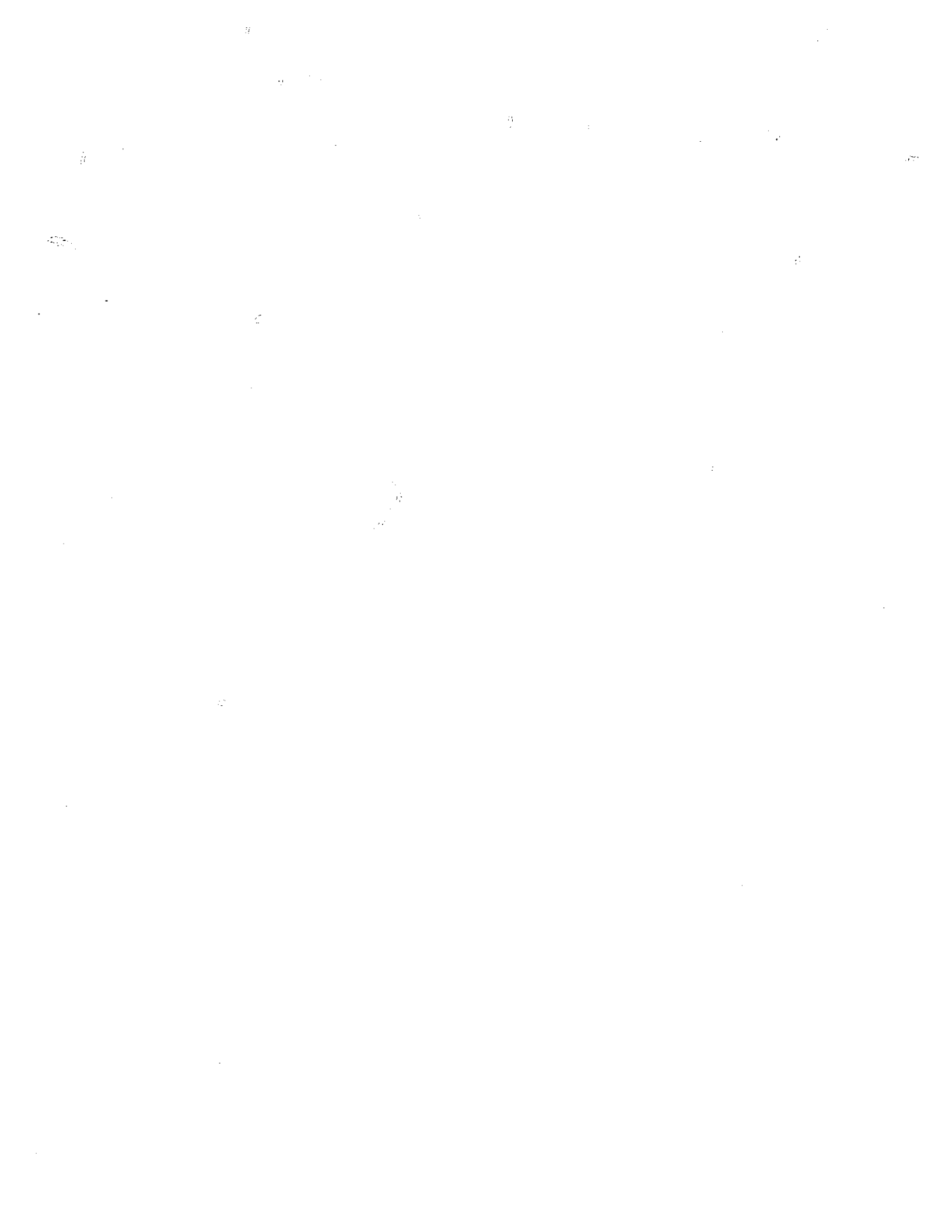
	page
Fig. 2.1 Schematic of laser block.	7
Fig. 2.2 Polishing jig used for removing metallization from diode lasers.	8
Fig. 2.3 Schematic of experimental apparatus	11
Fig. 2.4 Intensity distribution across the active region of gain guided laser.	13
Fig. 2.5 Dependence of focus on lens position.	14
Fig. 2.6 Degree of polarization distribution across the active region of a gain guided laser for aligned detectors and for detectors misaligned 10 and 20 μm .	16
Fig. 2.7 Spatially resolved EL map of damaged gain guided laser. The displacement in the vertical direction is proportional to the light intensity detected.	18
Fig. 2.8 Spatially resolved EL maps of rejected PBH laser for both orthogonal polarizations P1 and P2.	20
Fig. 2.9 (a) Three dimensional representation of degree of polarization along the active region of PBH laser. The data near the facets have been removed. (b) Two dimensional representation.	21
Fig. 2.10 Degree of polarization distribution across and along stripe for a gain guided laser with (a) the detectors aligned and (b) the detectors misaligned 20 μm .	23

Fig. 2.11	Two dimensional representation of degree of polarization distribution along the active region of a gain guided laser for aligned detectors (solid line) and for misaligned detectors (broken line).	24
Fig. 2.12	Degree of polarization along the stripe of PBH laser for two different set of data showing the reproducibility of the results.	25
Fig. 2.13	Degree of polarization along the stripe of PBH laser for different current levels: 20 mA, 30 mA, and 40 mA. The degree of polarization increases with increased current.	26
Fig. 3.1	Degree of polarization (ρ) distribution along the active region of PBH laser (laser G) for below threshold operation (solid line) and above threshold operation (broken line).	30
Fig. 3.2	Distribution of ρ along the active region of ABC laser (laser 3) with facet effects removed for below threshold operation (solid line), and above threshold operation (broken line).	32
Fig. 3.3	Distribution of ρ along the active region of a gain guided laser (laser e) for below threshold operation (solid line), and above threshold operation (broken line).	33
Fig. 3.4	Standard deviation vs. mean of below threshold degree of polarization (ρ) measurements, for gain guided lasers (lower case), PBH lasers (upper case) and ABC lasers (numbers).	34
Fig. 3.5	Discrete effective scattering ($\Delta\rho_d$) vs. total effective scattering ($\Delta\rho_t$) for gain-guided lasers (lower case), PBH lasers (upper case) and ABC lasers (numbers).	36
Fig. 3.6	Experimentally measured spectral output of (a) gain guided laser e, (b) ABC laser 3, (c) and (d) PBH laser G at two different operating temperatures.	39
Fig. 3.7	Experimentally measured spectral output of (a) PBH laser J, (b) PBH laser E, (c) PBH laser I, and (d) gain guided laser a.	40
Fig. 4.1	Schematic diagram of a laser (length L) with a scattering centre (solid dot) which exists a distance L_1 from the left hand facet and a distance L_2 from the right hand facet.	46

Fig. 4.2	Calculated longitudinal mode spectrum of a gain guided laser assuming no scattering centre exists ($\sigma = 0$).	55
Fig. 4.3	Measured longitudinal mode spectrum of a gain guided laser. The vertical scale is in units of intensity and the horizontal scale is in units of wavelength. Note the similarity between Figs. 4.2 and 4.3.	56
Fig. 4.4	Degree of polarization (ρ) distribution along the active region of a planar buried heterostructure (PBH) laser operating below (broken line) and above (solid line) threshold.	57
Fig. 4.5	Calculated longitudinal mode spectrum of the PBH laser from Figs. 4 and 6. The scattering parameters $\sigma = 0.0015$, $L_1 = 153\mu\text{m}$ and $L_2 = 97\mu\text{m}$ are calculated using the data from Fig. 4.4.	58
Fig. 4.6	Measured longitudinal mode spectrum of the PBH laser of Fig 4.4.	59
Fig. 4.7	Measured longitudinal mode spectrum of a PBH laser exhibiting a large modulation of the mode envelope.	61
Fig. 4.8	Calculated longitudinal mode spectrum of a PBH laser using the scattering parameters $\sigma = 0.0005$, $L_1 = 164\mu\text{m}$ and $L_2 = 86\mu\text{m}$. Note the similarity between Figs. 4.7 and 4.8.	62
Fig. 4.9	Calculated longitudinal mode spectra of a PBH laser at two different temperatures, using the scattering parameters $\sigma = 0.0005$, $L_1 = 79\mu\text{m}$ and $L_2 = 171\mu\text{m}$.	63
Fig. 5.1	Spontaneous emission at threshold vs. threshold current for arrowhead buried crescent (numbers), planar buried heterostructure (upper case), and gain guided (lower case) lasers.	68
Fig. 5.2	Spontaneous emission vs. current for (a) a gain guided laser with a threshold current of 160 mA, and (b) a PBH laser with a threshold current of 20 mA.	69
Fig. 5.3	Side mode suppression ratio vs. one over spontaneous emission for various values of scattering: i) $\sigma = 0$, ii) $\sigma = 0.0224$, iii) $\sigma = 0.0316$, iv) $\sigma = 0.0387$, v) $\sigma = 0.0447$.	73

Fig. 5.4	Side mode suppression ratio vs. the scattering parameter σ for various values of above threshold spontaneous emission: i) $c=0.036$, ii) $c=0.047$, iii) $c=0.067$, iv) $c=0.114$, v) $c=0.400$.	74
Fig. 5.5	Total (+) and discrete (O) scattering vs. output power for a PBH laser. Note the linear relationship indicating scattering is taking place in the laser.	76
Fig. 5.6	Discrete scattering vs. total scattering for arrowhead buried crescent (numbers), planar buried heterostructure (upper case), and gain guided (lower case) lasers.	77
Fig. 5.7	Worst case spectral output of gain guided (lower case) and index guided (upper case) lasers operating above threshold.	78
Fig. 5.8	Spontaneous emission masked scattering parameter σ/c for arrowhead buried crescent (numbers), planar buried heterostructure (upper case), and gain guided (lower case) lasers.	79
Fig. 6.1	Effective reflectance (R_m) for a laser with one scattering centre located $25 \mu\text{m}$ from a facet and $\sigma = 0.0009$.	88
Fig. 6.2	R_m for a laser with 9 scattering centres distributed $25 \mu\text{m}$ apart along the length of the active region each with $\sigma = 0.0001$.	89
Fig. 6.3	Theoretical spectra created using R_m from (a) Fig. 6.1, and (b) Fig. 6.2.	90
Fig. 6.4	Spatially resolved electroluminescence distributions showing absorptive regions for (a) laser C and (b) laser E.	91
Fig. 6.5	R_m for scattering centre located $10 \mu\text{m}$ from a facet in a $250 \mu\text{m}$ long laser (solid line), and $10.01 \mu\text{m}$ from a facet in a $250.01 \mu\text{m}$ long laser (broken line). Notice the shift in frequency of R_m .	92
Fig. 6.6	Theoretical spectra of a laser. The spectra is lasing in a central mode in (a) and (b), has shifted to shorter wavelength in (c), and then shifts to longer wavelength in (d), (e) and (f).	93

Fig. 6.7	Plots of R_m changing due to an increase in a $27 \mu\text{m}$ cavity of $0.02 \mu\text{m}$. The R_m plotted were used to create the theoretical spectra of Fig. 6.6 (a) and (c).	94
Fig. 6.8	R_m for a laser with a scattering centre located 50 (solid line) to $50.05 \mu\text{m}$ from a facet in a $250 \mu\text{m}$ long laser. Notice the movement of R_m to the right.	96
Fig. 6.9	Theoretical spectra for a $250 \mu\text{m}$ long laser with a scattering centre located 50 - $50.16 \mu\text{m}$ from one facet. Notice that the dominant lasing mode oscillates in frequency space as the scattering centre moves across the device.	97
Fig. 6.10	Measured spectrum of laser E, at mid point between shifting from longer wavelength to shorter wavelength with increasing current or temperature.	98
Fig. 6.11	Plots of changes in Ψ with the temperature gradient through device which is represented by the cooler current. Notice the oscillations of Ψ with respect to the temperature gradient.	99
Fig. A.1	Laser Driver Circuit.	106
Fig. A.2	Laser Cooler Circuit.	107
Fig. A.3	Motor Driver Circuit.	108
Fig. A.4	Wien Bridge Oscillator Circuit.	109
Fig. A.5	Position Sensor Circuit.	110
Fig. A.6	9-Pin Connector Diagram.	111



Chapter 1. Introduction

Diode lasers are normally assumed to be uniform along the length and width of the active region. This is evident from the theoretical models used to describe diode lasers. For example, rate equations, which were developed for gas lasers, are used to model the spectral properties of diode lasers. This theoretical approach assumes high reflectivity facets and assumes that the active region of the laser is uniform, two assumptions which are not valid for diode lasers. It is known that the facets of diode lasers are not high reflectivity and it is shown in this thesis that 1.3 μm InGaAsP semiconductor diode lasers are not uniform along their active regions.

An instrument which measures the spatially resolved and polarization resolved electroluminescence of 1.3 μm InGaAsP semiconductor diode lasers has been developed and is reported in this thesis. The electroluminescence data taken with the instrument provides information which has been previously unavailable. The data can be analyzed to provide information about the internal strain and scattering that exist along the active regions of 1.3 μm InGaAsP semiconductor diode lasers.

Analysis of measurements made with the instrument demonstrates that there is a distribution of strain along the active region of diode lasers. This distribution has not been observed previously, nor has it been expected. The distribution varies from one type of laser to another and even varies between lasers fabricated from the same wafer.

Analysis of the data recorded with the instrument shows that scattering exists along the active region of semiconductor diode lasers. Scattering has not been previously measured, although internal scattering near the facets of diode lasers has been used to explain the unusual far field patterns of certain lasers.[1]

A correlation is observed between the scattering properties of $1.3 \mu\text{m}$ InGaAsP semiconductor diode lasers and the spectral output of the lasers. It is found that lasers with strong scattering are more likely to operate single moded or multilongitudinal moded with highly modulated mode envelopes than are lasers with weak scattering. Lasers with similar scattering have similar spectral properties.

To gain an understanding of the correlations, models for the spectral properties of diode lasers were developed which consider the effect of non uniformities along the active region in the form of scattering and absorption centres. The effect of scattering was examined theoretically to provide an explanation for the observed correlations between scattering and the spectral properties of diode lasers. By using scattering centres in the model, the different spectral properties which are observed for diode lasers are explained; properties which range from single moded operation to multilongitudinal moded operation with a large modulation of the mode envelope. The observed correlation between scattering and the spectral properties of diode lasers and the model which explains the correlation are a significant contribution in this field of research.

Experimentally, diode lasers sometimes skip modes as they tune to longer wavelength with increasing current. This phenomenon is explainable if scattering centres are considered, and the modelling of such behaviour is presented. A small percentage of diode lasers tune to shorter wavelength with increasing current over a limited current range. By allowing for absorption centres the model succeeds in

giving an explanation into this negative tuning behaviour. These unusual tuning properties of diode lasers have not previously been explained.

The thesis is divided into seven chapters. In Chapter 2 the method and apparatus for obtaining spatially resolved and polarization resolved electroluminescence are discussed. Chapter 3 describes how strain, scattering and absorption data are measured and demonstrates the correlation between the spectral properties and the scattering properties of the lasers. Chapter 4 develops a model for the spectral properties of semiconductor diode lasers which considers the effect of one scattering centre inside the device. Results from the model are used to explain the spectral output of diode lasers. Chapter 5 re-examines the scattering which exists in diode lasers and studies the combined effect of scattering and spontaneous emission on the spectral properties of the lasers. Chapter 6 presents a model for diode lasers which allows for multiple scattering and absorption centres to exist along the active region, and shows how unusual spectral tuning characteristics can be explained. Finally Chapter 7 provides a summary, and suggestions for further research.

The research presented in this thesis is summarized in eight manuscripts which have been published in scientific journals,[2,3,4,5,6] submitted for publication,[7] or presented at refereed conferences.[8,9]

Chapter 2. Method and Apparatus

2.1 Introduction

The goal of this research project was to design and build an instrument capable of studying the internal properties of diode lasers and to relate these properties to the operating characteristics of the lasers. Possible methods of analysis included electroluminescence, photoluminescence, X-ray diffraction and ellipsometry. The last two methods were ruled out due to their cost and their inability to achieve the desired spatial resolution of approximately $2 \mu\text{m}$. Spatially resolved photoluminescence (PL) has been used to study elimination of defects with superlattices,[10] to test quality of III-V wafers,[11] to show the intensity variation in the PL of wafers which is related to defects,[12] and to observe degradation mechanisms in diode lasers,[13] all at various resolutions. Photoluminescence, albeit a viable method, was not chosen as the analysis tool since it is not capable of monitoring the internal properties of lasers while under operation.

Spatially resolved electroluminescence has been carried out using a thermal plotter to monitor defects in diode lasers for reliability studies.[14] More recently IR vidicons have been used for spatially resolved electroluminescence to study the quality of diode lasers after various fabrication methods,[15] and to study defects in semiconductor diode lasers.[16,17,18,19] Hartman and Koszi, in addition to using an IR vidicon, used a discrete detector with an aperture and moved

the laser under the detector with a translation stage.[16] They achieved a spatial resolution of about $2 \mu\text{m}$ and could measure changes of luminescence much more accurately than with the IR vidicon. Since this discrete method is much slower than the IR vidicon, it was only used to measure the full widths at half power of the electroluminescence produced across the stripe of the lasers studied. Even though this method is time consuming, it was used in this work because of the high spatial resolution and because of the ability to measure small changes in the electroluminescence produced along the active region of lasers. In addition, modifications could be made to the electroluminescence apparatus so that polarization data could be measured.

An instrument to provide maps of the spatially resolved and polarization resolved electroluminescence along the stripe of diode lasers was constructed. With the instrument it is possible to measure reproducibly changes of $\leq 1\%$ of the radiant emittance of the electroluminescence over distances $\leq 2 \mu\text{m}$ and thus provide a means for the correlation of device performance with the characteristics along the active region. The spatially resolved measurements provide information on dislocations,[20] whereas the polarization resolved measurements provide information on the amount of mechanical strain in the plane of the active region.[21,22]

Spatially resolved and polarization resolved maps of the electroluminescence were made on about forty $1.3 \mu\text{m}$ InGaAsP diode lasers. For the lasers to be measured special preparation was necessary. The lasers needed to be bonded active region down and have the top contact removed so that the emission could be imaged through the substrate. The top contacts were removed by mechanically polishing, and wire bonds for electrical contact were made to the InP

on the top of the laser away from the active region.

The results are very interesting. Even though the spatially resolved electroluminescence (EL) signal looks uniform for most devices, it is shown by analyzing the polarization resolved data that the distribution is not uniform. Changes are seen from one type of laser to another, and even between devices fabricated from the same wafer.

In this chapter the apparatus and method for obtaining maps of the spatially resolved and polarization resolved electroluminescence are presented. Section 2.2 outlines the procedure for sample preparation, Section 2.3 is a description of the instrument, outlines how the instrument is used, and shows its capabilities. Section 2.4 presents some spatially resolved and polarization resolved measurements, and Section 2.5 provides a summary.

2.2 Sample Preparation

The purpose of the sample preparation is to produce a device which may be pumped with current and which does not have metallization over the active region, so that the light which is produced in the active region may be measured through the top of the device. All the lasers studied were 250 μm long InP based semiconductor diode lasers operating at about 1.3 μm . The lasers were typically 100 μm thick mounted active region down on a diamond heatsink which in turn was mounted on a copper block (Fig. 2.1). The top or substrate side of the lasers were metallized with a surface layer of gold and were wire bonded to a large gold pad away from the laser. The electrical contacts used for driving the lasers are the copper

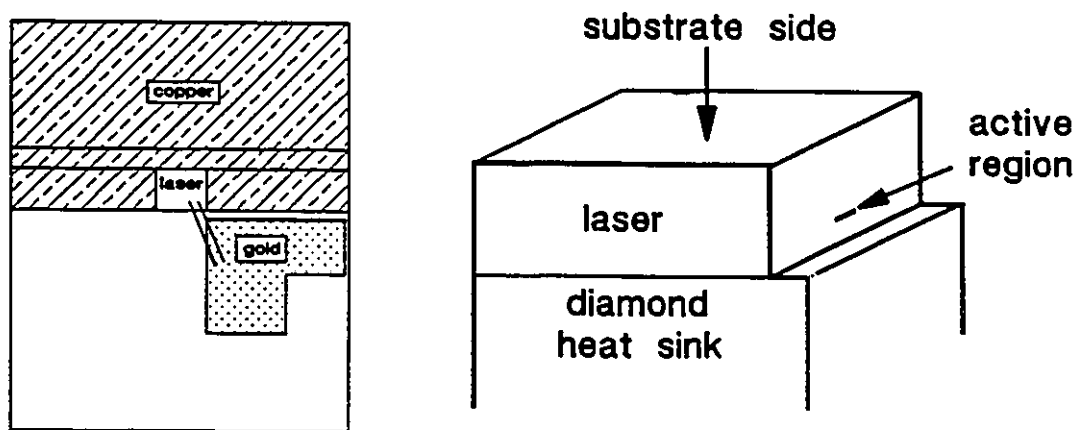


Fig. 2.1 Schematic of laser block.

(positive contact) and the gold pad (negative contact).

To measure light coming through the surface of the laser it is necessary to remove the substrate side surface metallization. The gold layer could easily be removed by an etch but under the gold layer was a titanium nitride thin film, and an etch could not be found which would remove this layer without damaging the InP. For this reason the metallization was removed by mechanical polishing.

Mechanically removing a few microns of metallization from the top of a 250 X 300 μm diode laser takes some care. A polishing jig was used whereby the surface to be polished is mounted on a stage controlled by a micrometer which is inside a steel cylinder (Fig. 2.2). In this way the amount to be polished can be carefully controlled by the micrometer. A nylon polishing cloth with 0.05 μm alumina powder was used to remove the metallization and leave the surface of the InP of optical quality.

The polishing procedure I use is as follows. First the laser block is

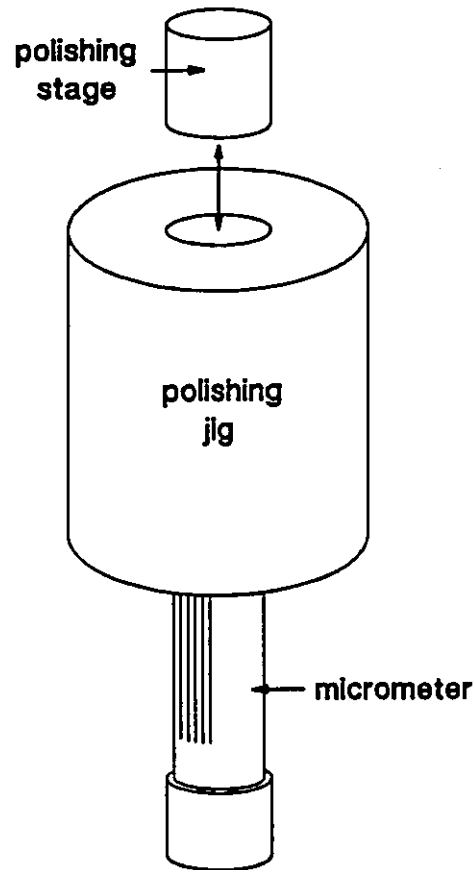


Fig. 2.2 Polishing jig used for removing metallization from diode lasers.

mounted with crystal bond onto the polishing stage. To protect the laser facets, the laser is then covered with a drop of crystal bond. It is important that there are no bubbles in this crystal bond coating, since this could lead to damage to the laser facets. Ensuring no bubbles is accomplished by not overheating the crystal bond when melting it ($< 120^{\circ}\text{C}$). The polishing stage is cleaned with soap to remove abrasive particles and then dried with methanol and compressed air before being inserted into the polishing jig (which has also been cleaned). The crystal bond is then slowly polished off by advancing the micrometer, initially in 10 to 20 μm increments.

Because the crystal bond is fairly transparent, it is possible to see the gold surface of the laser through a small thickness of the crystal bond. Using this fact and regular visual checks, it is possible to know when the surface of the laser is soon to be polished. At this point the micrometer is advanced slowly (about 1/3 of a 10 μm increment at a time) making sure the newly exposed crystal bond has been removed before the micrometer is advanced again. Once the gold surface disappears revealing a dark shiny surface, the micrometer is advanced about 2 μm followed by ample polishing. This is to ensure that all the metallization layers have been removed. Once the polishing is completed, the laser block is removed from the polishing stage. This can be done with acetone or by heating the stage to melt the crystal bond. Heating the stage is more efficient if a number of lasers are to be polished.

The crystal bond on the laser block is removed using two acetone baths. This is followed by a methanol bath to remove the acetone and finally the laser is dried with compressed air. I use two acetone baths because of the amount of crystal bond which dissolves into the first bath. Once the laser has been cleaned, new wire bonds are made from the laser to the gold pads.

A Hughes ball bonder has been somewhat successful using 25 μm gold wire and the following parameters: bond power 6-7, bond force 7-7.5 turns, bond time 9-10, and ball size 16-20. I make the first bond to the laser, and the second to the gold pad. Caution should be taken because if too large a force is used, or if the laser block is held down with vacuum suction or double sided tape there is a danger of destroying the laser. Leaving the laser block free allows less of the ultrasonic energy to be dissipated by the laser crystal. Additional caution should be taken with the second bond which tends not to be reliable even on a gold surface. If the second bond does not work, the first bond will likely be pulled off by the bonder. To

eliminate this problem, after the first bond is made the gold wire should be cut leaving enough wire to easily reach the gold pad. The free end of the gold wire can then be attached to the gold pad with an additional ball bond which squeezes the free end of the wire between the ball bond and the pad.

A Westbond wire bonder has also been used with success. This bonder is harder to use, but seems to be much gentler since no lasers have yet been chipped or destroyed while wire bonding. The Westbond wire bonder is therefore recommended. I have been successful using the following parameters with the ultrasonic bonding option: First bond power 100-150, first bond time 100, second bond power 100-150, and second bond time 100. With this bonder I make the first bond to the gold pad and the second to the laser.

Using either bonder the wire bond is made a sufficient distance from the active region so that light can be detected through the top of the device. During processing, some changes in threshold current may occur. Initially these threshold current changes were quite large (greater than five percent which is attributed to excessive bonding force using the Hughes ball bonder), although once experience was gained more than eighty percent of the lasers experienced very small changes in threshold current (less than two percent).

2.3 Apparatus

The instrument is designed to make maps of the spatially resolved and polarization resolved light produced in the active region of $1.3 \mu\text{m}$ InGaAsP semiconductor lasers and emitted through the substrate (Fig. 2.3). The spontaneous

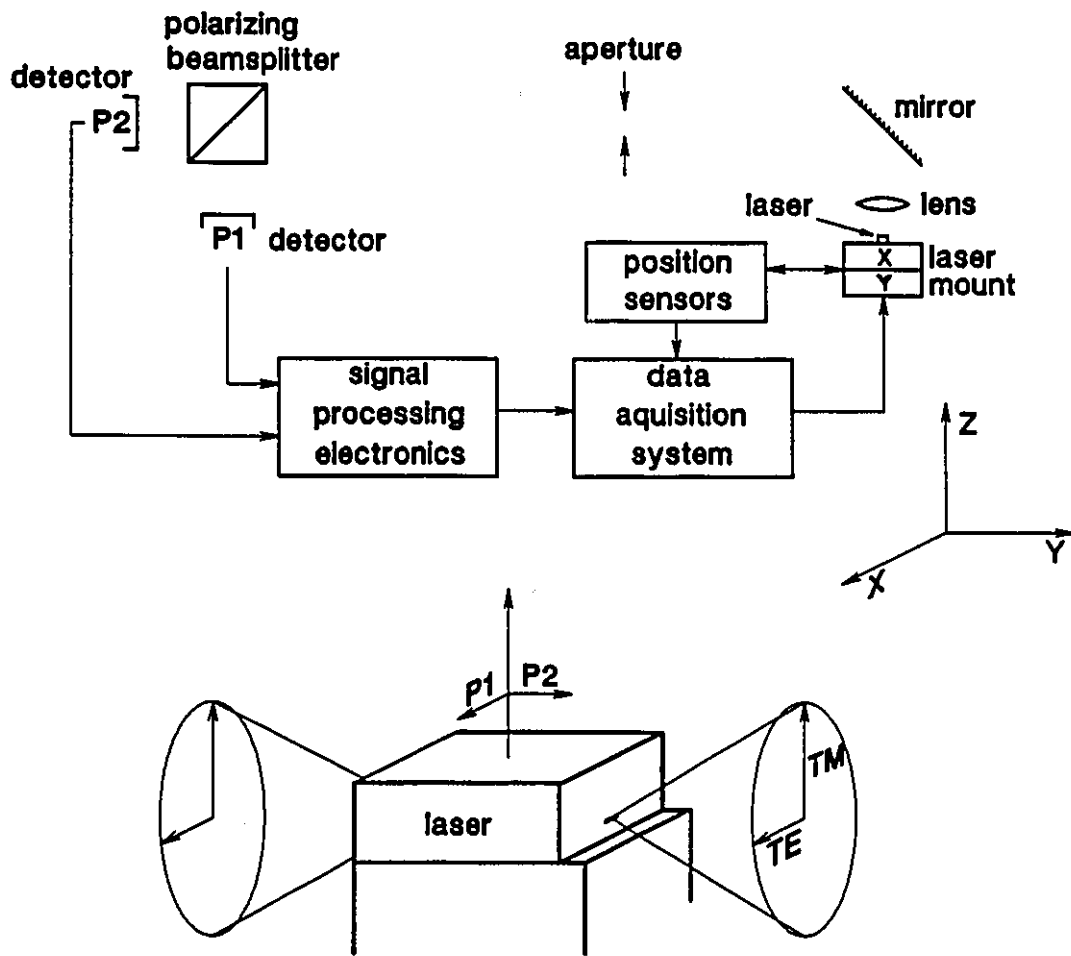
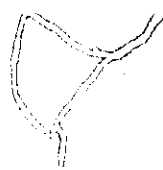


Fig. 2.3 Schematic of experimental apparatus

light emitted in the z-direction (perpendicular to the plane of the active region) and the stimulated light scattered into the z-direction will reach the detectors. Light polarized in the x-direction (the same polarization as the TE facet emission) is



designated as P1, and light polarized in the y-direction (along the stripe) before the mirror and polarized in the z-direction after reflecting off the mirror is designated as P2. Light polarized in the z-direction in the active region (same polarization as the TM facet emission) will not be emitted in a direction such that it reaches the detectors. The laser is attached to a mount which provides temperature control for standardization of the data and to make in situ accelerated aging possible. A photodiode is also present on the laser mount so that the output power of the laser can be measured.

While passing a modulated current (for phase sensitive detection) through the device so that light is produced, the laser is positioned under the lens such that light from the active region will reach the small area detectors. This is accomplished by moving the laser mount under computer control until the modulated light is detected. The instrument has a noise level of about 1 pW, therefore a signal of greater than 10 pW has been chosen as the detection threshold. Position gauges are used such that the movement of the laser mount can be controlled to submicron accuracy.

Once light from the active region is noticeable on the detectors, the instrument can be focused. Coarse focusing is accomplished simply by maximizing the signal on one of the detectors. This is done by moving the lens in the z-direction (also controlled to submicron accuracy) while making sure the laser is located directly under the lens by maximizing the signal with respect to the x and y directions.

For fine focusing the laser is translated under computer control across the stripe (in the x-direction). The signal from one of the detectors is recorded at discrete points so that an intensity profile across the stripe is generated. The resulting

profile is approximately Gaussian in shape (Fig. 2.4). The full width at half maximum

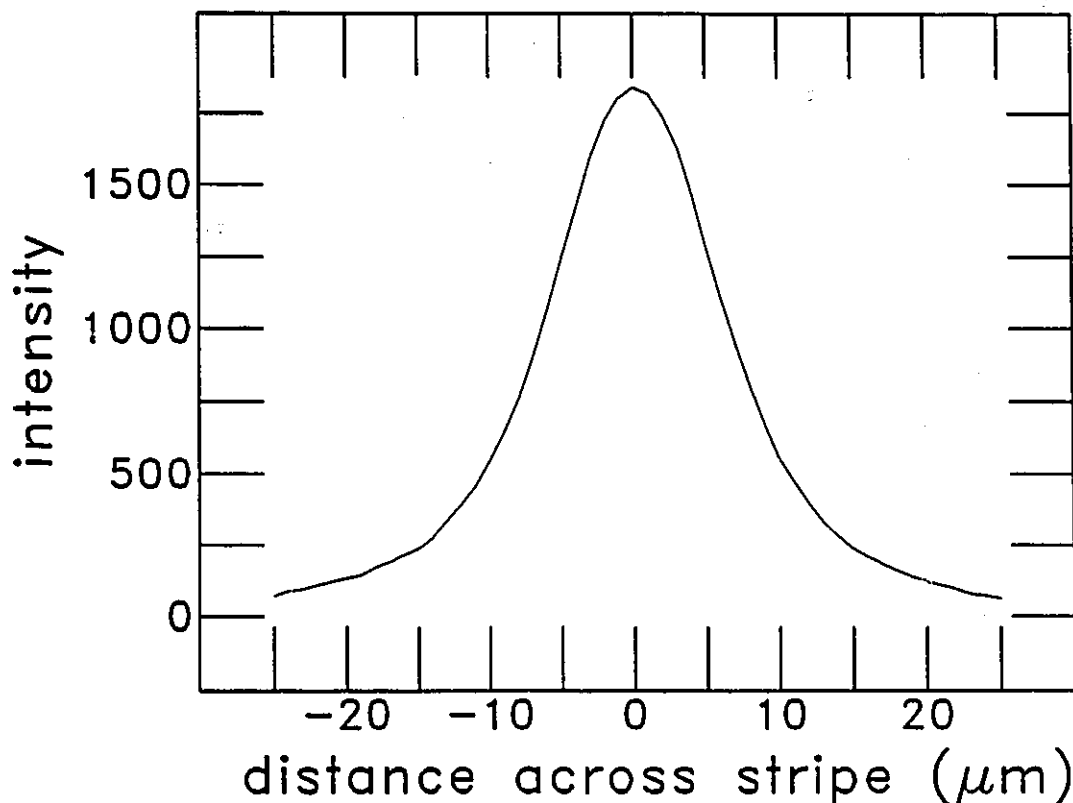


Fig. 2.4 Intensity distribution across the active region of gain guided laser.

(FWHM) of the intensity profile can then be minimized by moving the lens. Figure 2.5 provides a graph of the FWHM of the intensity profile vs. the position of the lens. Experimentally, it is found that when the FWHM is at a minimum, this is the point of best spatial resolution and hence optimum focus. The FWHM of the intensity profile is reduced by the aperture which lessens the field of view of the detectors, and thus further increases the spatial resolution. Polarization resolution is achieved by the polarizing beam splitter (Newport Optics model 10FC16PB.7) which separates the two orthogonal polarizations (P1 and P2) and directs each to one of the two detectors.

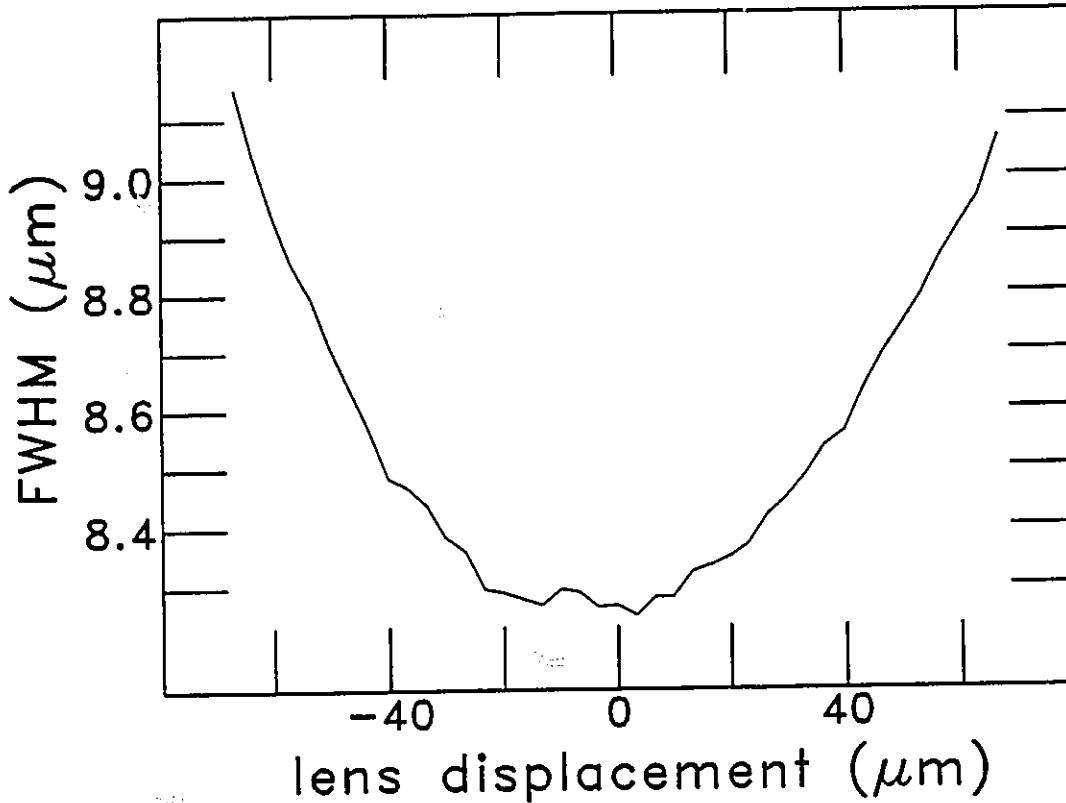


Fig. 2.5 Dependence of focus on lens position.

To ensure that both detectors receive light from the same part of the active region, the detectors must be accurately positioned relative to one another. This is done by repeating the computer controlled scan described for focusing, but this time recording the signal from both detectors. If the system is well aligned the centroids of the Gaussian like intensity distributions across the stripe will occur at the same position. Therefore rough alignment of the detectors is achieved by minimizing the difference between the centroids of the intensity distributions.

To achieve a higher degree of accuracy in positioning the detectors, the degree of polarization profile is calculated. The degree of polarization is defined as

$\rho = (P1-P2)/(P1+P2)$, where P1 and P2 represent the intensities of the two orthogonal polarizations (Fig. 2.3 (b)).

If the two polarizations yield intensity distributions across the active region which are Gaussian with the same FWHM given by 2.454σ and similar peak values of A and B, and the detectors are misaligned by a small amount a in the x -direction, then the degree of polarization distribution across the stripe $\rho(x)$ will be:

$$\rho(x) = \frac{A \exp\left(\frac{-x^2}{2\sigma^2}\right) - B \exp\left(\frac{-(x-a)^2}{2\sigma^2}\right)}{A \exp\left(\frac{-x^2}{2\sigma^2}\right) + B \exp\left(\frac{-(x-a)^2}{2\sigma^2}\right)}. \quad (2.1)$$

If the centroids of the distributions occur close to the same position then $\exp(a^2/2\sigma^2) \approx 1$ and

$$\rho(x) \approx \frac{A - B \exp\left(\frac{ax}{\sigma^2}\right)}{A + B \exp\left(\frac{ax}{\sigma^2}\right)}. \quad (2.2)$$

Near alignment $(ax/\sigma^2)^2 \approx 0$, and

$$\rho(x) \approx \frac{A - B}{A + B} - \frac{B}{A + B} \frac{ax}{\sigma^2}. \quad (2.3)$$

Now $A \approx B$ since $\rho(x)$ is typically < 0.03 and thus the slope of $\rho(x)$ is $\approx a/2\sigma^2$.

A least squares linear fit of the degree of polarization profile will then give a slope which represents the error in alignment. By minimising this slope the detectors can be aligned to within a few microns. Figure 2.6 shows a distribution of

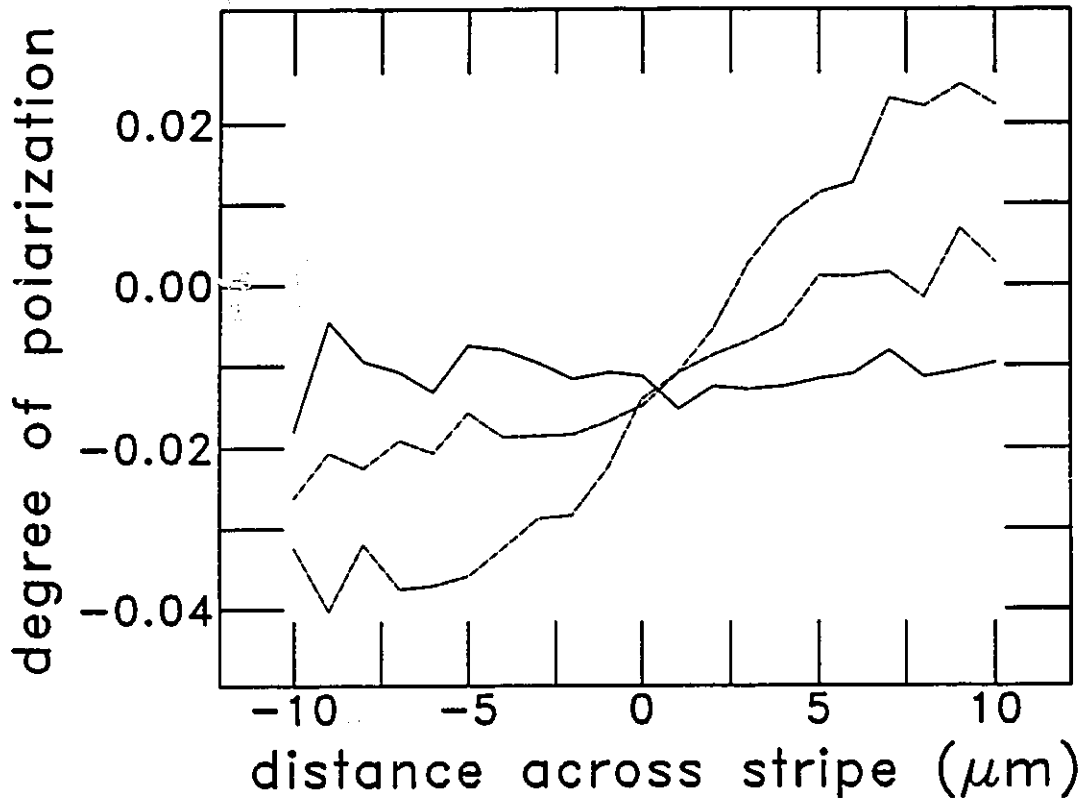


Fig. 2.6 Degree of polarization distribution across the active region of a gain guided laser for aligned detectors and for detectors misaligned 10 and 20 μm .

$\rho(x)$ for aligned detectors and for detectors misaligned by 10 μm and 20 μm . The large change on the slope of $\rho(x)$ for the misaligned detectors can be seen. This makes it possible to align the detectors to an accuracy of approximately 3 μm . Since the magnification of the optical system is ≈ 82 times, this means that the detectors are sampling light from volumes offset by less than .05 microns. This offset is less than the resolution of the system due to diffraction and lens aberration and thus the detectors detect light from essentially the same region.

To align the detectors in the remaining direction, the same procedure is followed with the laser repositioned with the active region parallel to the x-direction, and with the scan made in the y-direction. This also helps to calibrate the two detectors with respect to each other. Since the degree of polarization at a given location on the laser is constant for a given pumping level, the detectors can be calibrated to make sure that this is the case regardless of whether the laser stripe points in the x or the y direction.

The data collection has been completely automated and takes from 12 to 24 hours depending on the amount of averaging for noise reduction which is desired. A grid is used over which intensity and polarization data are taken for different current levels. The grid size is 101 points along the stripe (y-direction) and 37 points across the stripe (x-direction). For the lasers each grid point is $3\ \mu\text{m}$ apart along the stripe, and from 1 to $3\ \mu\text{m}$ apart across the stripe. At each grid point data for six different current or output power levels is taken. This guarantees that the position is identical for each current or output power level at the same grid point, and that any changes in degree of polarization due to current or output power changes are accurate. A large area detector is located on the laser mount to enable the measurement of light intensity vs. current data. This also allows for electroluminescence data to be taken for a given output power of the laser.

The apparatus is controlled by a personal computer via A/D and D/A cards. All circuits except for the lock-in amplifiers were designed and built as part of the system development. Schematics for the circuits which operate the laser,

detectors, motors and position sensors are located in the Appendix.

2.4 Results

Spatially resolved EL and PL has been used by others to evaluate lasers which exhibit large variations in the EL or PL signal along the stripe.[13-19] Figure 2.7 shows a light intensity vs. spatial dimension plot of a damaged gain guided laser.

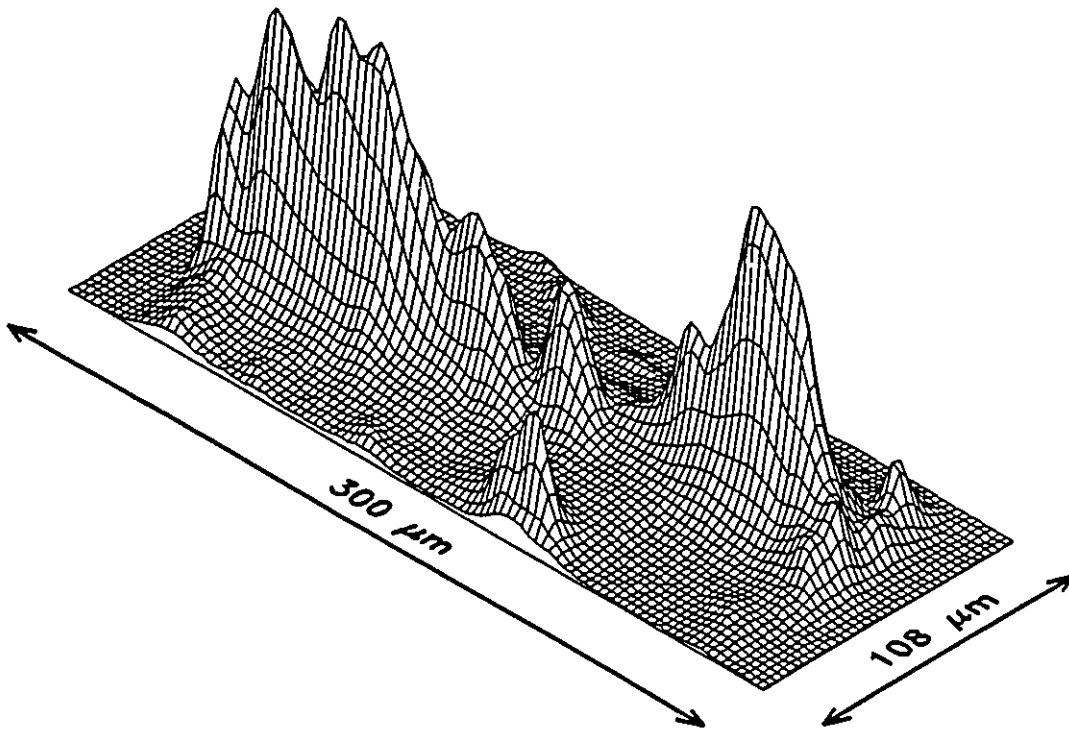


Fig. 2.7 Spatially resolved EL map of damaged gain guided laser. The displacement in the vertical direction is proportional to the light intensity detected.

The dark regions are immediately obvious and are consistent with the device

behaviour: it does not lase. Unfortunately using only spatial resolution one cannot distinguish between structures whose external properties (like threshold current) would be cause for rejection. Figure 2.8 shows the intensity maps of the two orthogonal polarizations of a laser which was rejected for production of toll grade laser transmitter modules. The maps were taken with the laser operating about 25 mA above threshold. The asymmetry of the EL map is caused by scattering of stimulated light off the gold coated diamond heat sink. The bottom part of Fig. 2.3 shows the bonding geometry of the laser on the diamond block; one end of the laser is lined up with the diamond block. Because the lasers are not all identical in length, the laser may be longer or shorter than the diamond block. Thus more light will be scattered for a short laser than for a long one because of the amount of the diamond exposed. Light will be scattered off the exposed part of the diamond block. Away from the facets no substantial changes in the intensity profile along the stripe are observable.

If a plot of the degree of polarization vs. the spatial dimensions is made, the results are much more interesting. Figure 2.9 (a) shows such a plot for the same laser as in Fig. 2.8, with the texture a result of the inherent difference between the intensities of the two orthogonal polarizations. Not all the data collected was used to make this plot. First, data corresponding to the scattered light from the ends of the laser was removed. Second, only the data which would fit in the FWHM of the light distribution across the stripe (in the x-direction) was used to calculate the degree of polarization. This is because as $(P1+P2)$ becomes small the error in the

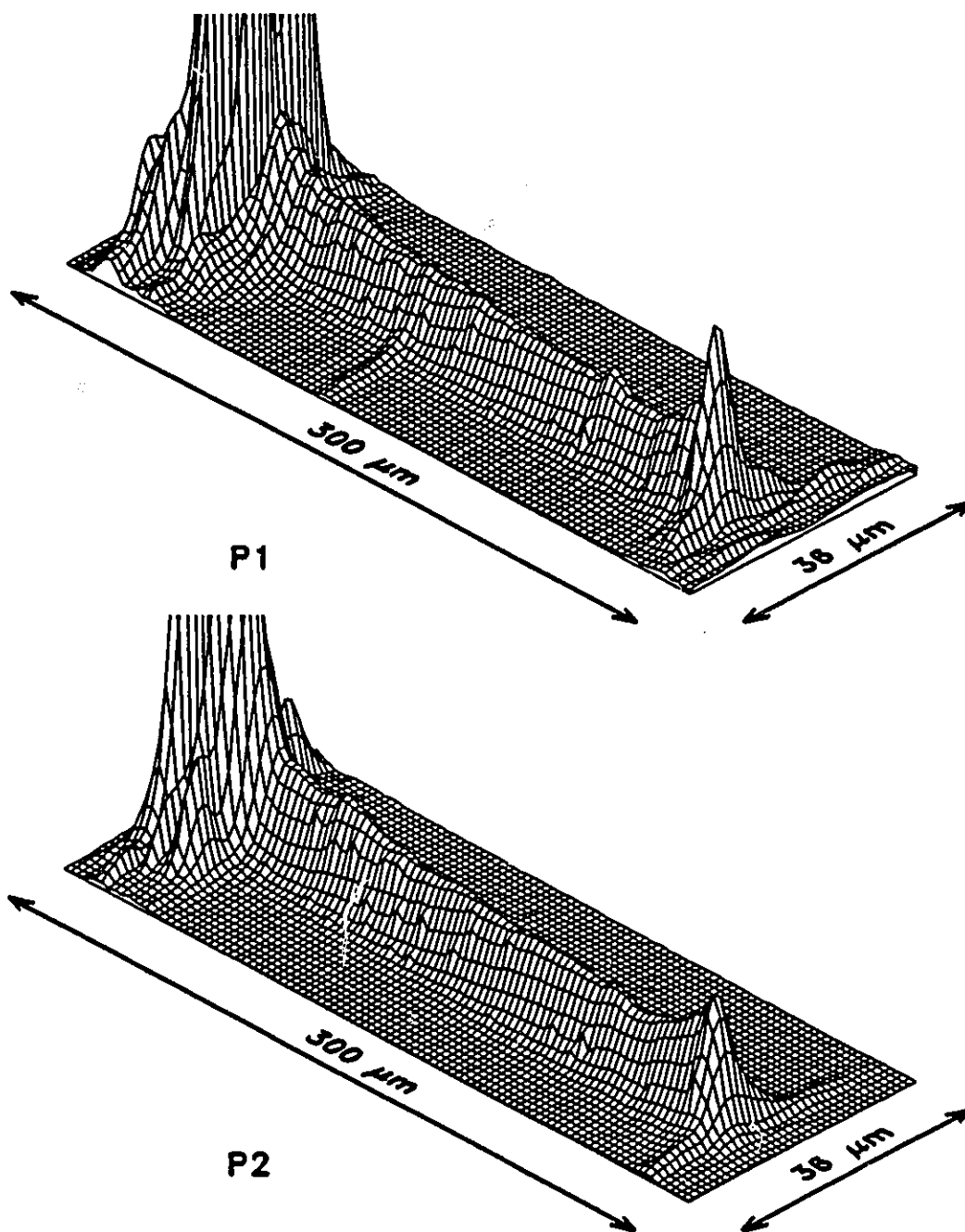


Fig. 2.8 Spatially resolved EL maps of rejected PBH laser for both orthogonal polarizations P1 and P2.

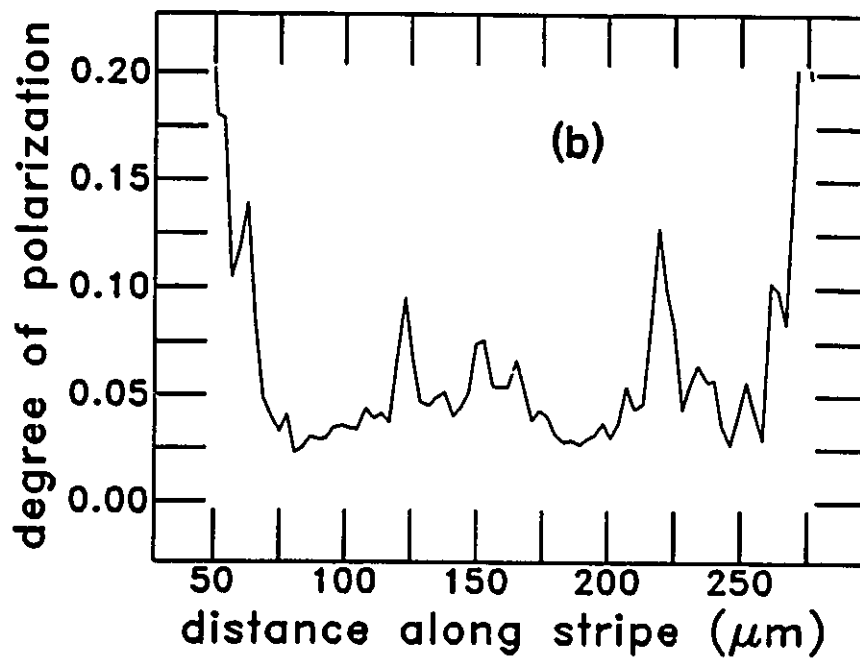
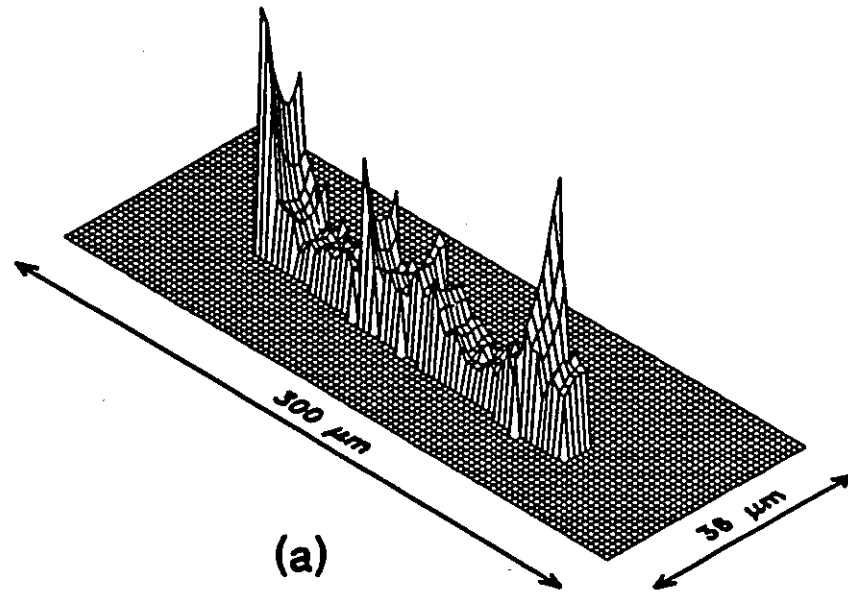


Fig. 2.9 (a) Three dimensional representation of degree of polarization along the active region of PBH laser. The data near the facets have been removed. (b) Two dimensional representation.

degree of polarization measurements becomes large due to additive noise corrupting the computation. The degree of polarization at all points outside the FWHM of the light distribution was set to zero.

One may notice that across the stripe (in the x-direction) there is not very much texture in the degree of polarization data. Therefore an efficient way to represent the data is to use a two dimensional plot of the degree of polarization along the stripe (ie. a y-z plot). Different graphs can be overlaid to demonstrate the effect of: aging, different current or output power levels and different sets of data for reproducibility. The degree of polarization (in the z-direction) is an average of those values of degree of polarization across the stripe which lie in the FWHM of the intensity distribution. Figure 2.9 (b) shows such a plot, which clearly shows the variations in the degree of polarization along the stripe.

The dependence of the two dimensional graph on positioning of the detectors was tested to ensure the reproducibility of results. The position of one of the detectors was misaligned about $20 \mu\text{m}$ to represent experimental error, and data was taken again. The resulting changes in the three dimensional graph were as expected: there was a definite slope in the degree of polarization across the stripe compared to when the detectors were aligned (Fig. 2.10). The two dimensional representation along the stripe of the degree of polarization was generated by averaging ρ across the stripe for each data point. This averaging removes the effect of a small alignment error (since the error is linear to first order) so that the resulting two dimensional graph should theoretically be identical to an equivalent

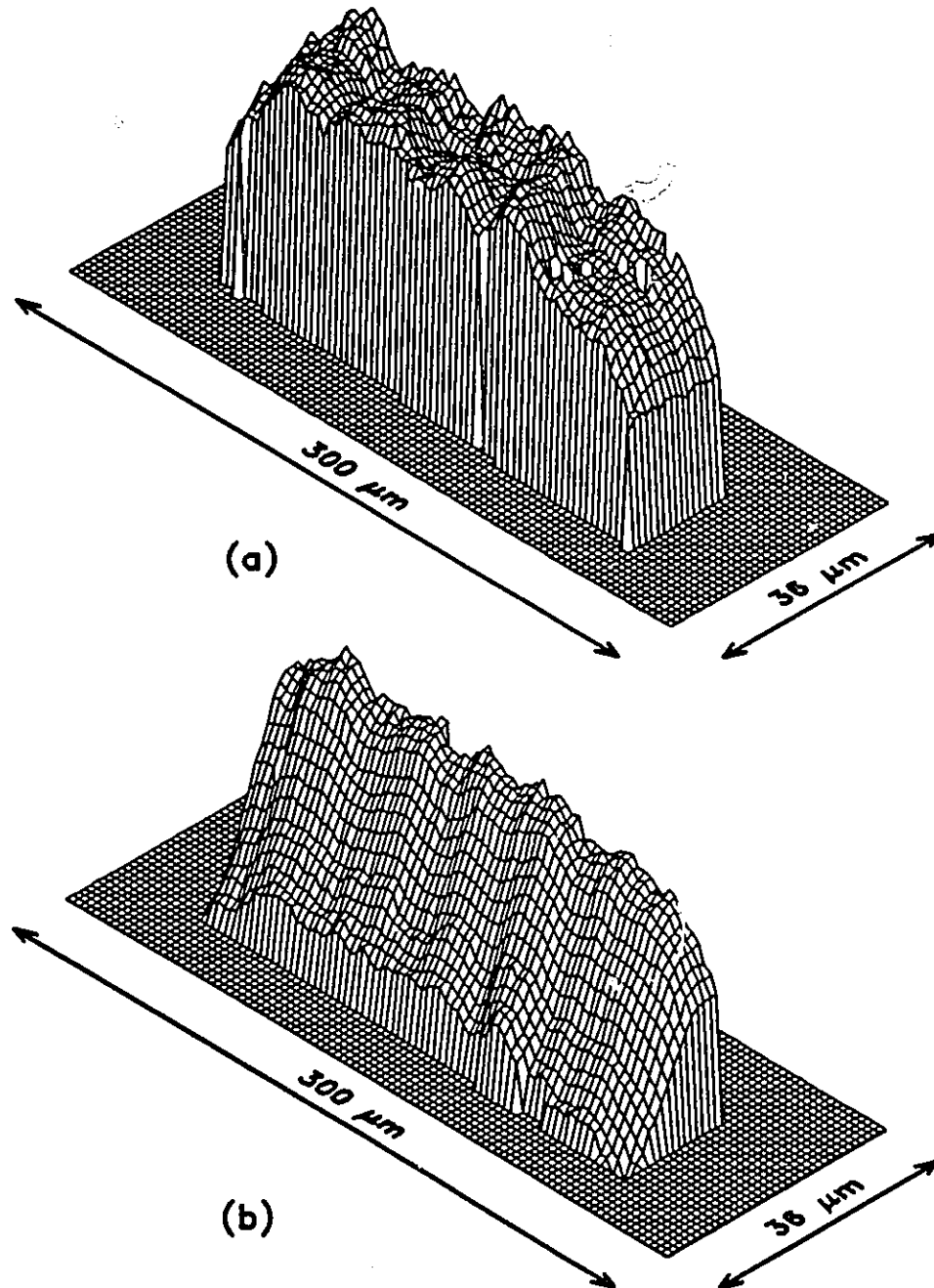


Fig. 2.10 Degree of polarization distribution across and along stripe for a gain guided laser with (a) the detectors aligned and (b) the detectors misaligned 20 μm .

graph generated from data with no alignment error of the detectors. Experimentally this is seen to be correct: differences between two sets of data with detectors well aligned are of the same order of magnitude as the differences between data corresponding to good and bad alignment (Fig. 2.11).

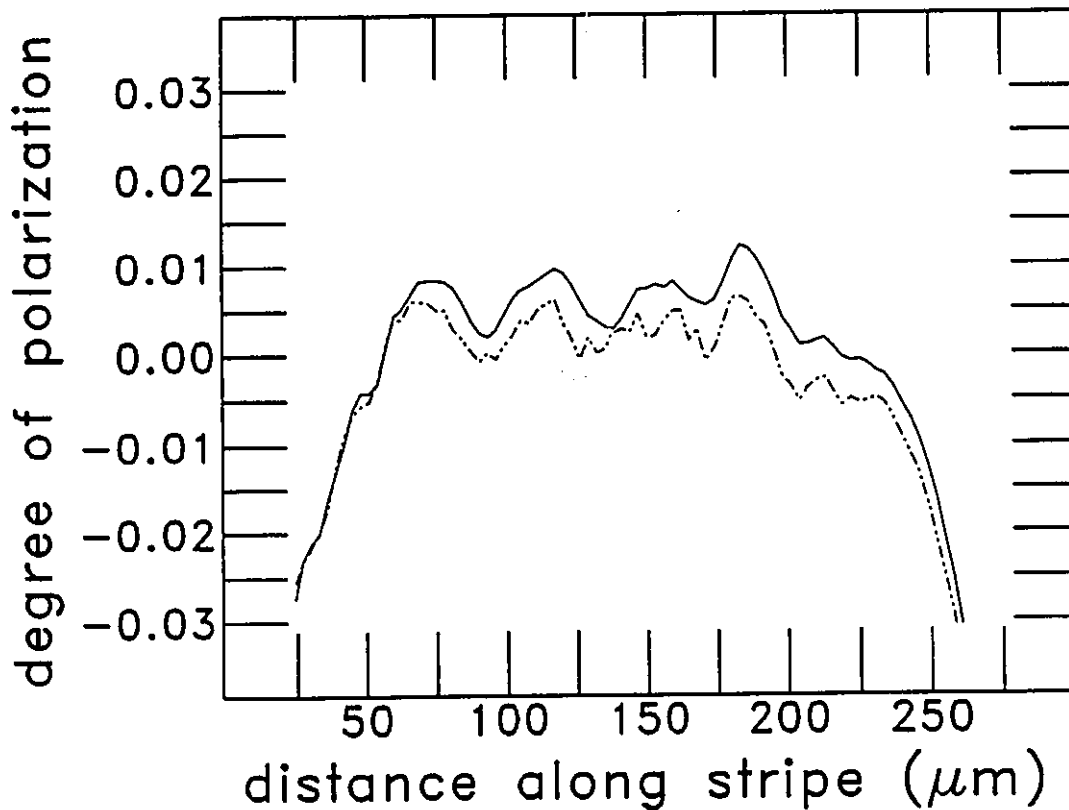


Fig. 2.11 Two dimensional representation of degree of polarization distribution along the active region of a gain guided laser for aligned detectors (solid line) and for misaligned detectors (broken line).

Thus the results are highly reproducible. The overlaid results in Fig. 2.12 are two sets of data taken days apart. The results have been shifted in the horizontal direction so that they overlap. Each scan was made with the entire set up procedure carried out (i.e., the laser was removed and the instrument misaligned and defocused

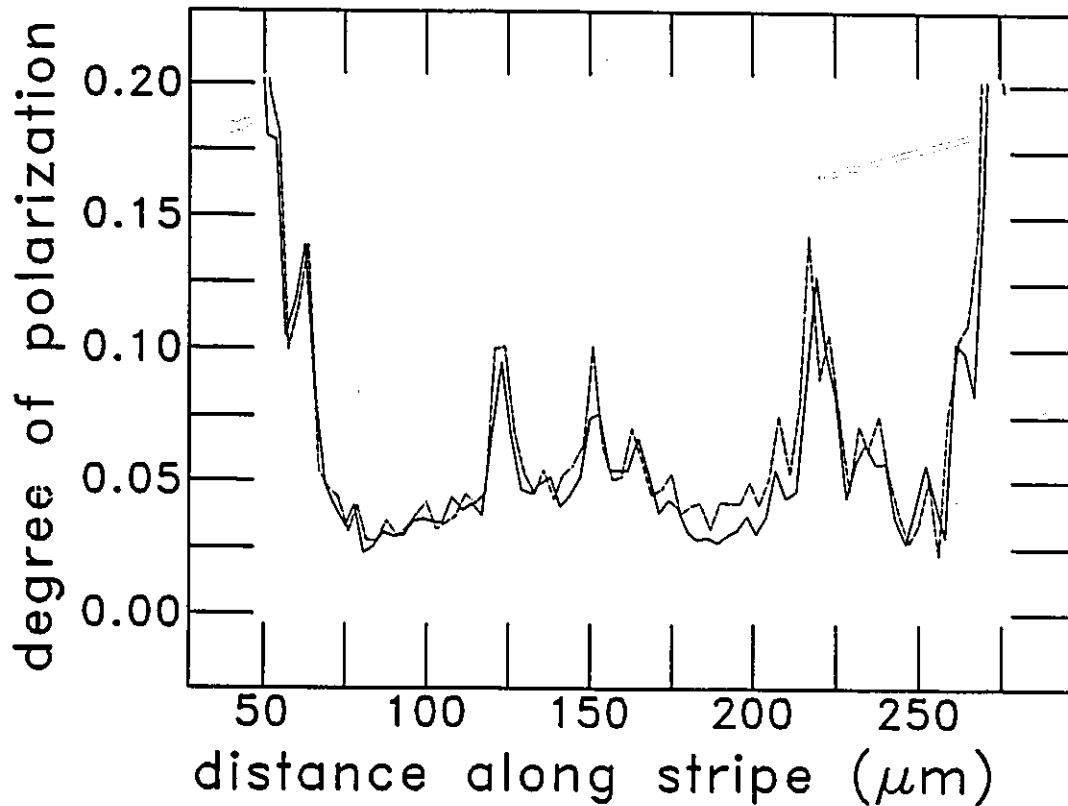


Fig. 2.12 Degree of polarization along the stripe of PBH laser for two different set of data showing the reproducibility of the results.

prior to reinstalling the laser). The results are very similar with the effect of the three micron grid in the y-direction being evident: If the peak in the degree of polarization graph lies between two data points in one scan, and lies on a data point in a subsequent scan the heights of the corresponding peaks appear to be different. The resolution of the instrument is therefore estimated at better than $2 \mu\text{m}$. Many measurements were done on the same lasers to test the accuracy of the measurements and the results indicate that the uncertainty (max.-min.) in the degree

of polarization data is ≤ 0.003 . This is the amount of uncertainty which will be assumed throughout this thesis for degree of polarization measurements unless stated otherwise.

During each scan, different current levels through the laser were used to observe the effects below and above threshold on the degree of polarization. At each spatial point all current measurements were taken to ensure that differences between the data at different current levels is meaningful. In Fig. 2.13 the degree of

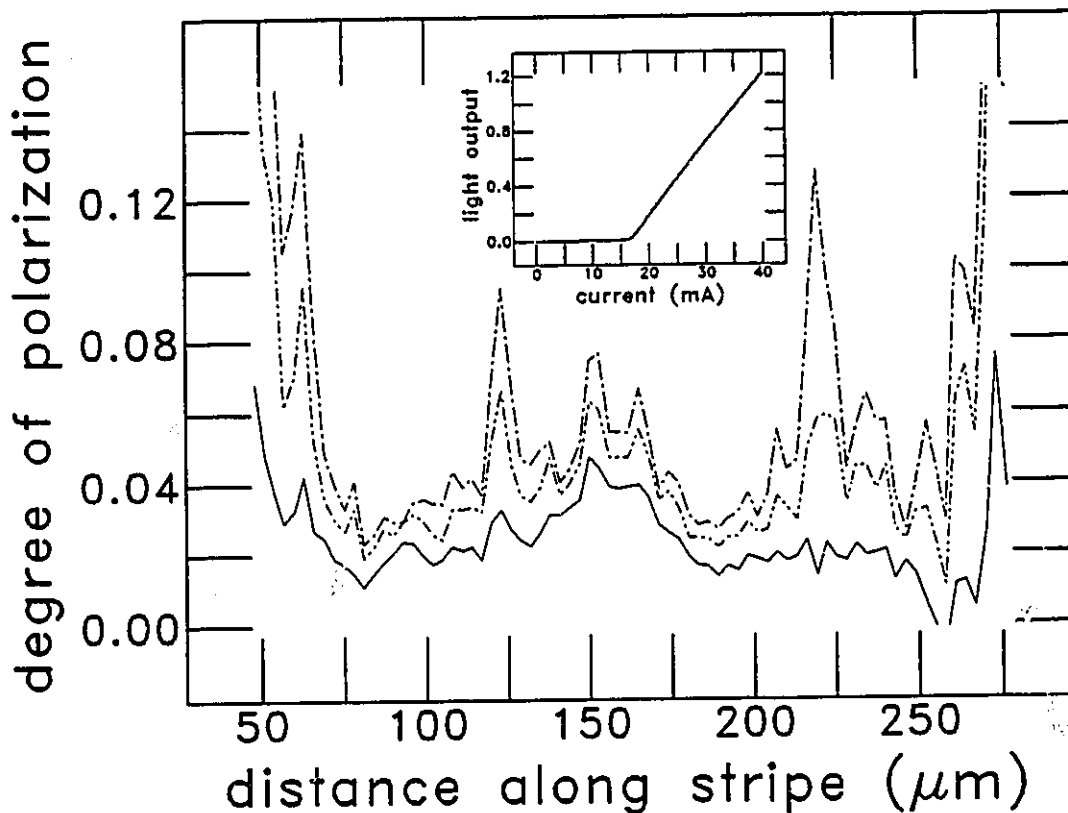


Fig. 2.13 Degree of polarization along the stripe of PBH laser for different current levels: 20 mA, 30 mA, and 40 mA. The degree of polarization increases with increased current.

polarization data is shown for three different current levels. The change in the degree

of polarization with current above threshold is interpreted as due to scattering and will be discussed at greater length in the next chapter.

2.5 Summary

An instrument has been developed to make spatially resolved and polarization resolved electroluminescence measurements and is capable of detecting small changes in the electroluminescence signal. A description of the instrument, its operation and its capabilities has been given. Spatially resolved and polarization resolved EL is shown to be a very useful technique. It has been shown to be capable of reproducibly measuring the internal properties of diode lasers. These internal properties will be used in the next chapter to correlate laser types and spectral outputs.

Chapter 3 Strain and Scattering

3.1 Introduction

Spatially and polarization resolved maps of the electroluminescence were taken for below and above threshold operation for three different diode laser structures: gain guided,[23] planar buried heterostructure[24] (PBH) and arrowhead buried crescent[25,26] (ABC) lasers. The amount of effective scattering ($\Delta\rho$) is correlated with the spectral properties of the diode lasers and provides some interesting results. The effective scattering is defined as the change in the degree of polarization (ρ) with the output power of the laser.

It is found that if a large amount of effective scattering exists in the device then the laser will tend to operate single moded or multilongitudinal moded with highly modulated mode envelopes. If the effective scattering is small then the device tends to operate multilongitudinal moded with smooth mode envelopes. It is also found that devices which have large positive internal strains tend to have a larger amount of effective scattering than devices with low or negative internal strains. The gain guided devices which were measured normally have very low or negative strain distributions with very low effective scattering; they tend to operate multilongitudinal moded with smooth mode envelopes. The PBH devices which were measured are under greater strain, have a larger amount of effective scattering, tend to operate more single moded than gain guided lasers, and may operate multilongitudinal

moded with a large modulation of the mode envelopes. The strain and effective scattering distributions in the ABC diode lasers which were measured lie between the distributions of gain guided devices and the PBH devices. Also, in keeping with these material properties, the ABC device, which was found to have the lowest strain distribution and the lowest effective scattering of the ABC devices which were measured, did not exhibit multilongitudinal moded behaviour with highly modulated mode envelopes or strong single moded operation over normal operating conditions. It is concluded that semiconductor diode lasers operate single moded or multilongitudinal moded with highly modulated mode envelopes as a result of the interference caused by the scattering of stimulated emission inside the device. This scattering will result in the formation of weak Fabry Perot cavities within the laser cavity and is modelled in Chapters 4 and 6. The dependence of the spectral output on the scattering properties of the active region is consistent with the results observed for intentionally introduced scattering [27] or loss centres.[28]

In this Chapter an analysis of the EL data to produce strain and scattering information is given, and a correlation between the scattering properties of the devices and their spectral properties is presented. Section 3.2 describes the measurement of strain in the active region, Section 3.3 outlines the measurement of the effective scattering, Section 3.4 shows the correlation which exists between the effective scattering and the spectral properties of diode lasers, and Section 3.5 provides a summary.

3.2 Strain Measurements

The below threshold degree of polarization measurements are used to obtain information about the internal strain which exists in the plane of the active region of the semiconductor diode lasers.[21,22] The distribution of the degree of polarization (ρ) along the length of the active region of a typical PBH laser (laser G) is shown in Fig. 3.1 for below threshold (solid line) and above threshold (broken

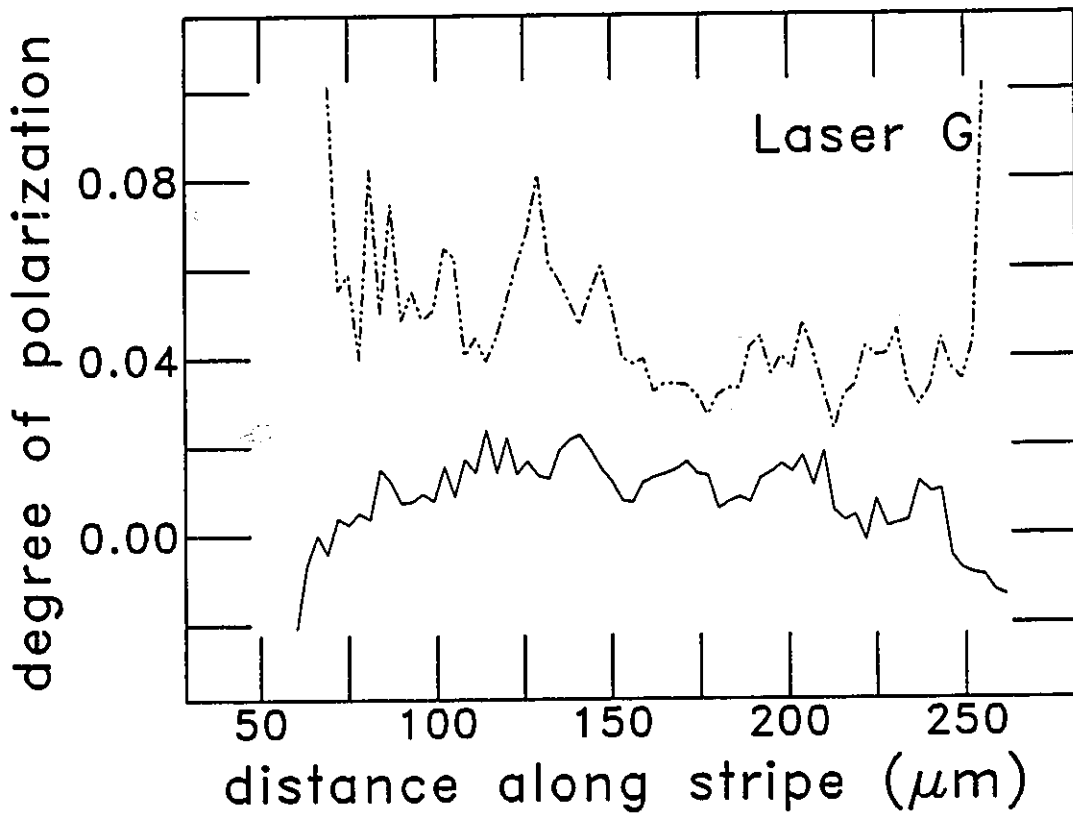


Fig. 3.1 Degree of polarization (ρ) distribution along the active region of PBH laser (laser G) for below threshold operation (solid line) and above threshold operation (broken line).

line) operation. Note that a substantial difference exists between ρ measured above and below threshold. This difference is not attributed to a change in the internal

strain of the active region with bias, but rather the difference is interpreted as an effect caused by the scattering of stimulated emission inside the device. ρ stays constant with current below threshold and increases with current above threshold (Fig. 2.13), and this corresponds to an increase of P1 light over P2 light above threshold. Since the lasing mode is TE polarized, scattered stimulated light will be seen as P1 light and will result in ρ increasing. Below threshold the amount of spontaneous light dominates over the scattered light and the effect of the scattered light on ρ is negligible. Therefore only the below threshold degree of polarization data (ρ_b) is used to estimate the distribution of strain in the device.

To quantify the internal strain of the devices, the results of graphs such as Fig. 3.1 for the laser operating below threshold are summarized. Two parameters have been chosen for this purpose: the mean and the standard deviation of the degree of polarization along the length of the device. These values were calculated for data corresponding to below threshold operation. Figure 3.2 shows ρ calculated along the active region of an arrowhead buried crescent (ABC) laser (laser 3), for below threshold (solid line) and above threshold (broken line) operation. The mean and standard deviation of the ρ is calculated over this region for the below threshold data. Laser e is a typical gain guided structure whose above and below threshold degree of polarization distribution is shown in Fig. 3.3.

Figures 3.1 to 3.3 show distributions of ρ along the active region of the lasers, results which are highly reproducible. The standard deviation of ρ along the stripe is not a measure of the accuracy of the data, but rather a measure of the variation in ρ which exists along the stripe. Because ρ can be measured reproducibly, the values of the mean and standard deviation of ρ along the stripe are accurate and are numbers which are characteristic of the internal strain of the laser. The

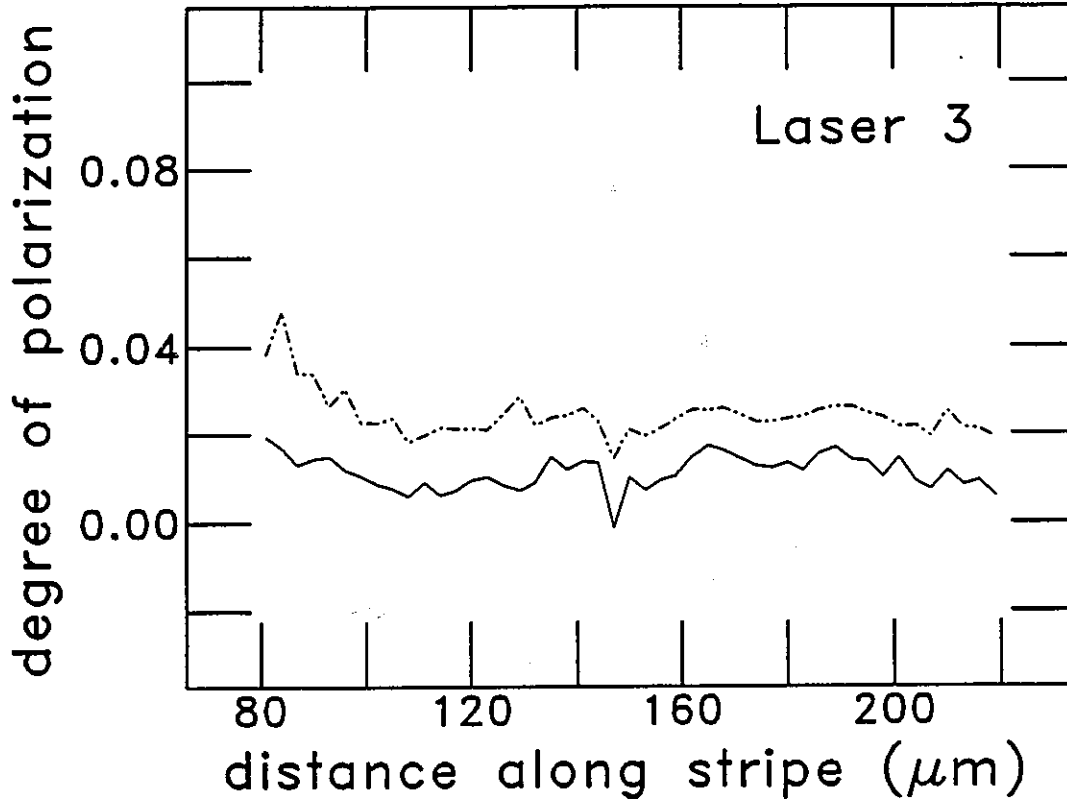


Fig. 3.2 Distribution of ρ along the active region of ABC laser (laser 3) with facet effects removed for below threshold operation (solid line), and above threshold operation (broken line).

uncertainties associated with these numbers are low; typically <0.003 for the mean and almost an order of magnitude smaller for the standard deviation as discussed in Chapter 2.

Once the mean and standard deviation of ρ along the active region are calculated for all the lasers, the results can be compared. Figure 3.4 shows the below threshold results of the mean and standard deviation of ρ , for the gain guided, PBH, and ABC lasers which were measured. The lower case letters represent gain guided lasers, the upper case letters represent PBH lasers and the numbers represent ABC

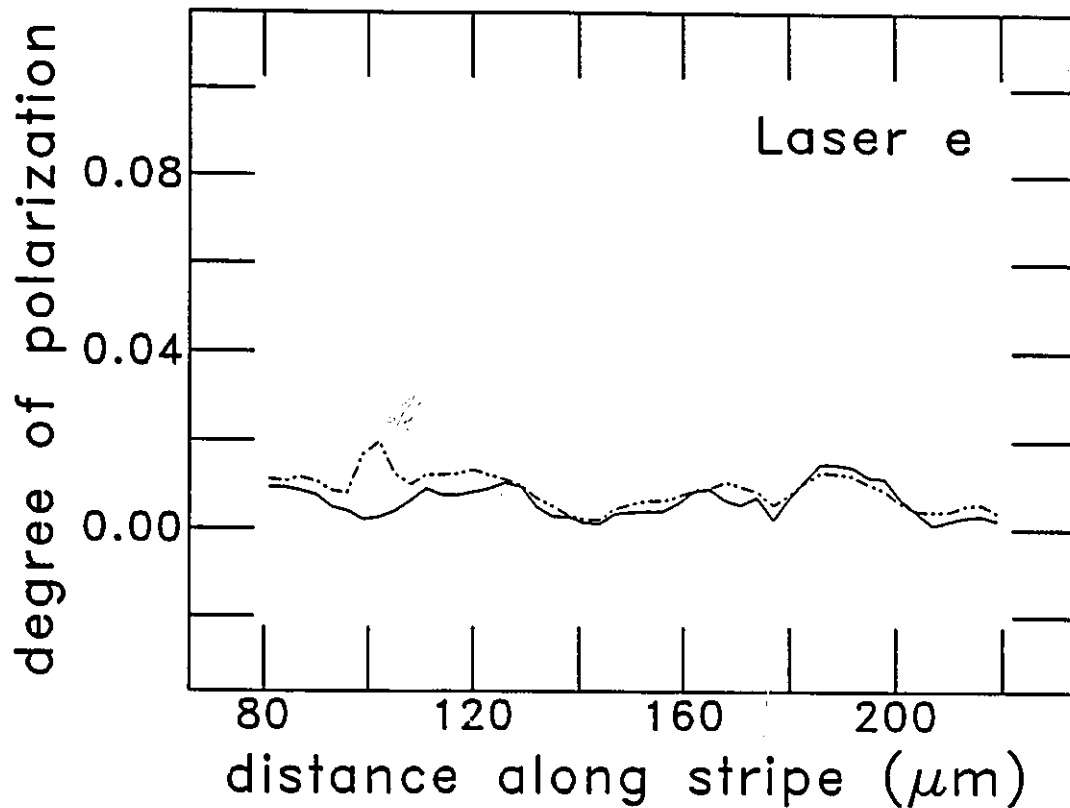


Fig. 3.3 Distribution of ρ along the active region of a gain guided laser (laser e) for below threshold operation (solid line), and above threshold operation (broken line).

lasers. By comparing the mean values of ρ_b one can immediately see that the gain guided lasers have lower strains in their active region than the PBH or the ABC lasers. Since the standard deviation of ρ_b measures the variation of the strain distribution along the length of the device, one can also conclude that diode lasers do not have uniform strain distributions along their active regions and on average the gain guided lasers have a more uniform distribution of strain than the index guided lasers.

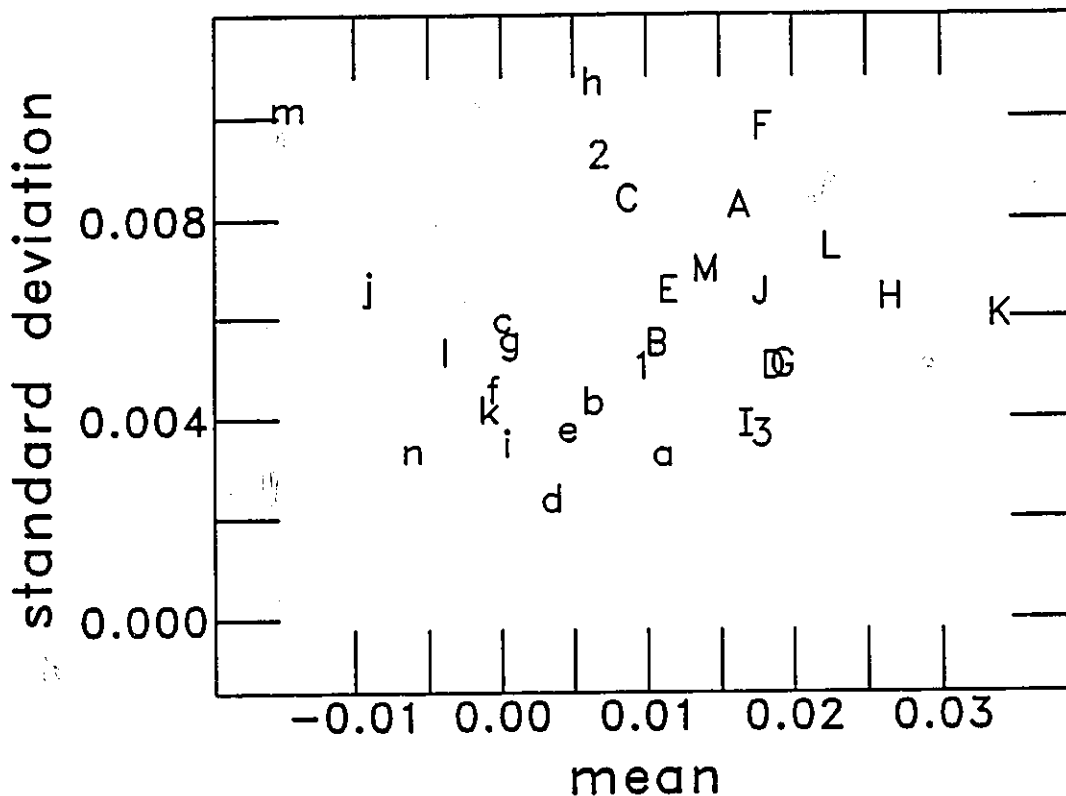


Fig. 3.4 Standard deviation vs. mean of below threshold degree of polarization (ρ) measurements, for gain guided lasers (lower case), PBH lasers (upper case) and ABC lasers (numbers).

3.3 Effective Scattering Measurements

The above threshold degree of polarization measurements (ρ_a) are used to estimate the amount of effective scattering which exists near or in the active region. The increase of ρ above threshold ($\rho_a - \rho_b$) is interpreted as due to the scattering of stimulated emission, and is assumed to be the result of material defects, or growth irregularities. This means that the amount of scattering which exists in a device is a measure of the quality of the material properties of the active region.

The data of Fig. 3.1 shows that the PBH laser G is not uniform along the length of the active region. There exists scattering from uniformly distributed scattering centres which is evidenced by the difference in the baseline between ρ_a and ρ_b and scattering from discrete or isolated centres which is observable as peaks in ρ_a . For all three figures (Figs. 3.1-3.3) the above threshold data (ρ_a) was taken when the lasers were operating at approximately the same output powers.

Figure 3.2 shows ρ_a (broken line) and ρ_b (solid line) for an ABC device (laser 3). The device is not uniform along the length and the effective total and discrete scattering in this device is less than the PBH laser of Fig. 3.1.

Fig. 3.3 shows ρ_a (broken line) and ρ_b (solid line) for a gain guided device (laser e). Note that this device is also not uniform along the length of the active region, and that the effective scattering of the gain guided device is lower than either the ABC laser of Fig. 3.2 or the PBH laser of Fig. 3.1.

These lasers (G, 3, and e) are typical in terms of their effective scattering properties of the samples measured of their structure. That is, the effective scattering seen in gain guided lasers is typically weak, PBH lasers exhibit a large amount of effective scattering, and ABC lasers are intermediate to the gain guided and PBH lasers in terms of their effective scattering characteristics. To demonstrate this a compact scheme for presenting the ρ_a - ρ_b data for the lasers measured is required. One method is to plot the discrete effective scattering $\Delta\rho_d$ against the total effective scattering $\Delta\rho_t$. This is done in Fig. 3.5. Data for gain guided lasers are plotted with lower case letters, data for ABC lasers are plotted with numbers, and data for PBH laser are plotted with capital letters. Note that the amount of effective scattering in the gain guided devices tested tends to be less than for the index guided devices (PBH and ABC lasers) and that lasers G, 3, and e are typical of their structure. A

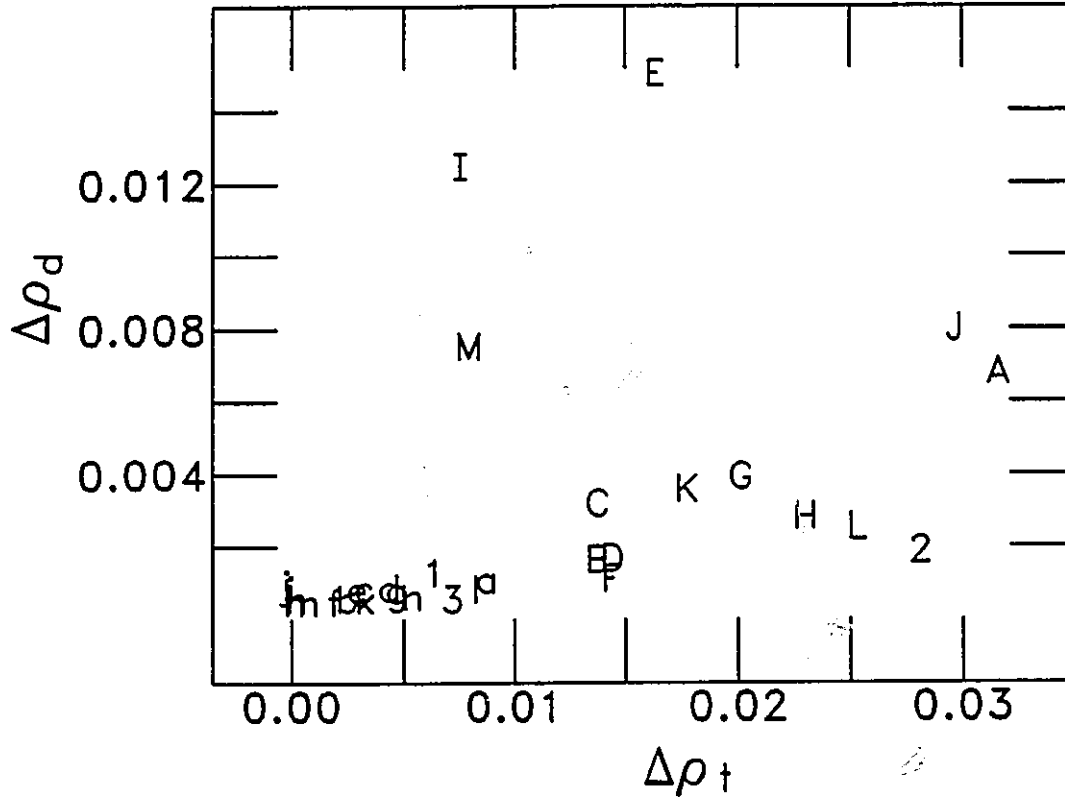


Fig. 3.5 Discrete effective scattering ($\Delta\rho_d$) vs. total effective scattering ($\Delta\rho_t$) for gain-guided lasers (lower case), PBH lasers (upper case) and ABC lasers (numbers).

comparison of Figs 3.4 and 3.5 shows that lasers with large positive internal strains are more likely to have large amounts of effective scattering than are lasers with low or negative strains.

The parameter $\Delta\rho_t$, the total effective scattering has been defined as:

$$\Delta\rho_t = \sum_{i=1}^N [\rho_a(y_i) - \rho_b(y_i)]/N, \quad (3.1)$$

where N is the number of data points, and the y_i are the data points in the y -

direction (along the length of the active region). $\Delta\rho_t$ measures the difference between the mean values of ρ_a and ρ_b and roughly corresponds to the vertical distance between ρ_a and ρ_b in Figs. 3.1-3.3. A value of $\Delta\rho_t=0$ corresponds to ρ_a and ρ_b , on average, lying on top of each other. The parameter $\Delta\rho_d$, has been defined as:

$$\Delta\rho_d = \left\{ \sum_{i=1}^N [\rho_a(y_i) - \rho_b(y_i)]^2 / N \right\}^{1/2} - \Delta\rho_t. \quad (3.2)$$

The function $\Delta\rho_d$ weights large values of the difference $\rho_a - \rho_b$ more than small values of the difference. Thus $\Delta\rho_d$ is the discrete effective scattering found from the data presented in Figs. 3.1-3.3. $\Delta\rho_d$ is sensitive to variations in $\rho_a - \rho_b$ along the length of the device. If $\rho_a(y_i) = \rho_b(y_i) + \Delta$ for all y_i , then $\Delta\rho_d = 0$, where the y_i are the discrete data points.

The parameters $\Delta\rho_d$ and $\Delta\rho_t$ are referred to as effective scattering because they describe the fraction of scattered light which is seen over the spontaneous emission background. For example, an increase in the amount of scattered light due to an increase in the output power of a laser, will be more noticeable in terms of $\Delta\rho$ for a laser which produces a small amount of spontaneous emission (small P1 and P2) than for a laser which produced a large amount of spontaneous emission (large P1 and P2).

3.4 Scattering and the Spectral Properties

From Fig. 3.5 it can be seen that gain guided devices tend to have very low values of $\Delta\rho_d$ and $\Delta\rho_t$, whereas the index guided lasers, and in particular the PBH lasers, tend to have large $\Delta\rho_d$ and $\Delta\rho_t$ values. The scattering data is correlated with the longitudinal mode spectra of the lasers. The spectra of diode lasers was recorded with the temperature and current adjusted to produce the most single mode operation or the worst modulation of the mode envelope. The reason for this is as follows: if scattering centres through resonant enhancement of selected modes affect the spectral output, then the effect of the scattering centres will be most pronounced when the gain peak is centred over the selected modes. By adjusting the temperature and current, the position of the gain peak relative to the modes can be adjusted.

Figure 3.6 is made up of the worst case spectra for laser e, laser 3, and laser G at two different temperatures. Note that laser e is a gain guided device, laser multilongitudinal moded with a smooth mode envelope, and has low values of $\Delta\rho_d$ and $\Delta\rho_t$. Laser 3 is an ABC laser and operates more single moded than the gain guided laser e. Laser 3 also exhibits larger values of $\Delta\rho_t$ and $\Delta\rho_d$ than laser e. Laser G runs either single moded or multilongitudinal moded with a modulated mode envelope, depending on the temperature. Laser G also has significantly higher values of $\Delta\rho_d$ and $\Delta\rho_t$ than the other two lasers.

The relationship between the scattering properties and the spectral properties of lasers can be further demonstrated by examining the spectral properties

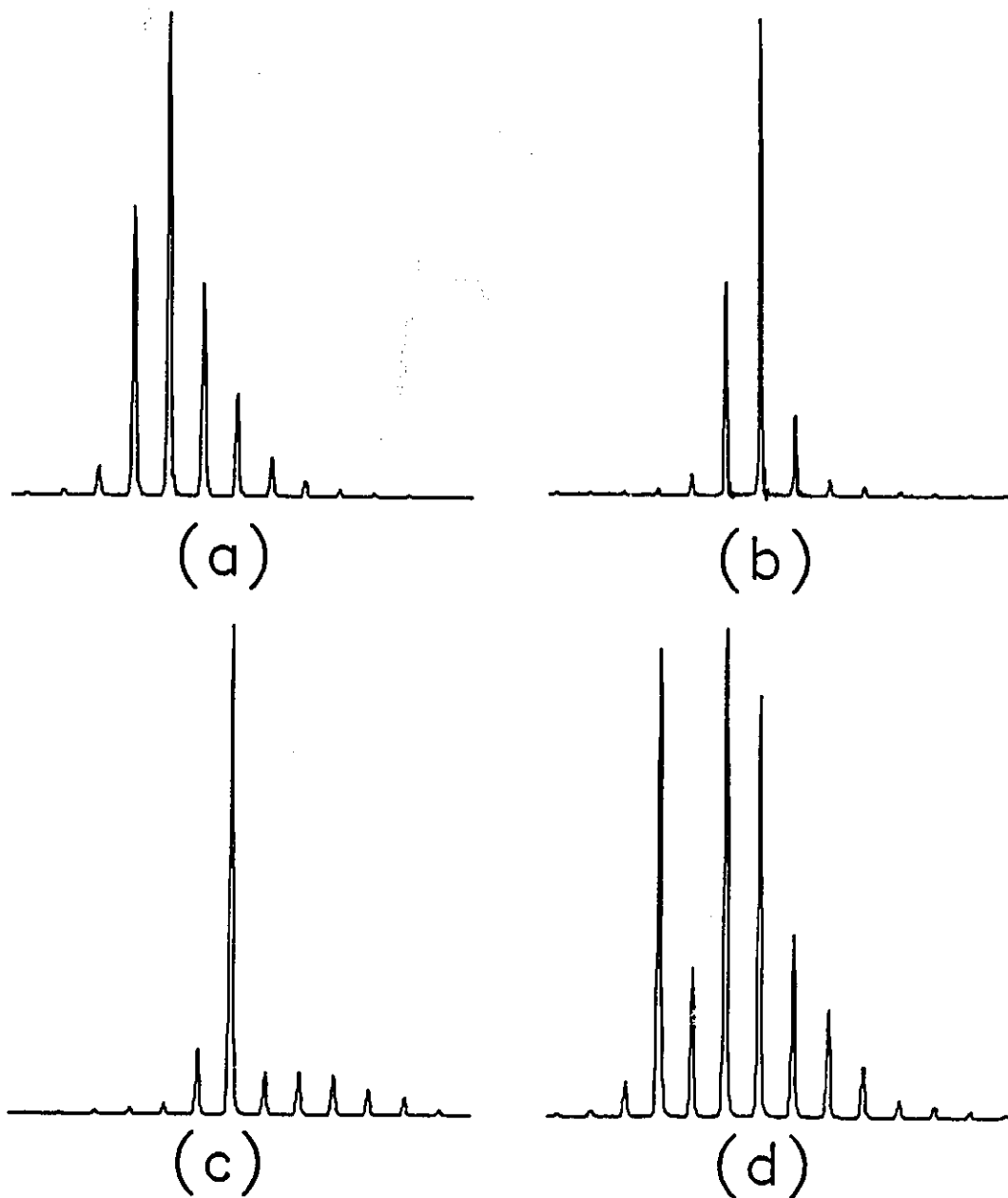


Fig. 3.6 Experimentally measured spectral output of (a) gain guided laser e, (b) ABC laser 3, (c) and (d) PBH laser G at two different operating temperatures.

of lasers which exist in the extremes of the graph of Fig. 3.5. Figure 3.7 shows the

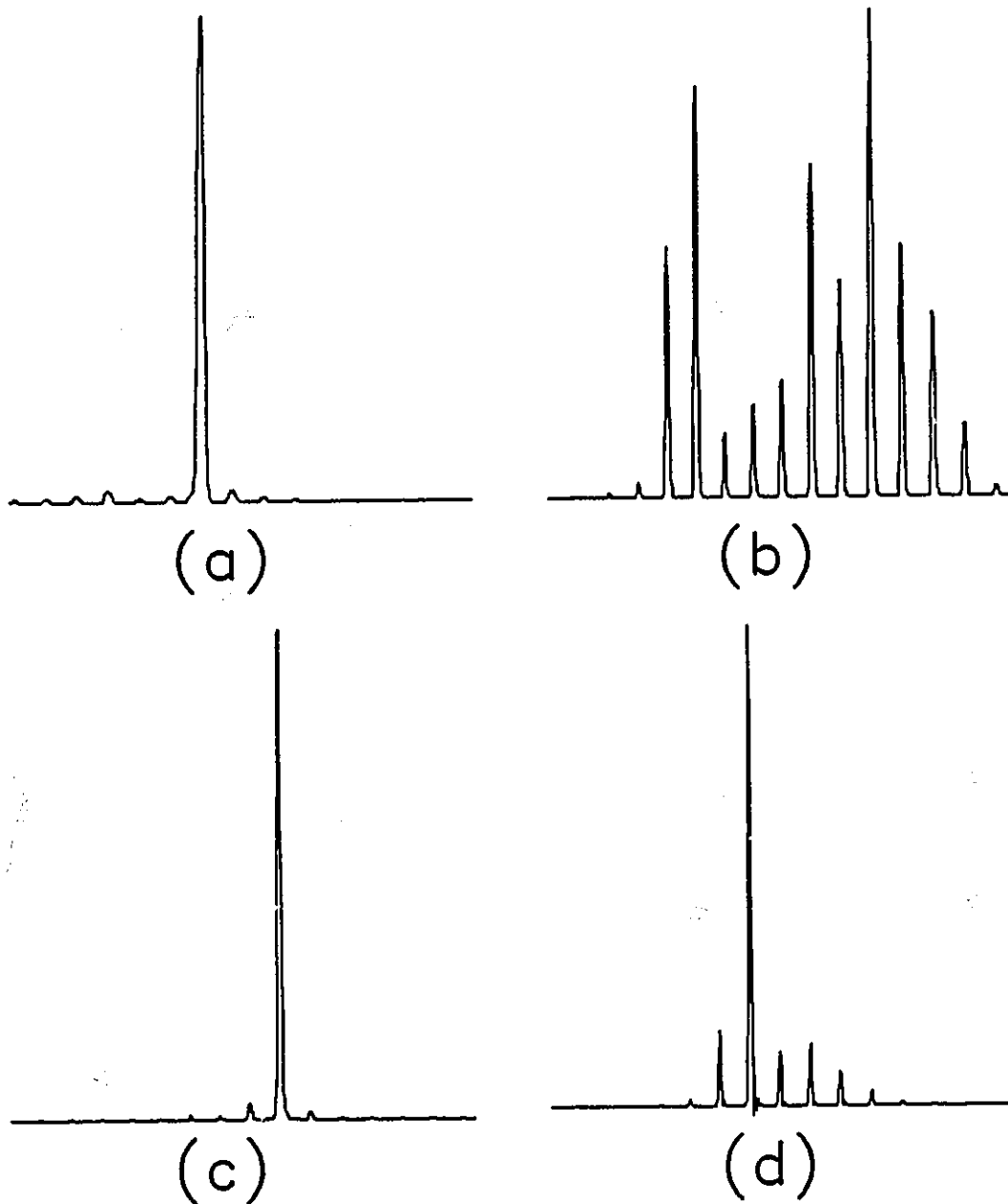


Fig. 3.7 Experimentally measured spectral output of (a) PBH laser J, (b) PBH laser E, (c) PBH laser I, and (d) gain guided laser a.

spectral output of lasers J, E, I, and a. Laser E operates multilongitudinal moded

with highly modulated mode envelopes and has large values of $\Delta\rho_d$ and $\Delta\rho_t$. Laser E also is one of only two lasers measured which tuned to shorter wavelength with increasing current, an unusual characteristic in lasers. Lasers I and J operated strongly single moded and had large values of $\Delta\rho_d$ and $\Delta\rho_t$. Laser a whose spectral output is multilongitudinal moded with a small amount of modulation of the mode envelope exhibited very low values of both $\Delta\rho_t$ and $\Delta\rho_d$ compared with the index guided devices, but large values of $\Delta\rho_t$ and $\Delta\rho_d$ compared with the gain guided devices such as laser e. On the basis of data such as Figs. 3.5-3.7 it is concluded that the material properties of the active region affect the spectral output of semiconductor diode lasers.

3.5 Summary

Spatially resolved and polarization resolved electroluminescence measurements of 1.3 μm InGaAsP semiconductor diode lasers have been made, and the material properties of the active region have been derived from the data. The degree of polarization (ρ), which is defined as the difference of the two orthogonal polarizations of the EL signal divided by the sum, is used to derive these properties. Measurement of ρ along the length of the active region for below threshold operation gives an estimate of the strain distribution. The mean of this distribution provides a measure of the strain distribution and a convenient technique to compare

lasers. Likewise, measurements of the difference between ρ for above and below threshold operation along the length of the active region ($\rho_a - \rho_b$) reveals the presence of scattering centres.

The larger the effective scattering which exists in a laser, the more likely it is that the laser will operate single moded or multilongitudinal moded with highly modulated mode envelopes. The PBH lasers tested were found to have the highest strains and the largest values of effective scattering and they tend to operate the most single moded or multilongitudinal moded with the most modulated mode envelopes. The gain guided devices measured were found to have the smallest strains, lowest values of effective scattering and operate the most multilongitudinal moded with the smoothest mode envelopes. The ABC lasers tested were found to have strain and scattering properties somewhere between the gain guided and the PBH lasers which were measured. The spectral output of the ABC lasers had smoother mode envelopes than the PBH lasers tested but more single moded and multilongitudinal moded with a larger modulation of the mode envelopes than the gain guided lasers measured. Thus the spectral output is correlated with the material properties of the lasers, as found from measurements and analysis of ρ . It is concluded that the difference in the spectral properties of lasers can be attributed to the difference in material properties of the active region. This will be examined theoretically in the next chapter.

Chapter 4 Single Scattering Model

4.1 Introduction

In Chapters 2 and 3 measurements were presented which demonstrate that semiconductor diode lasers are not uniform along their active regions. Models which predict the spectral output of semiconductor diode lasers assume that lasers are uniform along the length of the active region. They also often make the magnitude of the spontaneous emission factor and the shape of the gain profile dependent upon the structure of the laser. For gain guided lasers the spontaneous emission factor is taken to be large (as compared to that for index guided lasers) and the gain profile is taken to be smooth and parabolic, while for index guided lasers the spontaneous emission factor is assumed to be small (as compared to that for gain guided devices) and the shape of the gain profile is taken to be non-parabolic. The predictions of the models with the input parameters adjusted as described then agree with the observation that index guided lasers tend to run more single longitudinal moded than gain guided lasers. The input required for the models has been justified by considering the effects of spectral hole burning [29], population beating [30], and astigmatic beams.[31]

Experimentally, the measured spectra of a semiconductor diode laser may be single moded or multilongitudinal moded with a smooth mode envelope, may be very asymmetric, and may be multilongitudinal moded with a highly modulated mode

envelope. Also the spectra of diode lasers can change dramatically with temperature and operating current. The spectra of a laser may change from single moded to multilongitudinal moded with highly modulated mode envelopes. Such behaviour has not been explained. In chapter 3 a correlation was shown between the spectral properties of diode lasers and their effective scattering properties. It was shown that lasers which exhibit large amounts of effective scattering are more likely to operate single moded or multilongitudinal moded with highly modulated envelopes than are lasers with small amounts of effective scattering.

Therefore, a model has been developed for the longitudinal mode spectra of diode lasers which includes the effect of one scattering centre inside the diode laser. Any effects caused by hole burning, population beating, or astigmatic beams have been ignored, so that the effect of scattering may be isolated. The model not only explains asymmetric longitudinal mode spectra and multilongitudinal mode spectra with highly modulated mode envelopes but also provides an explanation, based on the material properties of the devices, as to why index guided lasers tend to operate more single moded than gain guided lasers.

In this Chapter the model and its predictions are presented. Section 4.2 gives the derivation of the model, Section 4.3 shows the results of the model and how the predictions of the model compare with existing devices, and Section 4.4 provides a summary.

4.2 Laser Model with Scattering Centre

The purpose of the theoretical analysis is to estimate the effect on the spectral output of semiconductor diode lasers of a scattering centre which exists in or near the active region. The approach is to define effective reflectivities which include the effect of the scattering centre so that the analysis can be transformed into a simple Fabry Perot laser model.[32,33] This is similar to the method used for modelling cleaved coupled cavity (C^3) lasers,[34] with the following differences. The current density is assumed to be equal in each section of the laser bounded by the scattering centre and the facets, and an effective reflectivity which accounts for the scattering centre is defined for each facet. The model is valid for both below and above threshold operation. Typical models of C^3 lasers define an effective reflectivity which accounts for the air gap and the shorter cavity in such a way as to restrict the model to below threshold operation in the shorter cavity.

The physical picture from which the model is formed can be stated as follows: light exiting from one facet is composed of light reflected at the other facet plus a contribution from light which is reflected off the scattering centre and directed back into the mode. This contribution is wavelength dependent and may be positive or negative depending on whether the interference between the component reflected off the facet and the scattered light is constructive or destructive. Thus the scattering centre effectively enhances or suppresses the reflectivity of the facet depending upon the phase of the scattered light relative to the phase of the light reflected off the facet. An equivalent statement can be made about the apparent reflectivity of the other facet.

The theoretical approach starts with a description of the electric fields in

the cavity. The electric fields at the left and right hand ends of the cavity and which are propagating in the positive y direction (see Fig. 4.1) are denoted a_1 and a_2 . The

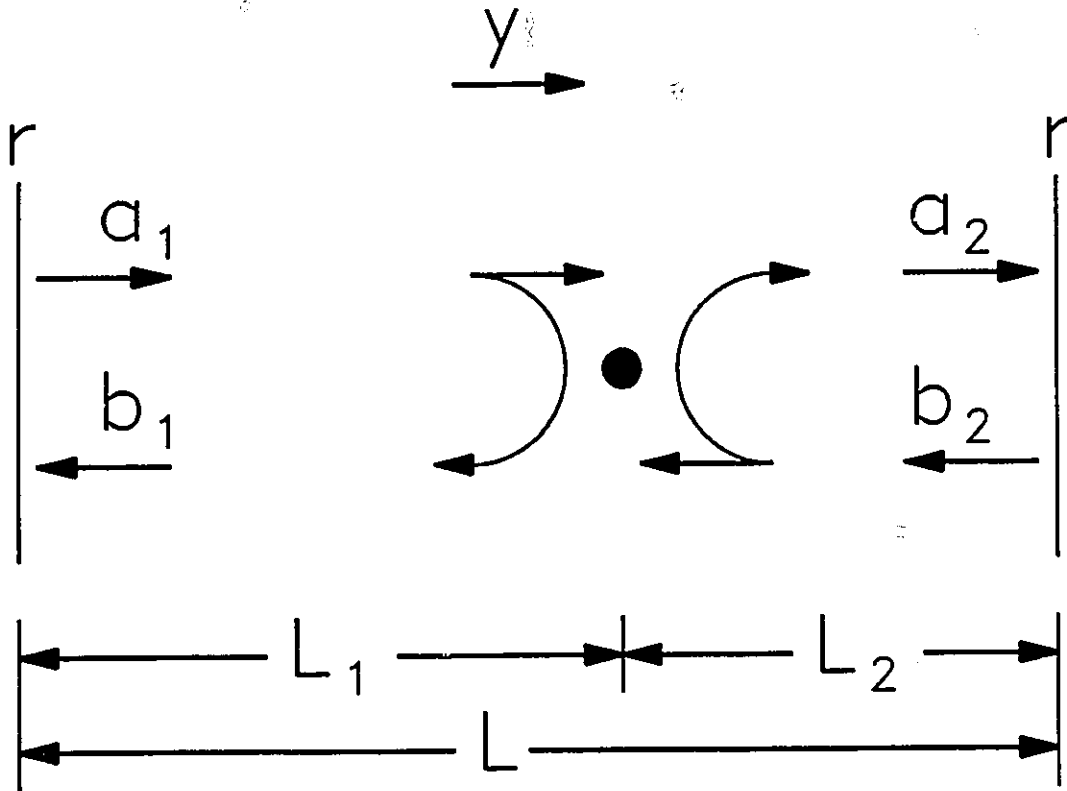


Fig. 4.1 Schematic diagram of a laser (length L) with a scattering centre (solid dot) which exists a distance L_1 from the left hand facet and a distance L_2 from the right hand facet.

electric fields at the facets which propagate in the negative y direction are denoted b_1 and b_2 . The cavity is taken to have a length $L=L_1+L_2$. A scattering centre is assumed to be located a distance L_1 from the left hand facet and a distance L_2 from the right hand facet. The fraction of the electric field which is scattered at the scattering centre is $1-\tau$, and the fraction of the electric field which couples back into the mode after scattering is σ . All variables used are defined in Table 1.

The amplitude of the electric field which propagates in the positive y

Table 1

a_i	electric field amplitudes travelling in the (+) y directions
b_i	electric field amplitudes travelling in the (-) y directions
r	reflectivity of laser facets
r_i	effective reflectivity of laser facets
L	length of laser cavity
L_i	distance from facet i of scattering centre
σ^2	fraction of light intensity which is scattered and couples back into the mode
τ^2	fraction of light intensity which is not scattered
t_i	transmission coefficient through region L_i
t	transmission coefficient across total cavity with no scattering centre
g_i	gain of E-field across region L_i
g	gain of E-field across total cavity
$ \delta^\pm ^2$	flux of spontaneous emission in the (+) and (-) y directions
k	$2\pi/\lambda$ λ - wavelength of light
$2\phi_i$	phase factor of complex variable r_i
R	$ r ^2$ - reflectance of laser facets
R_i	$ r_i ^2$ - effective reflectance of laser facets
G	$ g ^2$ - single pass gain through device with no scattering centre
G_i	$ g_i ^2$ - single pass gain through region L_i
$\langle I \rangle$	time averaged light intensity
β	spontaneous emission factor
β_{opt}	collection efficiency of optical system
Γ	gain profile of laser
B	spontaneous emission profile of laser
ρ	degree of polarization
P_1, P_2	intensities of two measured orthogonal polarizations
X_m	variable X evaluated at the centre frequency of the mode m

direction at the right facet (a_2) is the amplitude of the electric field from the left facet which propagates in the same direction (a_1) multiplied by the propagation coefficients (t_1 and t_2 which include phase information and gain or attenuation), and by the transmission coefficient through the scattering centre (τ), plus the amount of the electric field from the right facet which propagates in the negative y direction and is scattered back into the mode (σb_2) multiplied by the propagation coefficient through the cavity L_2 (t_2), plus the spontaneous emission which propagates in the positive y direction and couples into the mode (δ^+). The electric field which

propagates in the negative y direction at the left facet can be derived in the same way, and therefore

$$\begin{aligned} a_2 &= a_1 t_1 \tau t_2 + b_2 t_2^2 \sigma + \delta^+ , \\ b_1 &= b_2 t_2 \tau t_1 + a_1 t_1^2 \sigma + \delta^- . \end{aligned} \quad (4.1)$$

The right and left propagating electric fields at each facet are related directly through the reflection coefficient r at the facets, i.e.,

$$a_1 = r b_1 , \quad b_2 = r a_2 . \quad (4.2)$$

To calculate the amplitude of the electric field at the left hand facet and hence the output of the laser, the amplitude of the electric field b_1 is determined by solving equations (4.1) and (4.2), so that

$$b_1 = \frac{\frac{r t_1 t_2 \tau \delta^+}{(1 - r t_1^2 \sigma)(1 - r t_2^2 \sigma)} + \frac{\delta^-}{(1 - r t_1^2 \sigma)}}{1 - \frac{r^2 t_1^2 t_2^2 \tau^2}{(1 - r t_1^2 \sigma)(1 - r t_2^2 \sigma)}} . \quad (4.3)$$

Equation (4.3) can be simplified by defining effective reflectivities

$$r_1 = \frac{r \tau}{1 - r t_1^2 \sigma} , \quad r_2 = \frac{r \tau}{1 - r t_2^2 \sigma} . \quad (4.4)$$

Once effective reflectivities are substituted into equation (4.3), the result appears to be similar to that for a simple Fabry Perot laser. The simplified expression for b_1 is

$$b_1 = \frac{(r_2 t_1 t_2 \delta^+ + \delta^-)/(1 - r_1^2 \sigma)}{1 - r_1 r_2 t_1^2 t_2^2} \quad (4.5)$$

The effective reflectivities r_1 and r_2 incorporate the effects of the scattering centre located a distance L_1 and L_2 from the facets. Optical frequencies which are resonant with any of the cavities of length L , L_1 and L_2 will be enhanced while optical frequencies antiresonant with any of the cavities will be suppressed.

To solve for the intensity of the light field, explicit expressions for the phase and gain of the propagation coefficients and for the effective reflectivities are required. In terms of the single pass gains g_1 and g_2 in the cavities of length L_1 and L_2 and the phases ϕ_1 and ϕ_2 of the effective reflectivities

$$t_1 = g_1 \exp(ikL_1), \quad t_2 = g_2 \exp(ikL_2), \quad (4.6)$$

$$r_1 = |r_1| \exp(2i\phi_1), \quad r_2 = |r_2| \exp(2i\phi_2). \quad (4.7)$$

These expressions are used in equation (4.5) to calculate the time averaged light intensity. A convention is adopted to simplify the notation such that an upper case variable equals the magnitude squared of a lower case variable. Thus $R = |r|^2$, $G_1 = |g_1|^2$ and therefore

$$\langle I \rangle = \langle b_1^* b_1 \rangle = \frac{(|\delta|^2)(1 + R_2 G) / [1 - 2\sqrt{R G_1} \sigma \cos(2kL_1) + R G_1^2 \sigma^2]}{(1 - \sqrt{R_1 R_2} G)^2 + 4\sqrt{R_1 R_2} G \sin^2(kL + \phi_1 + \phi_2)} \quad (4.8)$$

This formula (Equation 4.8) gives the time averaged light intensity $\langle I \rangle$ at the left facet of the device as a function of optical frequency. The effects of the

scattering centre are incorporated into the variables R_1 and R_2 . To derive equation (4.8) spontaneous emission travelling in the positive and negative y directions (δ^- and δ^+) was assumed to be uncorrelated in time and thus $\langle |\delta^+ \delta^-| \rangle = 0$. Also, the spontaneous emission was assumed to be isotropic, so that $\langle |\delta^+|^2 \rangle = \langle |\delta^-|^2 \rangle = \langle |\delta|^2 \rangle$.

The power in each longitudinal mode of the laser is calculated by integrating $\langle I \rangle$ over one free spectral range of the total laser cavity (length L). [32] Because the intensity profile of the mode for above threshold operation approaches a delta function, the factors ϕ_1 and ϕ_2 which are small ($\sim \sigma$), become negligible in the integration, and the variables R_1 , R_2 and $\cos(2kL_1)$ are treated as constants evaluated at the centre of the mode. The intensity of the m th mode is therefore

$$I_m = \frac{\langle |\delta|^2 \rangle (1 + R_{2m} G_m) / [1 - 2\sqrt{R} G_{1m} \sigma \cos(2k_m L_1) + R G_{1m}^2 \sigma^2]}{1 - R_{1m} R_{2m} G_m^2} \quad (4.9)$$

This is the desired result. This equation predicts the intensity of each mode for scattering centres of different strengths (different values of σ), and for different locations (L_1 , L_2) in the laser cavity. These predictions can be compared with the measured spectra of existing devices. The subscript m for variables on the right hand side means that the quantity is evaluated at the centre frequency of the m^{th} mode. In equation (4.9) the denominator is the critical part in the formation of the mode structure. As long as a scattering centre exists $\sigma \neq 0$, and R_{1m} and R_{2m} are functions of the wavelength of the mode:

$$R_{1m} = \frac{R\tau^2}{1 - 2\sqrt{R}G_{1m}\sigma\cos(2k_m L_1) + RG_{1m}^2\sigma^2},$$

$$R_{2m} = \frac{R\tau^2}{1 - 2\sqrt{R}G_{2m}\sigma\cos(2k_m L_2) + RG_{2m}^2\sigma^2}.$$
(4.10)

Depending on whether the Fabry Perot cavities formed by the scattering centre and the laser facets are resonant or antiresonant, R_1 and R_2 may be greater than or less than the reflectance of the facets. Due to the resonant nature of the denominator of equation (4.9), $R_{1m}R_{2m}G_m^2 \leq 1$, and R_1 and R_2 can exert a large influence on the intensity of the mode and greatly enhance or suppress the intensity of any mode. Thus asymmetric, single mode moded spectra, and spectra with highly modulated mode envelopes can be modelled.

If more than one scattering centre is present then the mode pattern may be very complicated. There will be more than two weak Fabry Perot cavities which will affect the spectral output. Even though lasers rarely have only one scattering centre, modelling the laser with one scattering centre is sufficient to illustrate the effect that scattering centres have on the spectral output. A model which allows for multiple scattering is presented in Chapter 6.

If there is no scattering centre ($\sigma = 0$) then the effective reflectances have no wavelength dependence and are equal to the reflectances of the facets

$$R_1 = R_2 = R.$$

The mode intensities will be given by

$$I_m = \frac{\langle |\delta_m|^2 \rangle}{1 - RG_m}, \quad (4.11)$$

which is the result calculated using a Fabry Perot model and no scattering centre.[32,33] The mode intensities in equation (4.9) can be solved for since

$$\langle |\delta_m|^2 \rangle = \beta(B_m/\Gamma_m)(G_m - 1), \quad (4.12)$$

expressions for G_m are known, and values for B_m, Γ_m and β can be assumed.[33] When no scattering centre is present the product of the single pass gains $G_{1m}G_{2m} = G_m$. This relationship is also assumed to hold when a scattering centre is present. Thus $G_{1m} = G_m^{(L_1/L)}$ and $G_{2m} = G_m^{(L_2/L)}$ as this allows straight forward calculation of G_{1m} and G_{2m} .

4.3 Results

In this section an attempt is made to predict and explain the experimentally measured spectral outputs of both index guided and gain guided lasers. Both lasers types are modelled using the same gain and spontaneous emission profiles (Γ_m and B_m from [33]) and a spontaneous emission factor (β) of 0.005. The spontaneous emission factor (β) is a geometrical factor which gives the probability of emission of spontaneous light into a range of directions which constitute a longitudinal mode of the laser. β is a function of the waveguide dimensions,

materials, and the guiding mechanism.[31,35,36] For InGaAsP diode lasers, the dependence of β on the guiding mechanism is predicted and found to be small (≤ 2) [35,36,37], and thus the spontaneous emission factor for InGaAsP gain guided lasers is expected to be approximately double that for index guided devices whose active region dimensions are the same size as for the gain guide devices.[37] Changing β by a factor of two results in little change in the theoretical longitudinal mode spectrum.

To explain the experimental results, both gain guided and index guided lasers are modelled with the same value of β , since the results of Chapter 3 suggest that the effect of the scattering dominates the spectral output and the precise value of the enhancement factor is not known. Different lasers produce varying amounts of spontaneous emission, but all devices were modelled as producing the same amount of spontaneous emission so that the effective scattering would be related to the fraction of scattered light by the same amount for all lasers modelled (see Eq. 4.16) and so the correlation between the effective scattering and the spectral properties described in Chapter 3.4 can be tested. Thus the only variables adjusted to distinguish between gain guided and index guided devices are those which describe the scattering centre (τ and σ). To model a gain guided laser no scattering centre is used ($\sigma = 0$), while to model an index guided laser $\sigma \neq 0$.

The relationship between τ and σ is dependent on the type of scattering assumed in the device. If Rayleigh scattering is assumed, and if the fraction of light intensity scattered is $(1-\tau)^2$, then the fraction of light intensity which scatters back

into the mode is

$$\sigma^2 = \frac{3}{2}\beta(1 - \tau)^2 \quad (4.13)$$

The predicted spectral output was found to be very sensitive to changes in σ . Because the magnitude of σ can be estimated experimentally, σ is considered to be the independent variable in the analysis.

To model a gain guided device the strength of the scattering centre σ is set to zero. This is consistent with the experimentally measured effective scattering. Solving equation (4.9) for this case yields the theoretical longitudinal mode spectrum shown in Fig. 4.2. This is similar to that from a gain guided device as can be seen from the measured longitudinal mode spectrum in Fig. 4.3. This experimental spectrum is typical for gain guided lasers.

To model an index guided device a scattering centre is used. Experimental data is used to estimate the magnitude of σ . Figure 4.4 shows the measured degree of polarization profile along the length of the active region of a planar buried heterostructure (PBH) laser, taken by spatially resolved and polarization resolved electroluminescence (EL). The device has one scattering centre and was operated at about 2 mW output power. If P_1 and P_2 are the intensities of the two orthogonal polarizations of the EL signal and P_1 is the same polarization as the stimulated emission in the laser, then away from the scattering centre the degree of polarization ρ equals

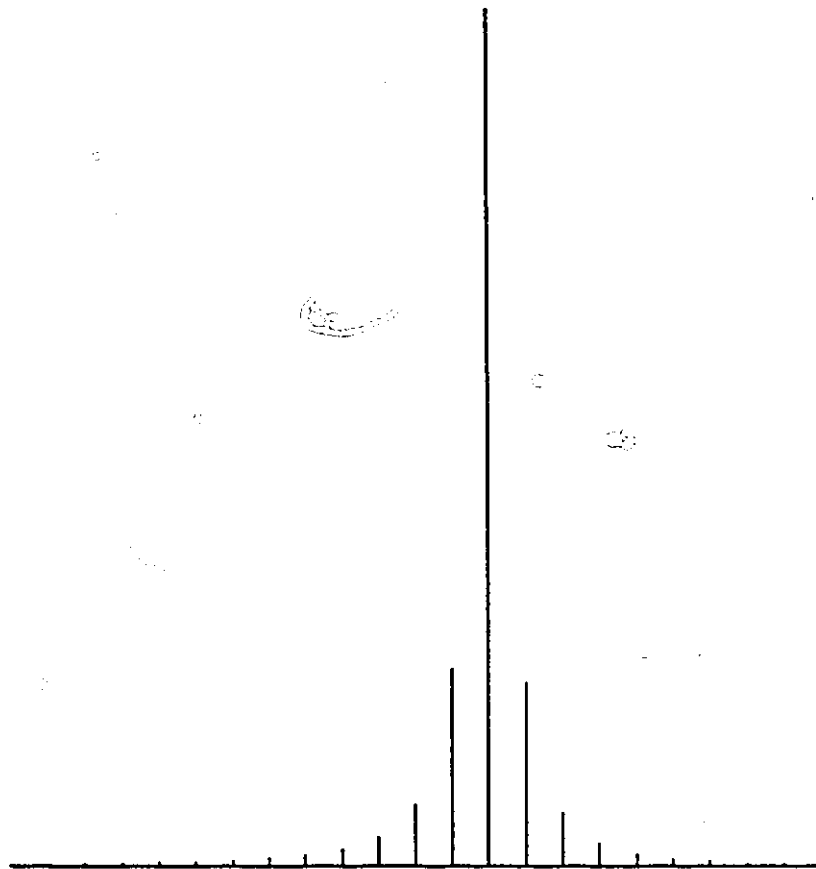


Fig. 4.2 Calculated longitudinal mode spectrum of a gain guided laser assuming no scattering centre exists ($\sigma = 0$).

$$\rho = \frac{P1 - P2}{P1 + P2} \approx \frac{P1 - P2}{2P2}, \quad (4.14)$$

because $P1 \approx P2$. At the scattering centre

$$\rho = \frac{(P1 + S\Sigma I_m) - P2}{(P1 + S\Sigma I_m) + P2} \approx \frac{(P1 + S\Sigma I_m) - P2}{2P2}, \quad (4.15)$$

where S is the fraction of stimulated light which scatters and reaches the detector,

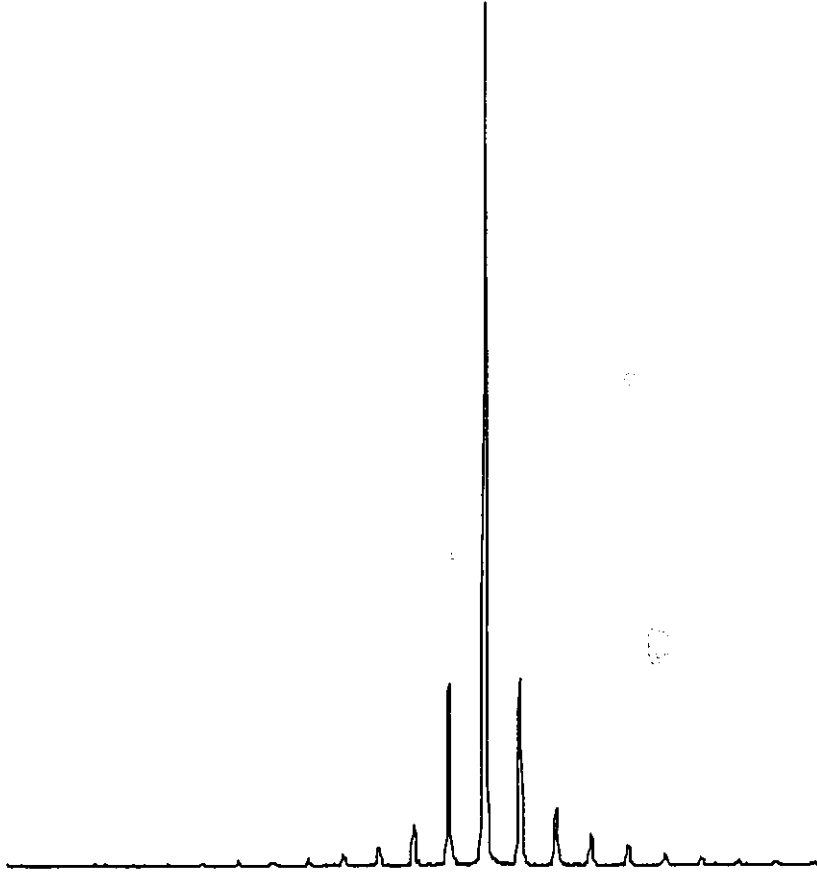


Fig. 4.3 Measured longitudinal mode spectrum of a gain guided laser. The vertical scale is in units of intensity and the horizontal scale is in units of wavelength. Note the similarity between Figs. 4.2 and 4.3.

ΣI_m is the total amount of stimulated light inside the cavity and $S\Sigma I_m \ll P_1$.

Therefore the change in the degree of polarization due to the scattering centre is

$$\Delta\rho = S\Sigma I_m/2P_2 . \quad (4.16)$$

The effective scattering $\Delta\rho$ is proportional to the output power (ΣI_m) and is the ratio the fraction of scattered light S and P_2 which is proportional to the amount of spontaneous emission produced.

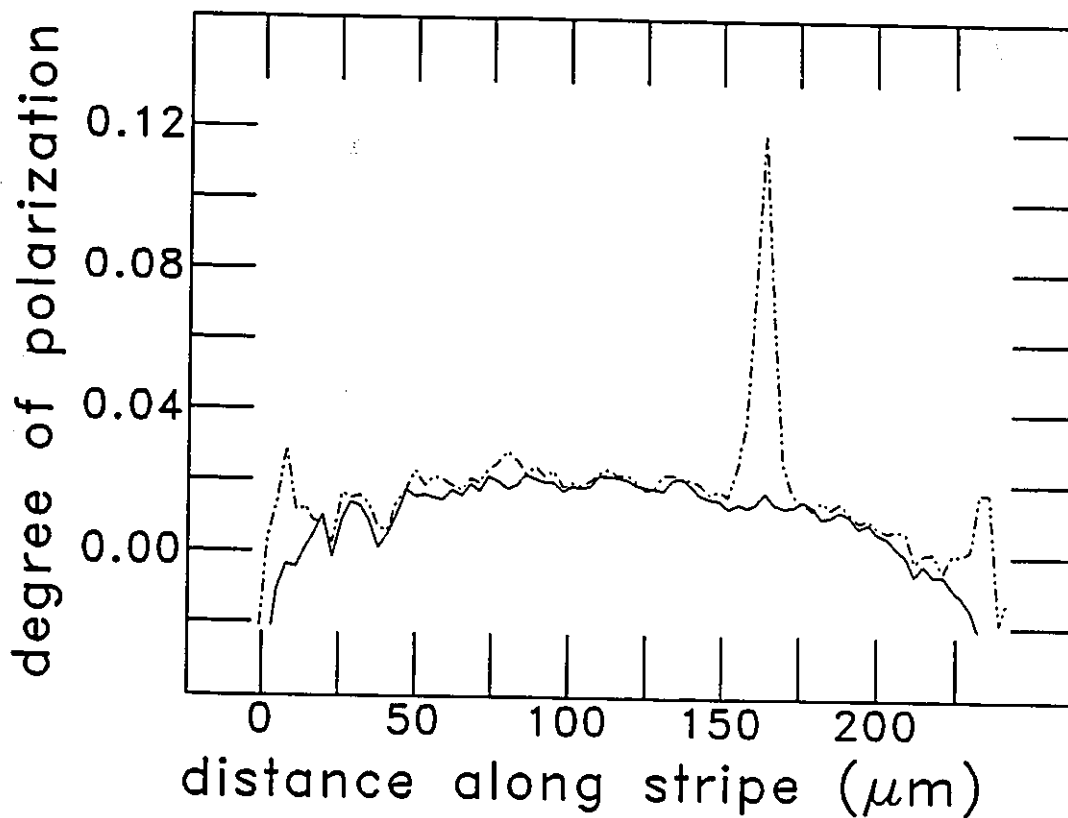


Fig. 4.4 Degree of polarization (ρ) distribution along the active region of a planar buried heterostructure (PBH) laser operating below (broken line) and above (solid line) threshold.

If β_{opt} is the collection efficiency of the optical system, then the amount of stimulated emission which scatters back into the mode (σ^2) can be calculated as

$$\sigma^2 = \frac{\beta S}{\beta_{opt}} \approx \frac{\beta}{\beta_{opt}} \frac{2\Delta\rho P_2}{\sum I_m} \quad (4.17)$$

This equation is derived assuming small angles, such that the scattering intensity can be considered constant across the solid angles β and β_{opt} . Since β is used as a fitting parameter it is set to 0.005 and β_{opt} is measured to be ≈ 0.0002 , thus the

small angle approximation is valid, and the magnitude of σ can be estimated directly from the measurement of ρ . From the raw data of Fig. 4.4 the value of P1 was measured to be about 1 nW at an output power of 2 mW and the value of $\Delta\rho$ is approximately 0.1. Thus, the magnitude of $\sigma^2 \approx 2 \cdot 10^{-6}$ ($\sigma \approx 0.0015$), which means that about two parts in a million of the power of the stimulated emission is scattered back into the mode.

Figure 4.5 is a plot of the spectral output calculated using the model

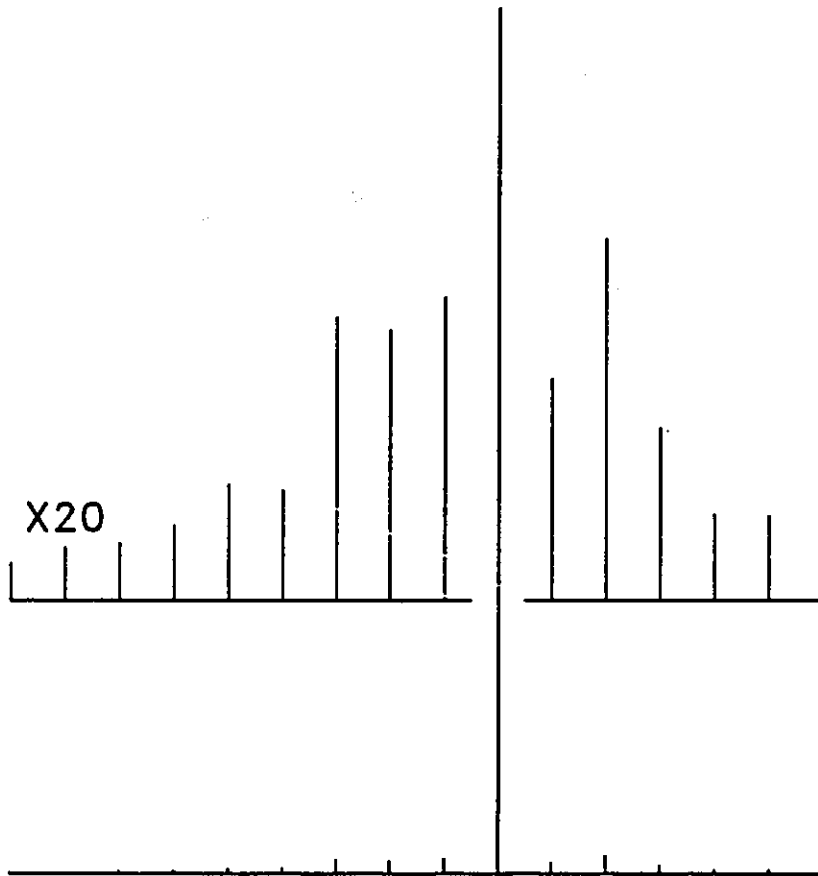


Fig. 4.5 Calculated longitudinal mode spectrum of the PBH laser from Figs. 4 and 6. The scattering parameters $\sigma = 0.0015$, $L_1 = 153\mu\text{m}$ and $L_2 = 97\mu\text{m}$ are calculated using the data from Fig. 4.4.

presented. The scattering parameter $\sigma = 0.0015$ was calculated from the data shown in Fig. 4.4. The parameters $L_1 = 153\mu\text{m}$ and $L_2 = 97\mu\text{m}$ were also taken from Fig. 4.4 and adjusted within the range of experimental uncertainty to fit the measured spectrum. Note that the measured spectral output (Fig. 4.6) of the laser of Fig. 4.4

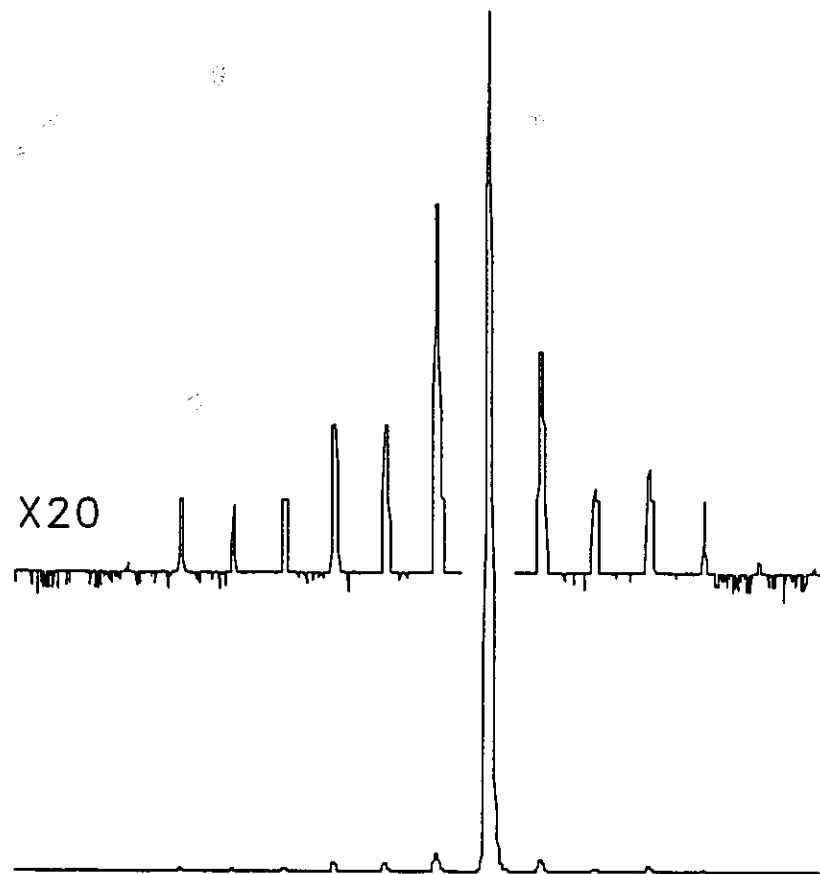


Fig. 4.6 Measured longitudinal mode spectrum of the PBH laser of Fig 4.4.

is much more single moded than the measured spectral output of the gain guided structure (Fig. 4.3), and that this is predicted by the theoretical calculations (Figs. 4.2 and 4.5).

A close inspection of both the measured and theoretical spectral outputs

of the index guided laser reveals a modulation of the mode intensities; the envelope of the side modes is not a smooth curve but is modulated with respect to the mode number. The presence of such modulation in the measured longitudinal mode spectrum supports the concept of scattering centres causing the index guided devices to run more single moded than a device without a scattering centre.

The theoretical longitudinal mode spectra is strongly dependent on the location and strength of the scattering centres. By adjusting the parameters σ , L_1 and L_2 and the location in frequency space of the gain profile, many interesting mode profiles can be predicted. For example, Fig. 4.7. shows the measured longitudinal mode spectrum of a PBH laser which exhibits a large modulation of the mode envelope. A scattering centre placed $86 \mu\text{m}$ from one facet with a strength of $\sigma = 0.0005$ results in a calculated spectrum (Fig. 4.8.) which is similar to the measured spectrum. It should be noted that this value of σ is one third the value estimated from the results shown in Fig. 4.4, and is still sufficiently large to predict multilongitudinal moded operation with a large modulation of the mode envelope.

The model is capable of explaining how a diode laser may operate single moded at one temperature and current and operate multilongitudinal moded with highly modulated mode envelopes at another temperature and current. The spectra of a laser (Laser G) which shows this tendency was shown in Fig. 3.6 (c) and (d). By using a scattering parameter of $\sigma = 0.0005$, which is consistent with the measured scattering of the laser, the lasers spectral properties are modelled as shown in Fig. 4.9. A temperature difference which causes a shift of the location of the peak

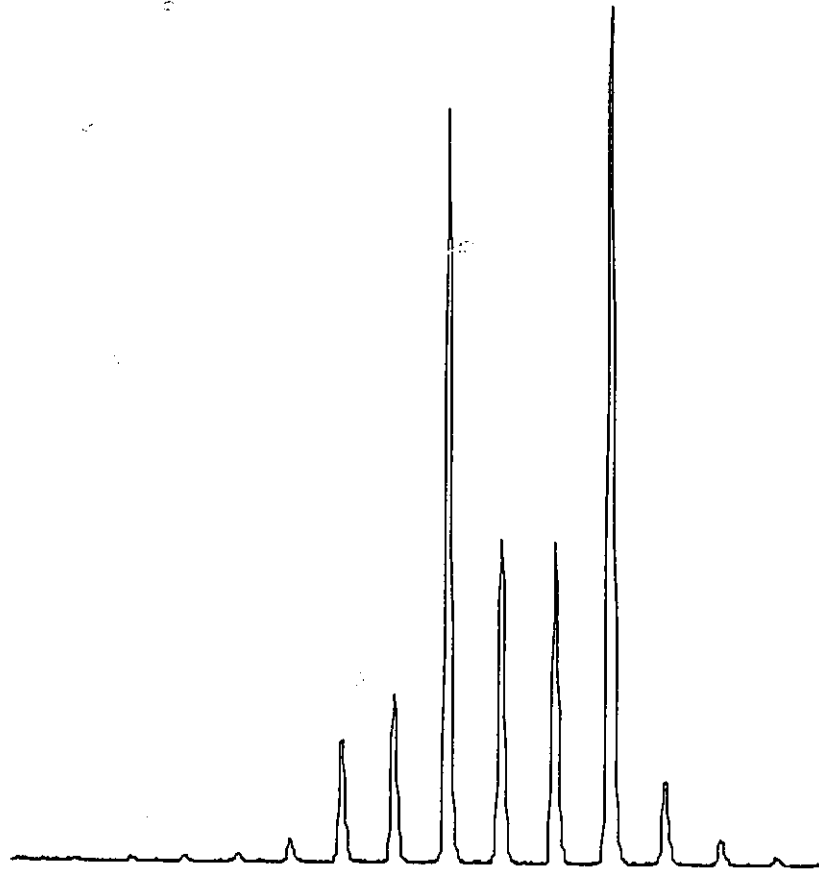


Fig. 4.7 Measured longitudinal mode spectrum of a PBH laser exhibiting a large modulation of the mode envelope.

of the gain profile was allowed for between the calculations of the spectra shown in Fig. 4.9 (a) and (b). One can see that there is good agreement between the experimental spectra of Fig. 3.6 (c) and (d) and the theoretical spectra of Fig. 4.9.

Thus the presence of even small scattering centres can cause the suppression of one or more longitudinal modes, and can be used to explain why index guided lasers tend to operate more single moded than gain guided lasers, and may operate multilongitudinal moded with highly modulated mode envelopes. The

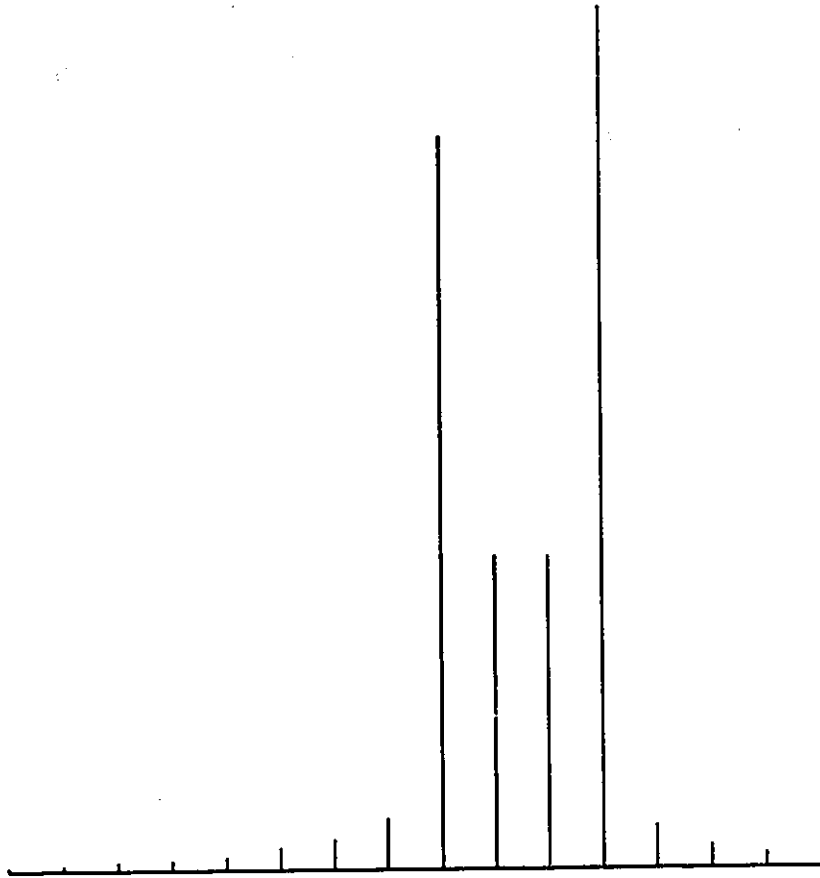


Fig. 4.8 Calculated longitudinal mode spectrum of a PBH laser using the scattering parameters $\sigma = 0.0005$, $L_1 = 164\mu\text{m}$ and $L_2 = 86\mu\text{m}$. Note the similarity between Figs. 4.7 and 4.8.

presence of scattering centres in a laser also explains how a laser can operate single moded at one set of operating conditions (temperature and current) and operate multilongitudinal moded with highly modulated mode envelopes at another set of operating conditions.

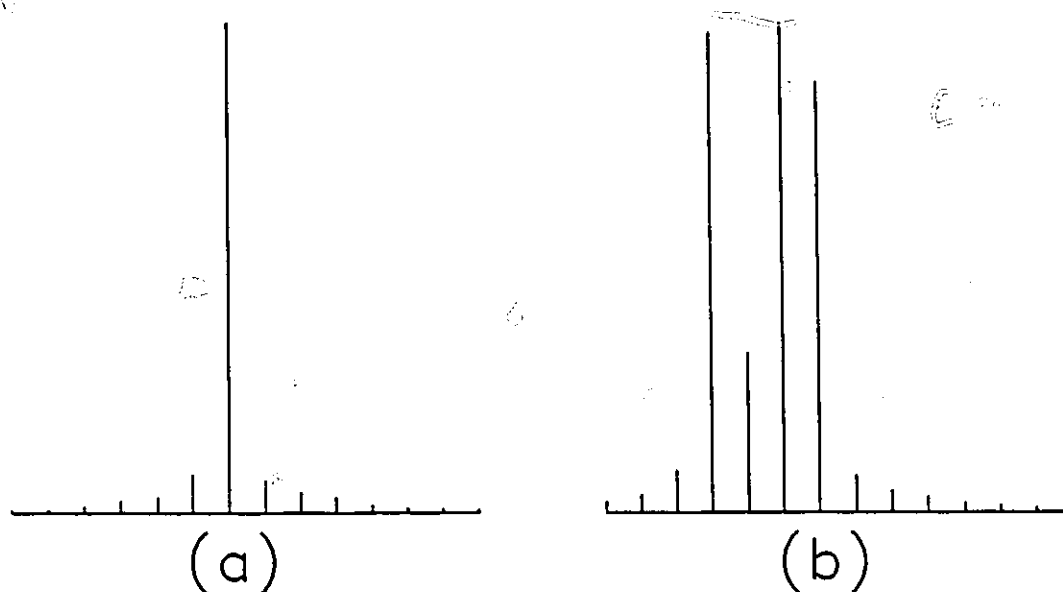


Fig. 4.9 Calculated longitudinal mode spectra of a PBH laser at two different temperatures, using the scattering parameters $\sigma = 0.0005$, $L_1 = 79\mu\text{m}$ and $L_2 = 171\mu\text{m}$.

4.4 Summary

There is great variety in the measured longitudinal mode spectra of semiconductor diode lasers. The lasers may operate single moded or multilongitudinal moded with smooth mode envelopes, may have asymmetric mode spectra and may operate multilongitudinal moded with highly modulated mode envelopes. Based on an analysis of spatially resolved and polarization resolved electroluminescence (EL) of semiconductor diode lasers, it is suggested that when predicting longitudinal mode spectra it is necessary to consider the effects of scattering of stimulated emission in or near the active region of the device.

In support of this hypothesis a laser model has been developed which includes the effect of one scattering centre in the device. By adjusting the amount of light which scatters and the position of the scattering centre in the device, the longitudinal mode spectra of both gain guided and index guided devices can be explained.

The theoretical model assumes that the astigmatism factor, and the gain profile of both gain guided devices and index guided devices are identical. These are reasonable assumptions for InGaAsP diode laser since the dependence of β on the guiding mechanism is weak for InGaAsP lasers [35,36,37], and for InGaAsP lasers emitting at the same wavelength the band structure will be the similar. If no scattering centre exists in a device, then the theoretical mode spectrum is multilongitudinal moded with smooth mode envelopes, which is typical of gain guided devices.

When a scattering centre is present some lasing modes will be enhanced and others suppressed, depending on the resonant conditions caused by the scattering inside the device. If the gain profile is centred near one of the preferred modes enhanced by the scattering centre, then the predicted mode spectrum tends to be much more single moded or multilongitudinal moded with highly modulated mode envelopes than the results obtained without a scattering centre. This spectrum is typical of index guided devices.

By adjusting the location of the gain profile in frequency space away from the resonant modes of the scattering centre, the theoretical mode spectrum may be

asymmetric or multilongitudinal moded with highly modulated mode envelopes. This provides an explanation for such behaviour, and explains how devices can operate both single moded and multilongitudinal moded with highly modulated mode envelopes at different operating conditions. Thus it is concluded that to explain the spectral properties of semiconductor diode lasers, internal scattering must be considered. In this chapter lasers were modelled using the effective scattering parameter by assuming they produced the same amount of spontaneous emission. In the next chapter the effect of spontaneous emission and the effect of the fraction of light that scatters inside the device will be considered.

Chapter 5 Spontaneous Emission and Scattering

5.1 Introduction

In Chapter 3 a correlation was shown to exist between the effective scattering and the spectral properties of semiconductor diode lasers. The effective scattering, which is the change in the degree of polarization ($\Delta\rho = \rho_a - \rho_b$, where ρ_a is the distribution of ρ above threshold and ρ_b is the distribution of ρ below threshold) with output power of the laser, was shown in Chapter 4 to depend on both the internal scattering and the amount of spontaneous emission produced by the device. In this Chapter the effects of both the spontaneous emission and the internal scattering are discussed. It is shown that spontaneous emission masks the effect of internal scattering on the spectral output of lasers. Lasers which produce a large amount of spontaneous emission are not as affected by scattering as lasers which produce a small amount of spontaneous emission.

The measurement techniques for both the spontaneous emission and the internal scattering are presented in this chapter. It is shown that the magnitude of the scattering can be obtained from the slope of a line plotted from experimentally measured values. Section 5.2 demonstrates the effect of both the spontaneous emission and the internal scattering on the spectral properties of diode lasers, Section 5.3 shows the experimental method of measuring the internal scattering and shows experimental evidence in support of the theory of Section 5.2, and Section 5.4 is a

summary.

5.2 Spontaneous Emission

Figure 5.1 is a plot of the amount of spontaneous emission detected through the substrate for 1.3 μm InGaAsP index guided and gain guided devices as a function of the threshold current. Figure 5.1 helps to demonstrate that the amount of spontaneous light produced increases with increasing threshold. Note that the gain guided devices (lower case in graph) exhibit much higher threshold currents than the index guided devices (upper case and numbers in graph) and also produce 5-10 times as much spontaneous emission. The data for Fig. 5.1 were obtained with the instrument described in Chapter 2. The data was created by averaging P2 light (see Fig. 2.3) over the central section of the laser and normalizing to obtain an amount per unit length. P2 light was used because no single scattering event can couple TE light into this polarization[38] and hence a measure of P2 light should be an accurate measure of the spontaneous light produced since all the lasers tested lased TE. The lasers were biased at about 0.5 mW above threshold to obtain the data for Fig. 5.1. Figure 5.2 shows the saturation of the P2 light for a gain guided and an index guided device as a function of current. From the data of Fig. 5.2 one can conclude that the correlation presented in Fig. 5.1 does not depend strongly on pumping, provided that the pumping level is greater than the threshold current of the device.

Note that it is the amount of spontaneous emission which couples into the modes that is important and not just the fraction. To appreciate the distinction,

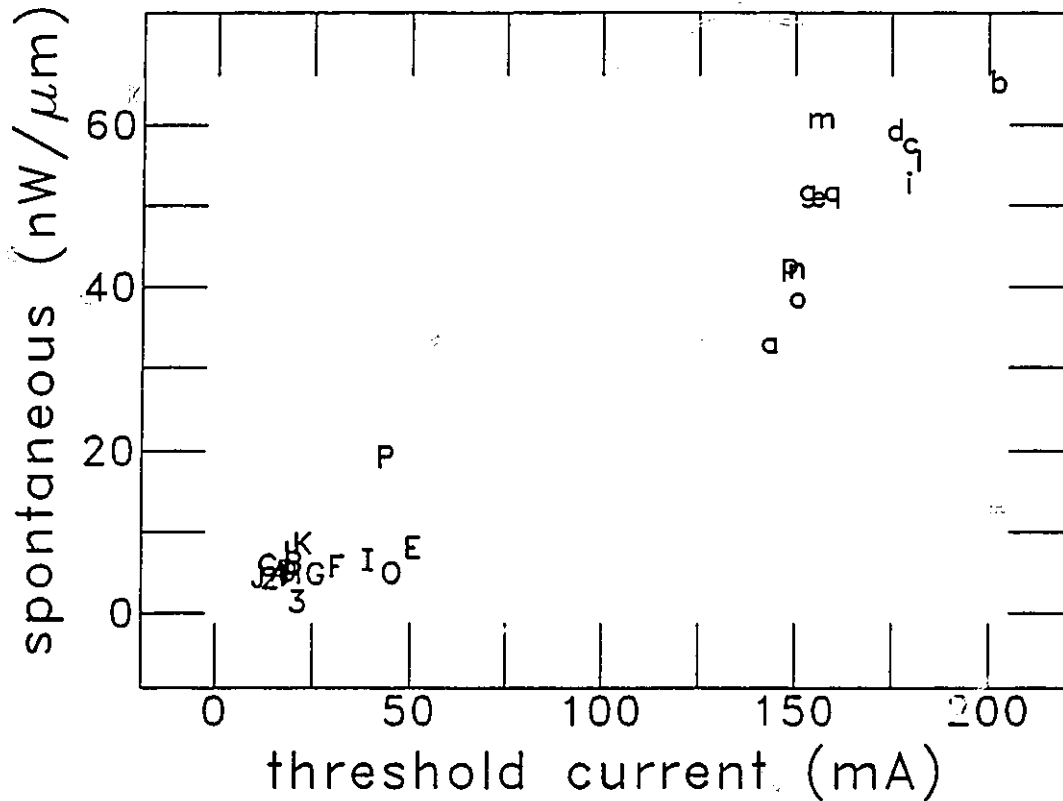


Fig. 5.1 Spontaneous emission at threshold vs. threshold current for arrowhead buried crescent (numbers), planar buried heterostructure (upper case), and gain guided (lower case) lasers.

consider the spectral output of a diode laser before and after anti-reflection (AR) coating of the facets. Experimentally, it is found that lasers run more multilongitudinal moded after AR coating.[39,40] AR coating the facets of diode lasers increases the inversion required to achieve lasing and hence increases the amount of spontaneous emission. Although the same fraction of the spontaneous emission may couple into the modes, the amount of spontaneous emission in the modes is increased, and the lasers run more multilongitudinal moded.[41,42] A similar argument can be made for lasers with differing amounts of absorption.[43]

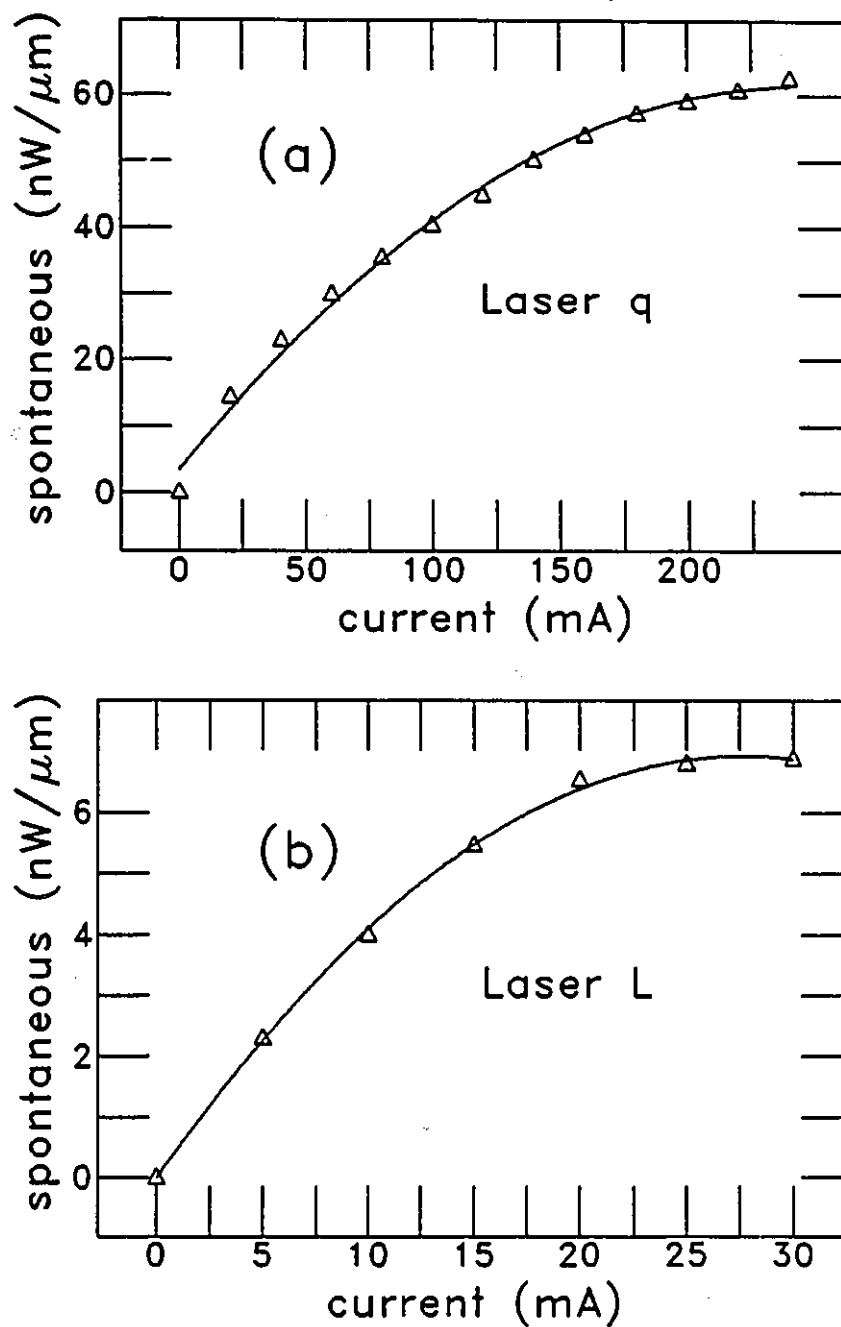


Fig. 5.2 Spontaneous emission vs. current for (a) a gain guided laser with a threshold current of 160 mA, and (b) a PBH laser with a threshold current of 20 mA.

Lasers with the larger threshold should run more multilongitudinal moded because of the increased amount of spontaneous emission produced and hence coupled into the modes.

The fraction of spontaneous emission which couples into a mode depends upon the probability $\beta = \beta_g \beta_s$ where β_g is a geometric spontaneous emission factor which represents the probability that the spontaneous emission is captured by the mode, and β_s is a spectral spontaneous emission factor which represents the probability that the spontaneous emission has the correct polarization and an energy lying in the interval defined by the mode.[37] It is expected that β_g is approximately the same for the lasers shown in Fig. 5.1 since the far fields subtend approximately the same solid angle.[31,35,36,37] It is expected that β_s is similar for all the lasers since the band structure of the active regions are nominally the same. Thus the amount of spontaneous emission which couples into the modes should follow the trend shown in Fig. 5.1 and hence lasers with larger thresholds should run more multilongitudinal moded than lasers with smaller thresholds. Since a large amount of spontaneous emission will reduce the value of the effective scattering, (as described in Chapter 3) the spectral output of lasers with larger thresholds (and thus large amounts of spontaneous emission) should be less affected by internal scattering than lasers with smaller thresholds. To appreciate this characteristic consider the side mode suppression ratio (SMSR) I_m/I_{m+1} where I_m is the power in the m^{th} mode and I_{m+1} is the power in an adjacent mode. In Chapter 4 the power I_m in the m^{th} mode for a laser with one scattering centre was shown to be:

$$I_m = \frac{c_m(G_m - 1)(1 + R_{2m}G_m)/[1 - 2\sqrt{R}G_{1m}\sigma \cos(2k_m L_1) + RG_{1m}^2\sigma^2]}{1 - R_{1m}R_{2m}G_m^2} \quad (5.1)$$

$$\text{where } R_{im} = \frac{R\tau^2}{1 - 2\sqrt{R}G_{im}\sigma \cos(2k_m L_i) + RG_{im}^2\sigma^2}, \quad i = 1, 2,$$

and $\langle |\delta| \rangle^2$ from Eq. 4.9 has been replaced by $c_m(G_m - 1)$ which is the amount of spontaneous emission which couples into the m^{th} mode.[33,42,43] The frequency dependant terms in the effective reflectances R_{im} have the same phase relationship for a given mode, that is

$$\cos(2k_m L_1) = \cos(2k_m L_2) \quad (5.2)$$

Using this fact Eq. 5.1 can be simplified by noting that for small values of scattering ($\sigma \ll 1$) $R_{1m} \approx R_{2m}$, so that

$$I_m \approx \frac{c_m(G_m - 1)}{1 - R_m G_m} \quad (5.3)$$

Then the SMSR is

$$\frac{I_m}{I_{m+1}} = \frac{1 - R_{m+1}G_{m+1}}{1 - R_m G_m} \quad (5.4)$$

if one ignores the small variations (<10%) in the amount of spontaneous emission which couples into the adjacent modes. Equation 5.4 can be manipulated to yield

$$\frac{I_m}{I_{m+1}} = 1 + \frac{I_m(1 - G_{m+1}/G_m)}{c_m(G_m - 1)} + \frac{I_m G_{m+1}(R_m - R_{m+1})}{c_m(G_m - 1)}, \quad (5.5)$$

since above threshold $1 - R_m G_m \approx 1$. For $\sigma \ll 1$ the factor R_m changes to first order in σ linearly with the fraction of the electric field scattered (c.f. Eq. 5.1). Also by using the definition of G_m from Ref. 33, one finds

$$\frac{I_m}{I_{m+1}} = 1 + \frac{I_m(1 - R^{(1-g_m/lg_m)} + F(g)\sigma)}{c_m(G_m - 1)}, \quad (5.6)$$

where g_m is the gain coefficient per unit length and is characteristic of the laser material, and $F(g)$ is a constant of the laser which depends on the laser material and the location of the scattering centre. Equation 5.6 shows that the SMSR scales inversely with the amount of spontaneous emission which is coupled into the modes. Also, devices with large amounts of spontaneous emission should be less sensitive to internal scattering than devices with small amounts of spontaneous emission.

Figure 5.3 is composed of plots of the side mode suppression ratio (SMSR) as a function of c^{-1} for different values of scattering (σ) for the same output powers. The plots were made by calculating the side mode suppression ratio using the model described in Chapter 4 for a laser with one scattering centre located $L_1/(L_1 + L_2) = 0.25$ from one facet and with the gain profile centred over a mode receiving constructive interference from the scattering centre. The plots are straight lines which confirms the inverse relationship between the side mode suppression ratio and the amount of spontaneous emission as derived in Eq. 5.6. They also show that the effect of scattering on the spectral output is masked by spontaneous emission. The SMSR for a laser with a large amount of spontaneous emission (small c^{-1}) and

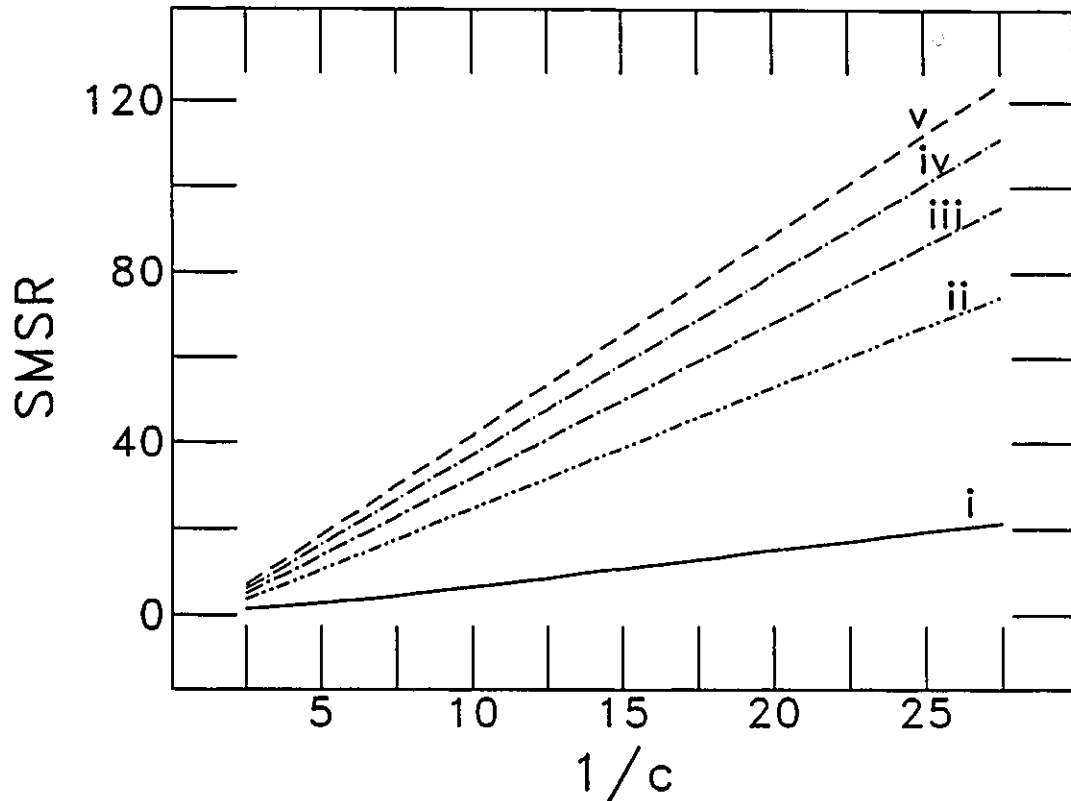


Fig. 5.3 Side mode suppression ratio vs. one over spontaneous emission for various values of scattering: i) $\sigma = 0$, ii) $\sigma = 0.0224$, iii) $\sigma = 0.0316$, iv) $\sigma = 0.0387$, v) $\sigma = 0.0447$.

scattering ($\sigma \neq 0$) is not much different than the SMSR for no scattering ($\sigma = 0$), whereas the SMSR for a laser with a small amount of spontaneous emission (large c^{-1}) is a strong function of σ .

When scattering exists it is evident from Eq. 5.6 that the side mode suppression ratio should change linearly with σ/c . The data used to generate Fig. 5.3 can be used to demonstrate the linear relationship between the SMSR and σ/c . Figure 5.4 shows a graph of the side mode suppression ratio as a function of σ for

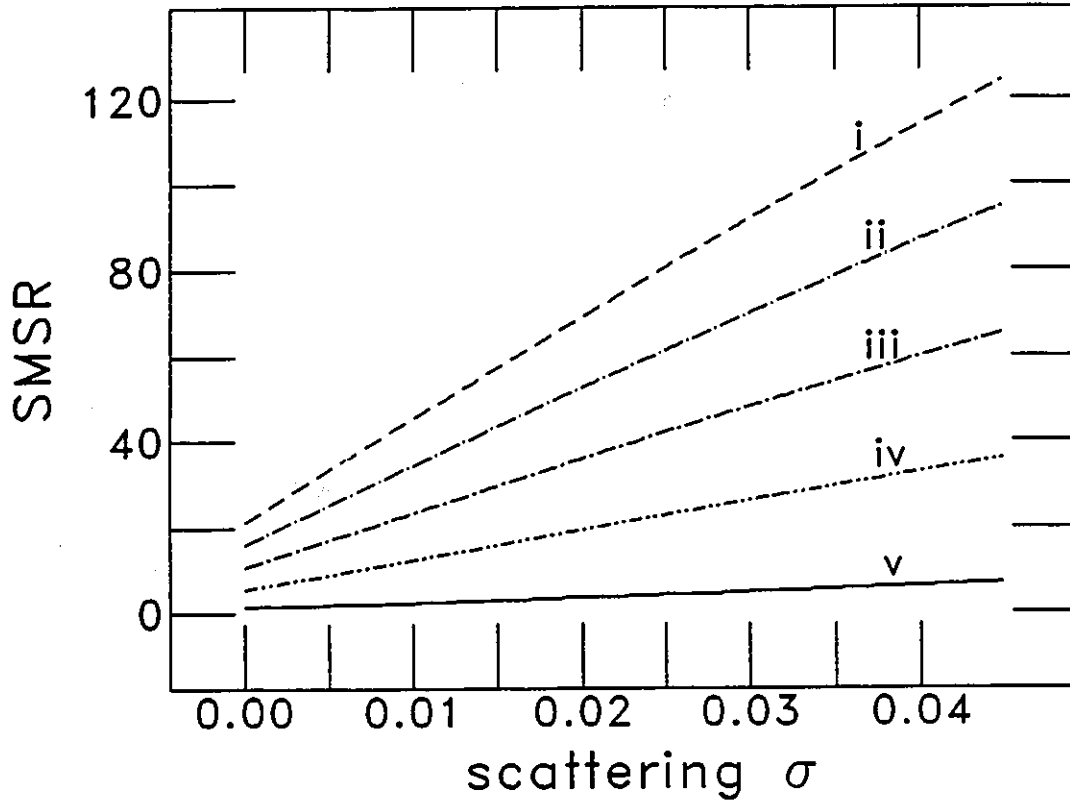


Fig. 5.4 Side mode suppression ratio vs. the scattering parameter σ for various values of above threshold spontaneous emission: i) $c=0.036$, ii) $c=0.047$, iii) $c=0.067$, iv) $c=0.114$, v) $c=0.400$.

various values of c . The values of c were chosen to be evenly spaced in c^{-1} so that the linear nature of the dependence on c^{-1} is evident. The data of Figs. 5.3 and 5.4 indicate that the quantity σ/c is a valid measure of the effect of scattering on the spectral properties of diode lasers and takes into account the masking effect of spontaneous emission.

5.3 Experimental Method

The scattering properties of 1.3 μm InGaAsP semiconductor diode lasers were determined using the data obtained from spatially resolved and polarization resolved electroluminescence (EL) measurements as described in Chapter 2. The fraction of light which is scattered back into the lasing mode as a function of position along the active region is given by Eq. 4.17. Thus, to measure σ^2 accurately, spatially resolved and polarization resolved EL measurements were made for five different output powers ranging from 0.5 to about 5 mW. From these measurements accurate estimates of σ^2 are possible since the slope of a $\Delta\rho P_2$ vs. $\sum I_m$ graph is proportional to σ^2 (Eq. 4.17).

The total amount of scattering and the amount of discrete (i.e., localized) scattering which takes place in a laser is of interest because the total amount of scattered light provides an estimate of the quality of the material in the active region, and the amount of discrete scattering gives an indication of the effect of scattering on the spectral properties of the devices. This was discussed in Chapter 3. Both the total effective scattering ($\Delta\rho_t$) and the discrete effective scattering ($\Delta\rho_d$) were calculated according to Eqs. 3.1 and 3.2 for the different output powers of the laser. This provides the data needed to calculate the total and discrete scattering (σ) for the lasers measured.

Figure 5.5 shows a graph of $\Delta\rho P_2$ vs. $\sum I_m$ for a planar buried heterostructure laser. Note that the curve is linear in $\sum I_m$ which is a clear indication

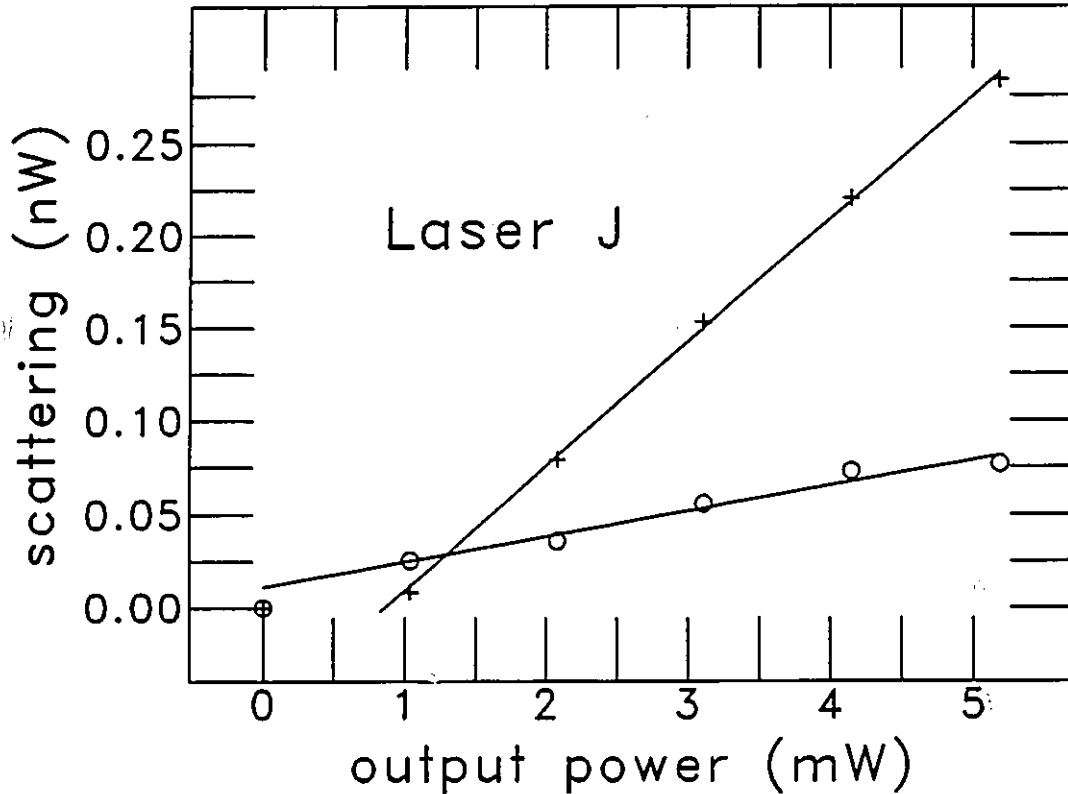


Fig. 5.5 Total (+) and discrete (o) scattering vs. output power for a PBH laser. Note the linear relationship indicating scattering is taking place in the laser.

of scattering. By performing a linear fit to this type of data, σ^2 information for all lasers tested can be compiled, and the results are displayed in Fig. 5.6. The sample variance was calculated for the least squares fit to give an estimate of the uncertainty of the fit. The uncertainty in σ was calculated to be typically $<2E-5$, although the uncertainty is higher for those data points at the origin of Fig 5.6. Figure 5.6 shows that the index guided lasers which were tested tend to scatter more light than the gain guided lasers which were tested.

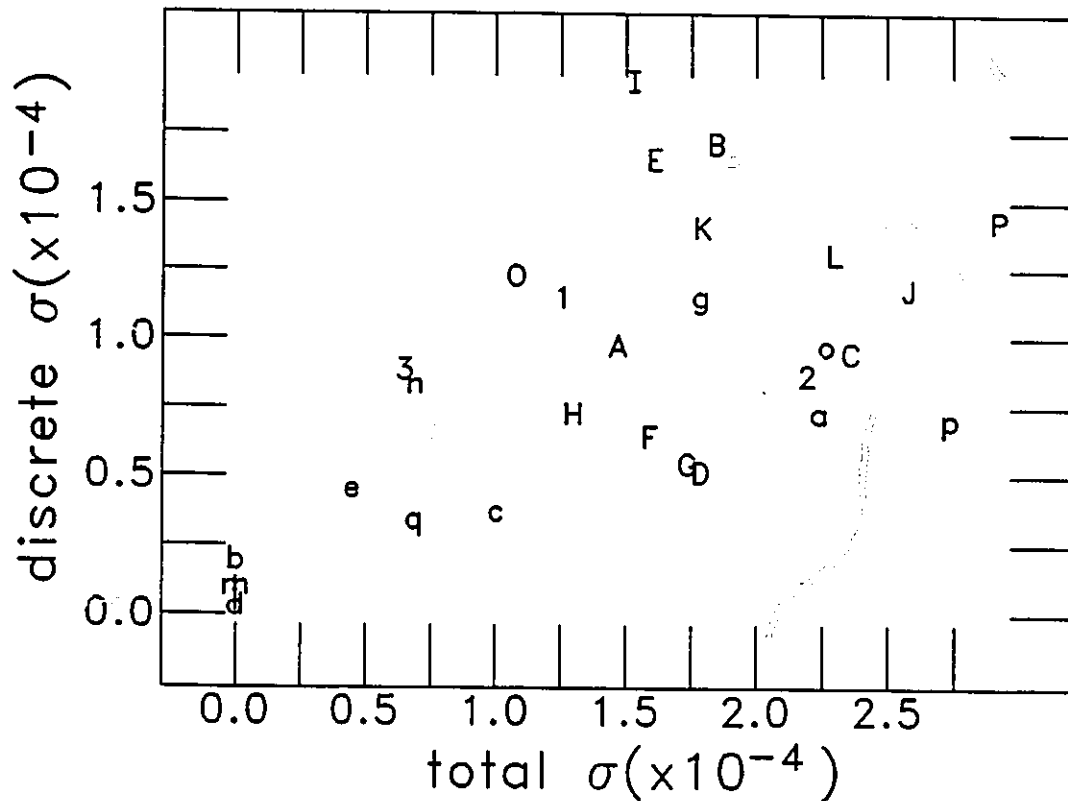


Fig. 5.6 Discrete scattering vs. total scattering for arrowhead buried crescent (numbers), planar buried heterostructure (upper case), and gain guided (lower case) lasers.

On the basis of the scattering data shown in Fig. 5.6, one might expect lasers a, p, A, F, and H to show a similar perturbation of the spectral output (i.e., to have regions of operation with similar SMSR or depth of modulation of the mode envelope), since the discrete scattering is approximately the same for these five lasers. Figure 5.7 shows the worst case spectral output of lasers a, m, p, A, F, and H. The spectral output of lasers A, F, and H are more affected by scattering than lasers a and p even though the lasers exhibit similar amounts of discrete scattering and

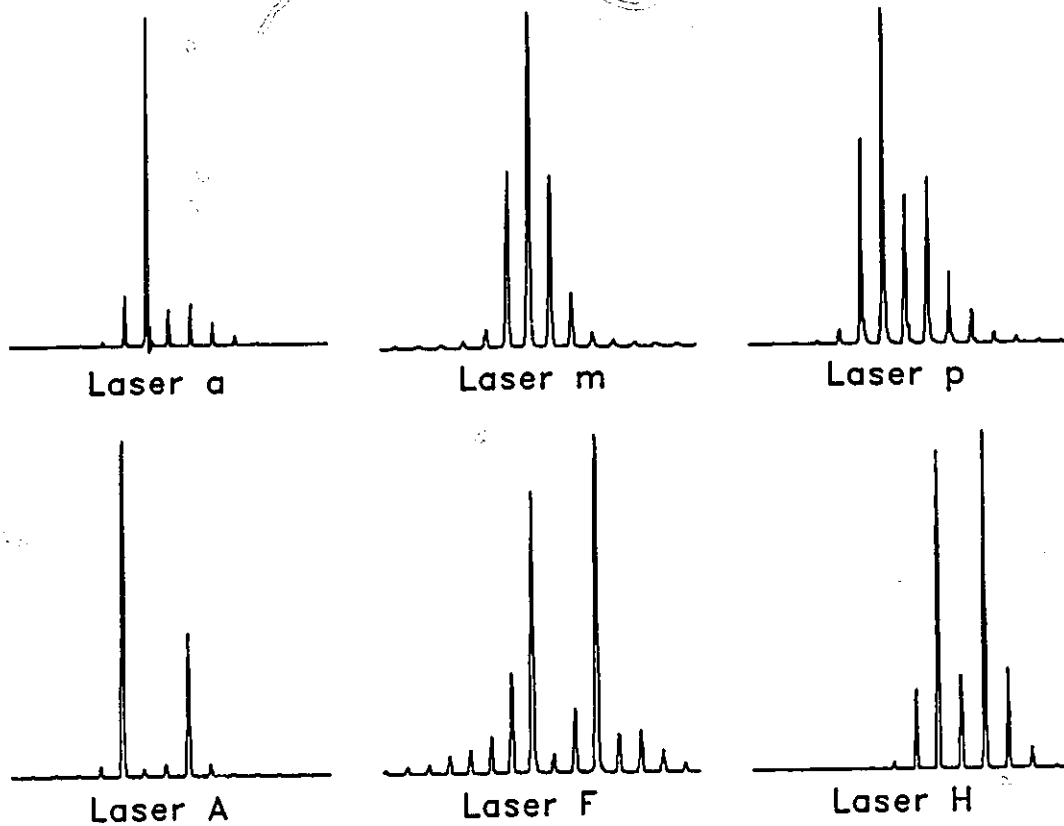


Fig. 5.7 Worst case spectral output of gain guided (lower case) and index guided (upper case) lasers operating above threshold.

lasers a and p exhibit more total scattering than the other lasers. This apparent contradiction exists because the effect of spontaneous emission has not been considered. Lasers a and p produce at and above threshold $\approx 10 \times$ as much spontaneous emission as lasers A, F, and H.

Since the effect of scattering on the spectral output is masked by spontaneous emission, a masked scattering parameter which includes spontaneous emission was chosen to give an indication of the expected effect of scattering on the

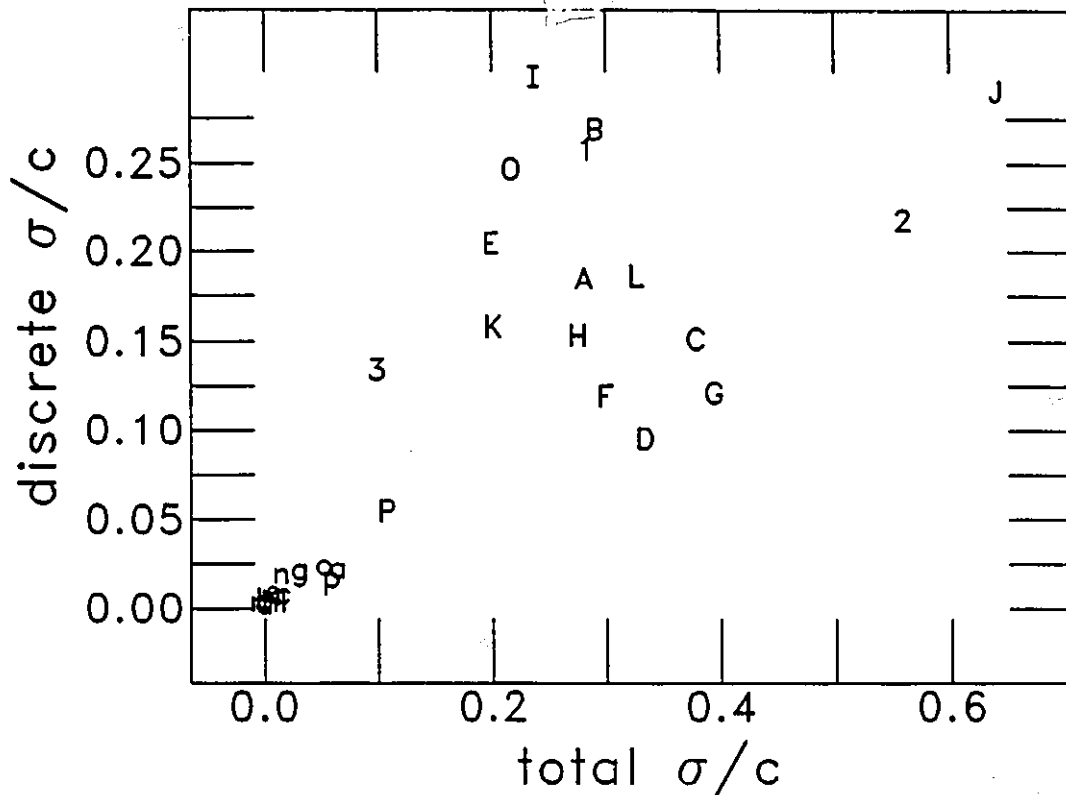


Fig. 5.8 Spontaneous emission masked scattering parameter σ/c for arrowhead buried crescent (numbers), planar buried heterostructure (upper case), and gain guided (lower case) lasers.

spectral output. In Section 5.2 it was shown that the SMSR varied inversely with c and proportionally to σ . Thus the quantity σ/c is used to describe the effect of scattering on the spectral output of diode lasers. The amount of spontaneous emission produced (c) is assumed to be proportional to the amount of P2 light measured (as was done for Fig. 5.1), therefore the measured P2 values are used to estimate c . Figure 5.8 shows a compilation of all the masked scattering values (σ/c) for the lasers tested. This masked scattering parameter is similar to the effective

scattering parameter ($\Delta\rho$) used in Chapter 3 as can be seen from Eq. 4.17, and so the correlation between σ/c values and the spectral properties of the lasers is similar to the correlation between $\Delta\rho$ and the spectral properties as shown in Chapter 3. Lasers with similar spectral output are grouped together in Fig. 5.8. Lasers a, m, and p operate multilongitudinal moded with weakly modulated mode envelopes (see Fig. 5.7), and have similar σ/c values. Lasers A, F, and H run multilongitudinal moded with strongly modulated mode envelopes and have large σ/c values. Thus the effect of scattering on the spectral output of diode lasers can be explained on the basis of the amounts of internal scattering and of spontaneous emission. Both must be considered for an understanding of the spectral properties. It is worth noting that there is a large difference in the σ/c values between those lasers which run multilongitudinal moded with weakly modulated mode envelopes (lower left portion of graph) and those which run single moded or multilongitudinal moded with strongly modulated mode envelopes. It is also worth noting that all the gain guided lasers which were tested lie in the lower left corner of the graph of Fig. 5.7, and that these lasers tend to run multilongitudinal moded with weakly modulated mode envelopes.

Figure 5.7 is very similar to Fig. 3.5 which graphs the effective scattering, and thus the correlation between scattering and spectral properties is the similar for both graphs. The major difference between Figs. 3.5 and 5.7 is that when the masked scattering parameter (σ/c) is used, the scale of the discrete σ/c gives an indication of the possible SMSR for the laser. This provides more information about the effect of scattering on any given laser. The data in Fig. 5.7 indicate that differences of two

orders of magnitude should exist between the SMSR of the lasers measured. Other differences do exist between the graphs of Fig. 3.5 and 5.7. For example in Fig. 3.5 lasers A and J are superimposed over each other, but since laser J produces less spontaneous emission than laser A, the masked scattering value of laser J is larger. The scattering properties of laser B have increased from Fig. 3.5 to Fig. 5.7 as a result of damage occurring between the measurements taken for Fig. 3.5 and Fig. 5.7. With only these few exceptions, the two figures are similar and both demonstrate differences in the material properties of lasers.

5.4 Summary

A study of the influence of spontaneous emission on the spectral properties of diode lasers when internal scattering exists along the length of the active region of the laser has been presented. It has been shown that the amount of spontaneous emission masks the effect of internal scattering on the spectral output of 1.3 μm semiconductor diode lasers. Internal scattering affects the spectral output through resonant enhancement of selected modes. The spectral output of lasers with large amounts of spontaneous emission which couples into the modes is not as affected by scattering as the spectral output of lasers with small amounts of spontaneous emission which couples into the modes.

A masked scattering parameter (σ/c) was derived which can be used to

orders of magnitude should exist between the SMSR of the lasers measured. Other differences do exist between the graphs of Fig. 3.5 and 5.7. For example in Fig. 3.5 lasers A and J are superimposed over each other, but since laser J produces less spontaneous emission than laser A, the masked scattering value of laser J is larger. The scattering properties of laser B have increased from Fig. 3.5 to Fig. 5.7 as a result of damage occurring between the measurements taken for Fig. 3.5 and Fig. 5.7. With only these few exceptions, the two figures are similar and both demonstrate differences in the material properties of lasers.

5.4 Summary

A study of the influence of spontaneous emission on the spectral properties of diode lasers when internal scattering exists along the length of the active region of the laser has been presented. It has been shown that the amount of spontaneous emission masks the effect of internal scattering on the spectral output of 1.3 μm semiconductor diode lasers. Internal scattering affects the spectral output through resonant enhancement of selected modes. The spectral output of lasers with large amounts of spontaneous emission which couples into the modes is not as affected by scattering as the spectral output of lasers with small amounts of spontaneous emission which couples into the modes.

A masked scattering parameter (σ/c) was derived which can be used to

estimate the effect of scattering on the spectral properties of a laser. This parameter is very similar to the effective scattering parameter ($\Delta\rho$) used in Chapter 3, so when comparing the internal properties of diode lasers the methods are similar.

The chapter provides an explanation for the spectral output of diode lasers, and for the difference in the spectral output between gain guided and index guided devices based on the influence of the internal scattering properties of the diode lasers and the amount of spontaneous emission produced and coupled into the modes of the lasers. Both the internal scattering and the amount of spontaneous emission are measured. This provides the parameters necessary for accurate modelling of semiconductor diode lasers. In the next chapter the theory of the last two chapters will be used to develop a model for the spectral properties of diode lasers that considers the effect of multiple scattering centres.

Chapter 6 Multiple Scattering and Absorption Model

6.1 Introduction

In Chapters 3 and 5 it was shown that light is scattered inside diode lasers from discrete scattering locations. In Chapter 4 a model was developed which included one scattering centre along the active region of the laser. In this chapter the model will be expanded to allow for multiple scattering centres, and other non uniformities.

Some effort has previously been made to model complex laser structures,[44,45] that is structures with non uniformities distributed along the active region. A numerical multi-element matrix approach has been developed for multiple cavity lasers. It was used to calculate mode lifetimes which could be coupled with rate equations to obtain an estimate of the device characteristics.[44] This numerical matrix approach was later adapted to analyze the performance of phase shifted distributed feedback structures.[45]

In this chapter a model is described which can include many non uniformities along the length of the device, and which allows for low reflectivity facets. This has been accomplished by coupling the numerical matrix approach to the model developed in Chapter 4. The model is used to examine the effect of multiple scattering and absorption centres which may exist along the stripe of diode lasers. The ability of multiple scattering centres to increase the side mode suppression ratio

of the spectral output of diode lasers is reported. Also an examination of the spectral tuning which exists with multiple scattering and absorption centres is presented.

Semiconductor diode lasers may have unusual tuning characteristics. Many of these characteristic such as skipping modes are explainable based on the existence of a single scattering centre as explained in Chapter 4. Some characteristics are not explainable due to scattering alone, such as negative tuning. This is when a iasers spectrum shifts to shorter wavelength with increased current. By measuring the emission which comes through the surface of the laser using spatially resolved and polarization resolved electroluminescence, it is found that lasers with negative tuning characteristics typically have absorption centres along the stripe. It will be shown using the Fabry Perot matrix model how an absorption centre coupled with multiple scattering centres can lead to negative tuning.

In Section 6.2 the theoretical model for multiple scattering and absorption centres is developed, Section 6.3 deals with the effect of multiple scattering on the spectral output of diode lasers, Section 6.4 provides an explanation into the negative tuning characteristics based on scattering and absorption, and a summary is given in Section 6.5.

6.2 Numerical Fabry Perot Matrix Model

The purpose of this section is to model semiconductor lasers which are complex due to internal scattering centres and absorption centres. Following the theoretical approach of Ebeling, the laser is considered to be one dimensional,[44] and can be divided into a number of uniform sections each of which is described by

a transfer matrix[45] given by:

$$\begin{aligned} \begin{pmatrix} a_{i+1} \\ b_{i+1} \end{pmatrix} &= \begin{pmatrix} m_{11} & m_{12} \\ m_{21} & m_{22} \end{pmatrix} \cdot \begin{pmatrix} a_i \\ b_i \end{pmatrix} \\ &= M \cdot \begin{pmatrix} a_i \\ b_i \end{pmatrix}. \end{aligned} \quad (6.1)$$

where M is the transfer matrix, the a_i 's are left propagating electric fields and the b_i 's are right propagating electric fields. In this analysis three types of transfer matrices are used to describe the laser. The matrix which describes the gain or loss medium with or without an absorber, is defined as:

$$M_g = \begin{pmatrix} e^{-\gamma L + ikL} & 0 \\ 0 & e^{\gamma L - ikL} \end{pmatrix} \quad (6.2)$$

where k is the wavenumber of the light, γ is the gain or absorption coefficient of the media and L is the partial length of gain medium which will be referred to as a pseudo cavity. The facets are described by

$$M_f = \begin{pmatrix} \frac{n_1 + n_2}{2n_1} & \frac{n_1 - n_2}{2n_1} \\ \frac{n_1 - n_2}{2n_1} & \frac{n_1 + n_2}{2n_1} \end{pmatrix} \quad (6.3)$$

where n_1 and n_2 are the indices of refraction for the semiconductor and air with the order depending on the facet. Finally the matrix which describes the scattering centre is:

$$M_s = \begin{pmatrix} \frac{1}{\tau} & -\frac{\sigma}{\tau} \\ \frac{\sigma}{\tau} & \frac{\tau^2 - \sigma^2}{\tau} \end{pmatrix} \quad (6.4)$$

where σ is the fraction of light which scatters back into the mode and τ is the fraction of light which is transmitted through the scattering centre and not scattered.

The product of such matrices becomes the transfer matrix for the laser so that

$$\begin{pmatrix} a_N \\ b_N \end{pmatrix} = \begin{pmatrix} m_{11} & m_{12} \\ m_{21} & m_{22} \end{pmatrix} \cdot \begin{pmatrix} a_1 \\ b_1 \end{pmatrix} \quad (6.5)$$

$$= \bar{M} \cdot \begin{pmatrix} a_1 \\ b_1 \end{pmatrix}$$

For a laser boundary conditions exist that there is no light input into the cavity, i.e., $a_N = 0$ and $b_1 = 0$. At the lasing condition a_1 is finite therefore $m_{11} = 0$. This condition can be calculated numerically by increasing the gain parameter γ (which is frequency dependant) until $m_{11} = 0$, revealing the threshold gains for each frequency. The effective reflectivity of each mode is then calculated by equating these threshold gains with the threshold condition of a laser as given by Eq. 5.3, that is:

$$1 - R_m G_m = 0 . \quad (6.6)$$

Here G_m is the single pass gain of the laser: $G_m = \exp(\gamma L_{tot})$, where L_{tot} is the total cavity length of the laser. Using the mode dependant reflectances (R_m) calculated by the numerical matrix model the results are adapted to the single scattering centre model such that Eq. 5.3 now describes the modal intensity output for a laser with

multiple scattering centres. If a localized absorber is present it will provide localized heating in the laser cavity. Localized absorbers have been observed in GaAs lasers with a temperature increase associated with the local absorbers of up to 40 K.[14] An increase in temperature will have the effect of changing the optical path length.[46] If scattering centres are present the optical path length of the small pseudo cavity defined by scattering centres which surround the localized absorber will increase relative to the rest of the laser cavity. The increase in length will change the effective reflectances of the cavity modes making the effective reflectances functions of the pumping level. The matrix describing the gain medium which contains an absorber will then have a length $L(\gamma)$ which changes with pumping level. With the new values of effective reflectivity, the modal intensities of the laser can be calculated using Eq. 5.3.

6.3 Spectral Output of Lasers with Multiple Scattering

In this section an effort is made to demonstrate how a complex semiconductor diode laser can be accurately modelled. Also spectra which cannot be accounted for with a single scattering model are shown. Multiple scattering can have a large effect on the spectral properties of diode lasers. Consider a 250 μm long laser with one scattering centre located 25 μm from one facet, with a scattering value of $\sigma = 0.0009$. Figure 6.1 shows a graph of the resulting effective reflectance (R_m). If nine

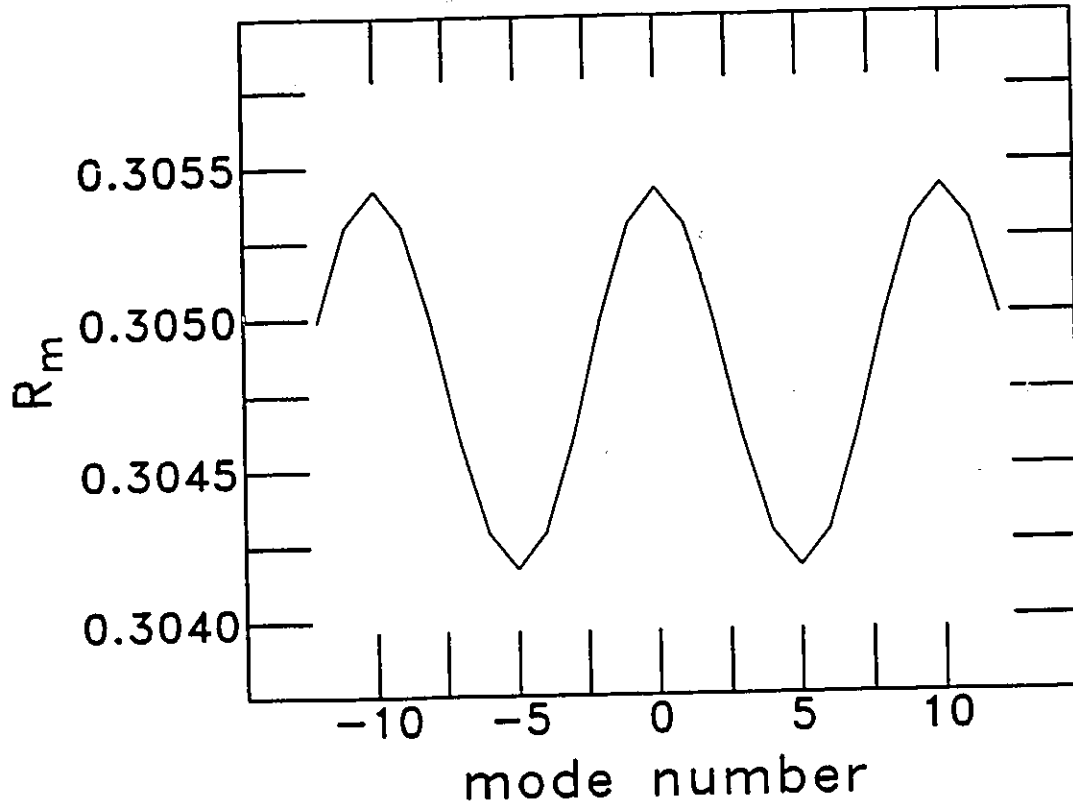


Fig. 6.1 Effective reflectance (R_m) for a laser with one scattering centre located $25 \mu\text{m}$ from a facet and $\sigma = 0.0009$.

scattering centres are located each $25 \mu\text{m}$ apart along the entire active region with scattering values of $\sigma = .0001$, so that the combined scattering amplitude is the same as before, then R_m will appear as in Fig. 6.2. This change in the effective reflectance has a large effect on the spectral output as can be seen from the theoretical spectra shown in Fig. 6.3. Even though the same amount of scattering was used for both theoretical spectra, the side mode suppression ratio is greater when multiple scattering centres are used.

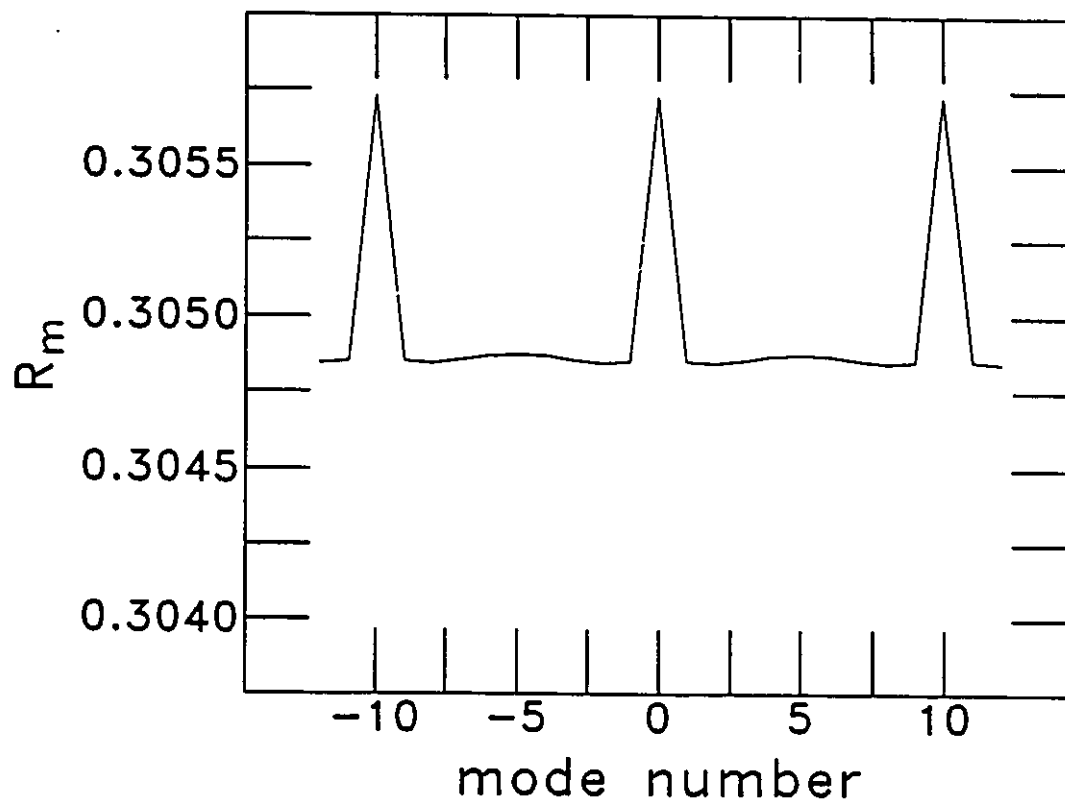


Fig. 6.2 R_m for a laser with 9 scattering centres distributed $25 \mu\text{m}$ apart along the length of the active region each with $\sigma = 0.0001$.

6.4 Negative Spectral Tuning

A small percentage of semiconductor diode lasers tune to shorter wavelength with increasing current over a limited current range. I have measured two lasers which exhibit negative spectral tuning. These lasers were the only lasing devices measured to have absorbing regions in them. Also, both scattered large amounts of light. Figure 6.4 shows the spatially resolved electroluminescence (EL) of the two lasers, with the absorbing regions noticeable as indentations in the EL

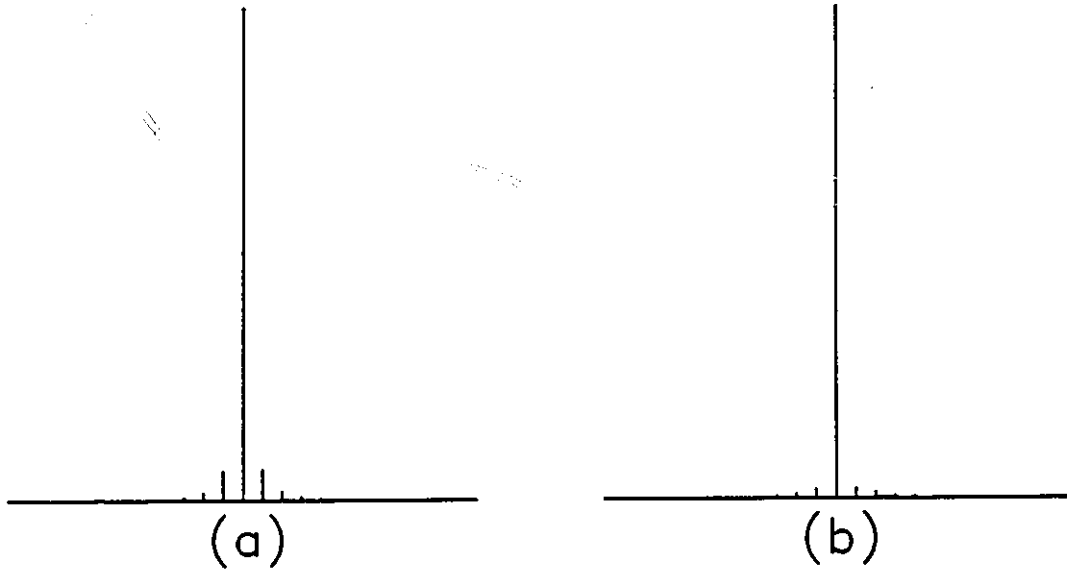


Fig. 6.3 Theoretical spectra created using R_m from (a) Fig. 6.1, and (b) Fig. 6.2.

profiles. The absorbing region in Fig. 6.4 (b) is much larger than in Fig. 6.4 (a), and the laser of Fig. 6.4 (b) tunes negatively over a larger range of operating conditions than does the other laser. It was hypothesised that negative spectral tuning may be explained by considering the effect of a localized absorber in a laser which contains multiple scattering centres. The theoretical approach used to test this hypothesis was to allow one of the pseudo cavities in the laser to grow with pumping, thus simulating the increase in the optical path length caused by localized heating. If the localized absorber is located in a small pseudo cavity, then R_m will shift slowly in frequency space as the cavity is increased. To demonstrate this, consider R_m for a laser with one strong scattering centre located $10 \mu\text{m}$ from a facet and R_m from the same laser if the $10 \mu\text{m}$ long pseudo cavity increases in length by $0.01 \mu\text{m}$. R_m for both cases is

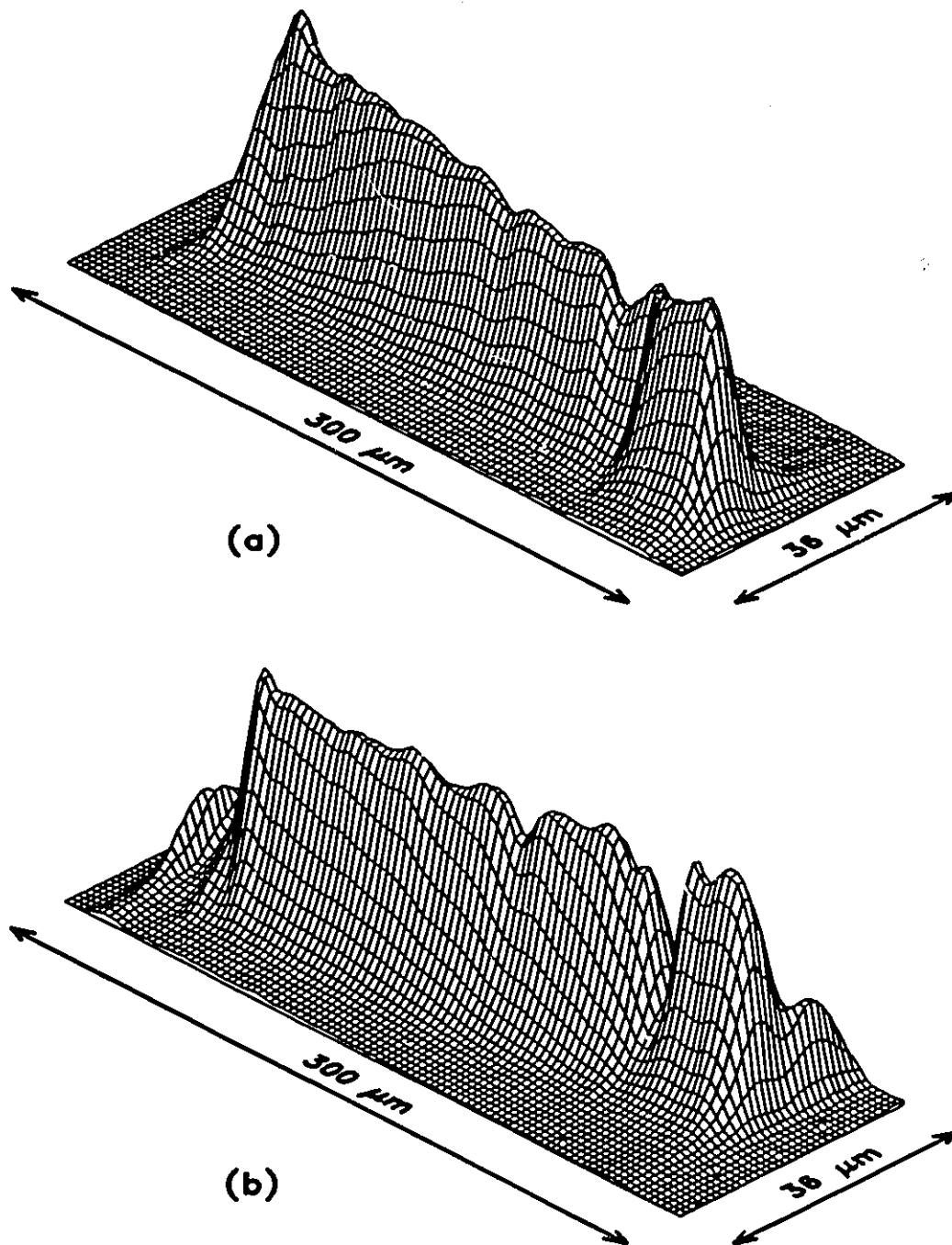


Fig. 6.4 Spatially resolved electroluminescence distributions showing absorptive regions for (a) laser C and (b) laser E.

shown in Fig. 6.5 and the shift in R_m with the optical path length increase is evident.

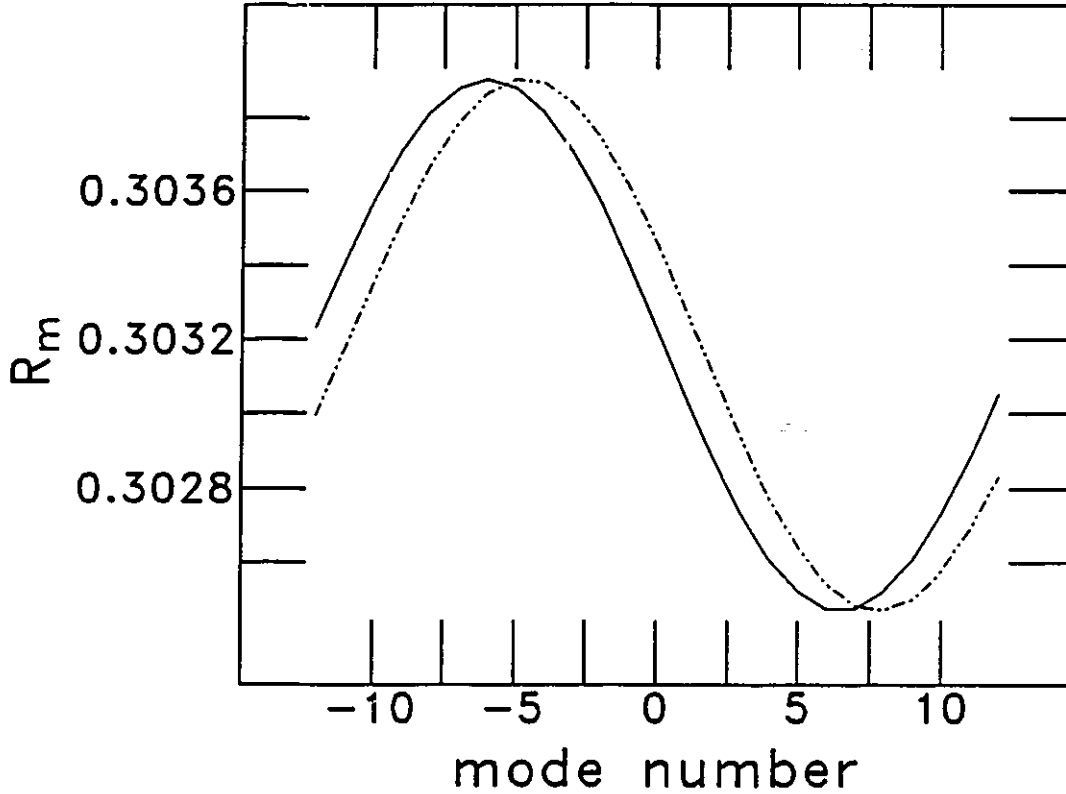


Fig. 6.5 R_m for scattering centre located 10 μm from a facet in a 250 μm long laser (solid line), and 10.01 μm from a facet in a 250.01 μm long laser (broken line). Notice the shift in frequency of R_m .

This frequency shift can be positive or negative depending on the pseudo cavity whose optical path length is growing. If only one scattering centre is assumed to exist and the absorber is modelled as increasing in temperature proportionally to the driving current, then the mode structure may be interesting, although no negative tuning will occur. This is because R_m shifts in frequency with driving current slower than the frequency shift of the gain peak with current. However, if multiple scattering centres are allowed to exist, the resulting R_m is a complicated function of the

scatterers, and peaks in R_m may change position much more rapidly with current due to changes of the relative phases of the scattering from the different scattering centres, resulting in negative tuning over a limited current range.

Figure 6.6 shows plots of theoretical spectra for a laser which tunes to

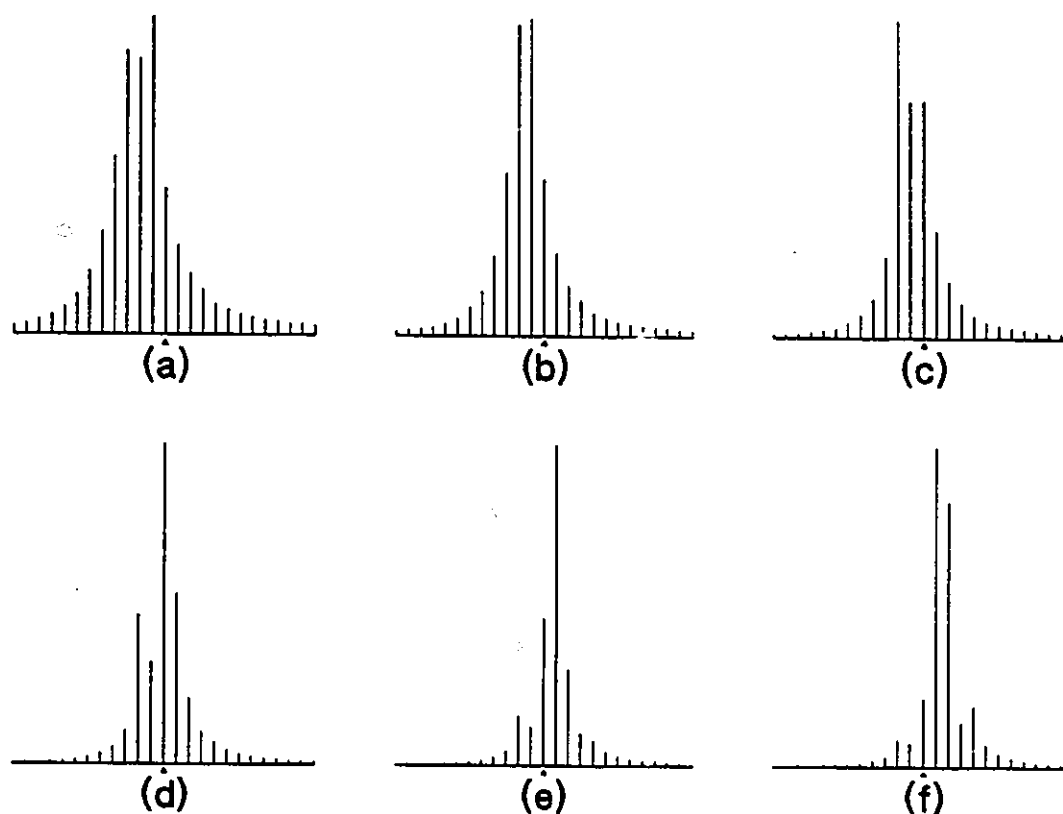


Fig. 6.6 Theoretical spectra of a laser. The spectra is lasing in a central mode in (a) and (b), has shifted to shorter wavelength in (c), and then shifts to longer wavelength in (d), (e) and (f).

shorter wavelength, even though the gain peak is shifting to longer wavelength. Six spectra are shown in the figure corresponding to an increase in the pumping from Fig. 6.6 (a) to (f). R_m used to create the spectra of Fig. 6.6 (a) and (c) is shown in Fig. 6.7 The change in R_m in the figure is associated with an increase of $0.01 \mu\text{m}$ in

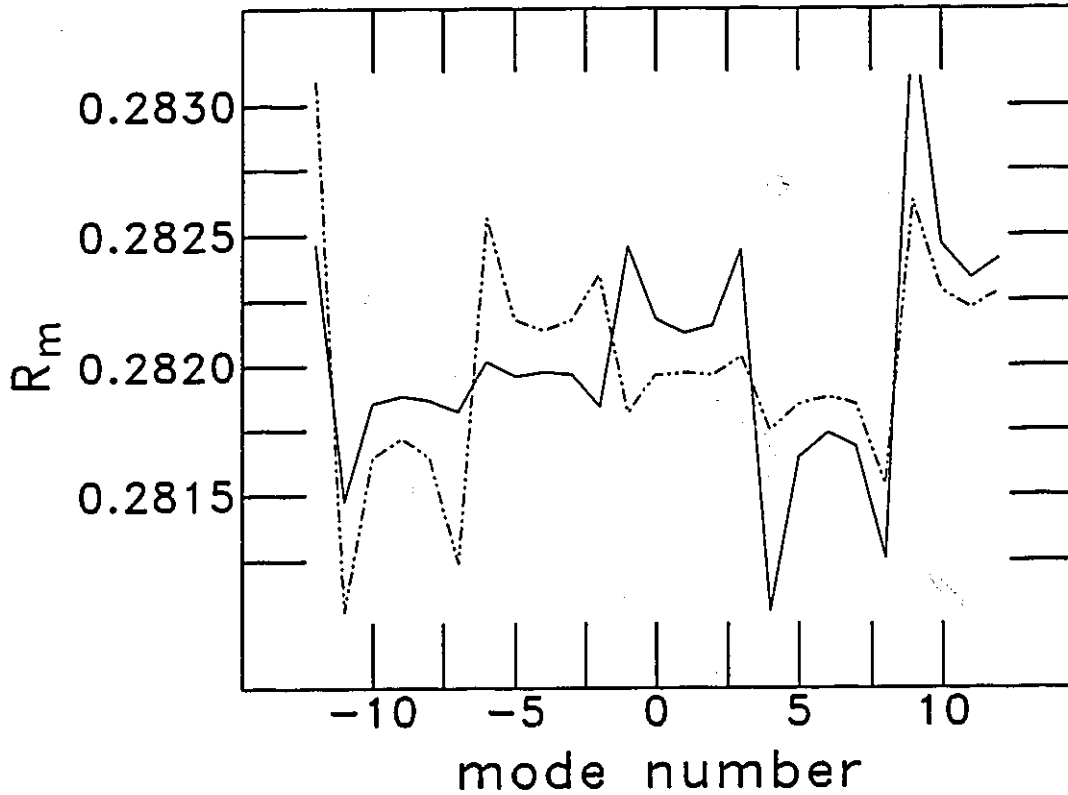


Fig. 6.7 Plots of R_m changing due to an increase in a $27 \mu\text{m}$ cavity of $0.02 \mu\text{m}$. The R_m plotted were used to create the theoretical spectra of Fig. 6.6 (a) and (c).

a $27 \mu\text{m}$ long pseudo cavity; an increase of 0.037% . Notice how much larger the change in R_m is in Fig. 6.7 than the change due to one scattering centre in Fig. 6.5. Based on measurements made of temperature tuning,[46] the increase of 0.037% corresponds to a temperature differential between the pseudo cavity and the rest of the laser of 48 K . This temperature differential is larger than would be expected, although it is expected that negative tuning could be modelled with smaller temperature differentials using different scattering parameters.

An effort was made to find experimental evidence to support the model of negative tuning, using a variable temperature gradient across a device which was seen to tune to shorter wavelength. Theoretically, a variable temperature gradient will have the same effect as scattering centres which move small distances inside the device. To explain this, consider a device with one scattering centre. The average temperature of the pseudo cavity on one side of the scattering centre will be larger than the average temperature of the pseudo cavity on the other side of the scattering centre. The temperature difference will result in a relative change in the optical path lengths of the two pseudo cavities, which is equivalent to the scattering centre moving a small distance. The effect on R_m of a moving scattering centre will be to shift R_m in frequency, similar to the effect shown in Fig. 6.5. A large enough range of the temperature gradient would shift the effective reflectivity continuously resulting in an oscillation of the lasing modes in frequency space. This can be explained using R_m for a laser with one scattering centre located $50 \mu\text{m}$ from one facet. The variable temperature gradient is modelled by moving the scattering centre in $.01 \mu\text{m}$ increments. The resulting values of R_m are shown in Fig. 6.8 for the first five increments. The theoretical spectra of this laser can be seen in Fig. 6.9 for various locations of the scattering centre. One can see that the lasing mode oscillates with the distance moved. If a large enough temperature gradient could be achieved more than one oscillation should be evident in the spectra as the temperature gradient changes.

The experiment was done on a laser (Laser E) which exhibited negative

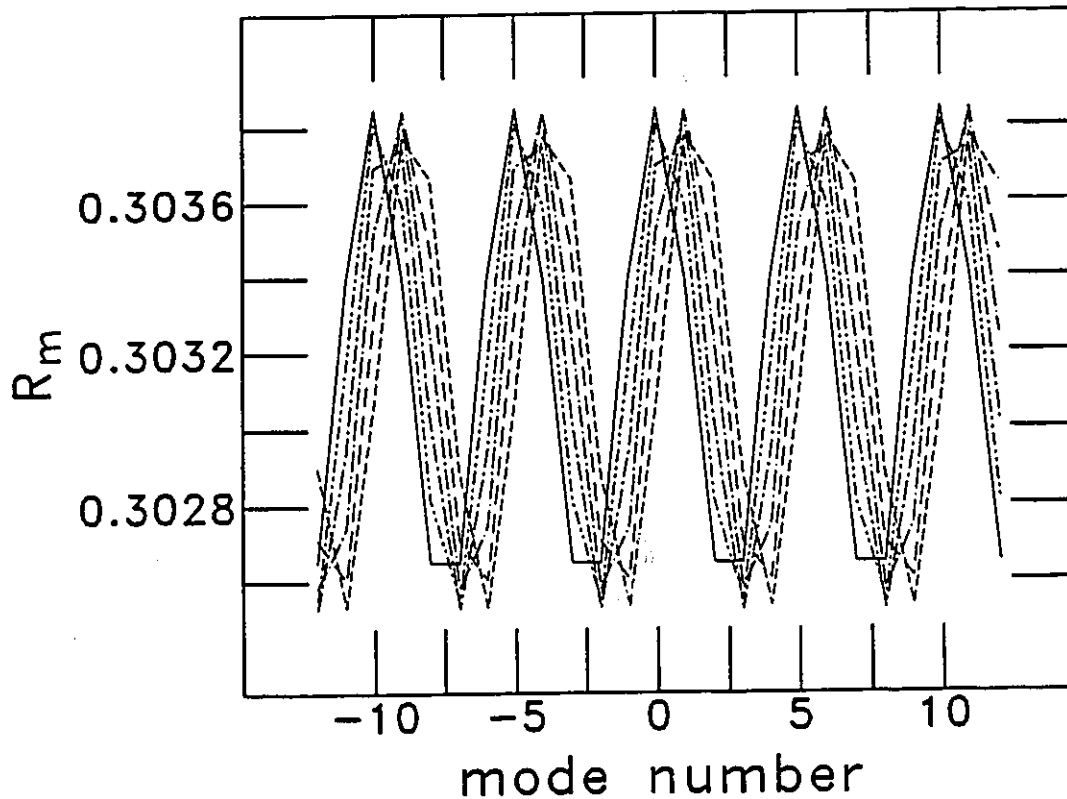


Fig. 6.8 R_m for a laser with a scattering centre located 50 (solid line) to 50.05 μm from a facet in a 250 μm long laser. Notice the movement of R_m to the right.

tuning. At low current the laser operated single moded and at higher current the laser also operated single moded, but at a shorter wavelength. To begin the experiment the laser was biased so that lasing would occur at both these frequencies; the spectrum is shown in Fig. 6.10. A probe which was attached to a soldering iron was brought close to a facet of the laser, so as not to touch the laser, and so no optical feedback would occur. The power to the soldering iron was turned off and then the laser cooler current and the spectra of the device were continuously

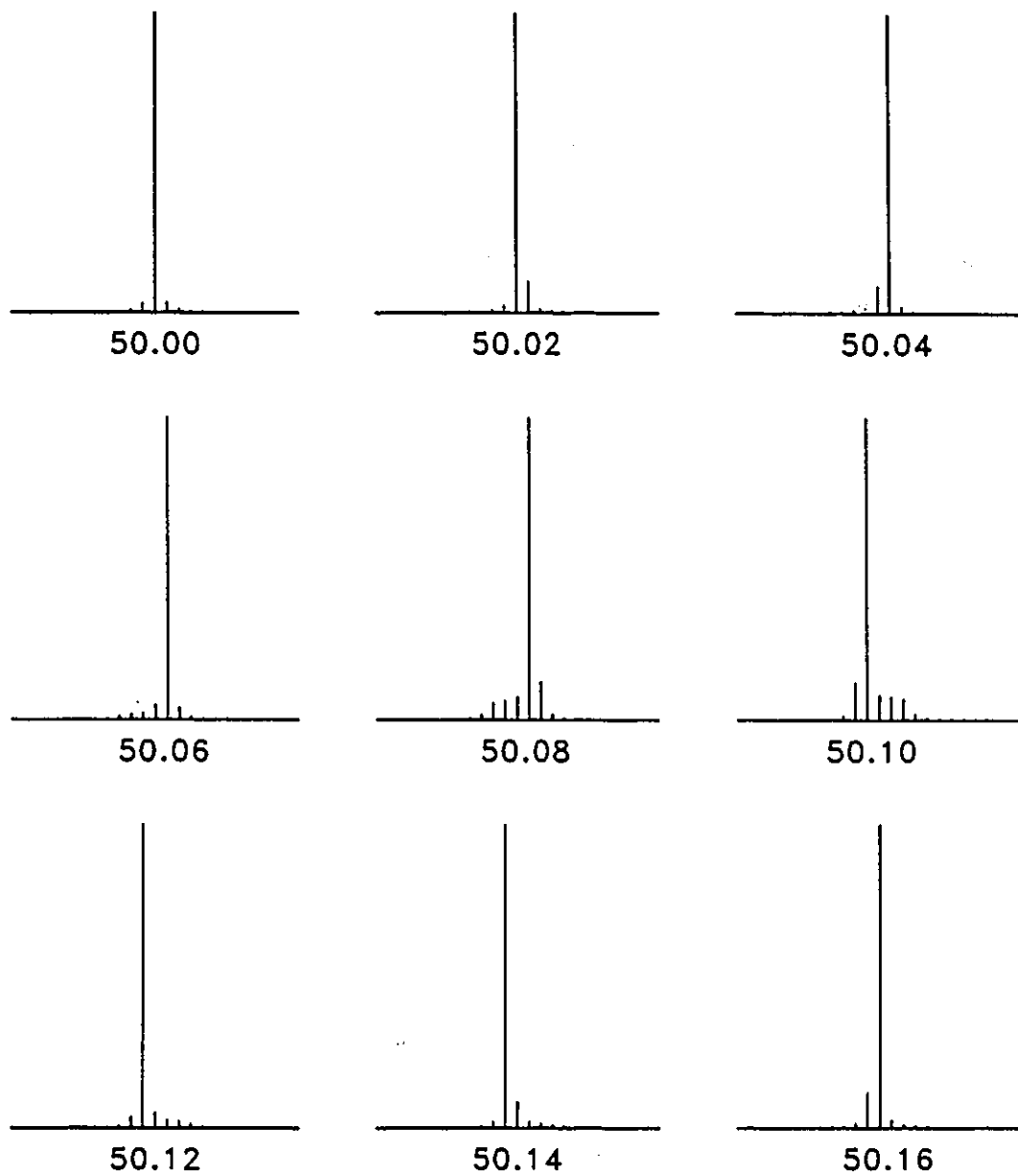


Fig. 6.9 Theoretical spectra for a $250 \mu\text{m}$ long laser with a scattering centre located $50\text{-}50.16 \mu\text{m}$ from one facet. Notice that the dominant lasing mode oscillates in frequency space as the scattering centre moves across the device.

monitored.

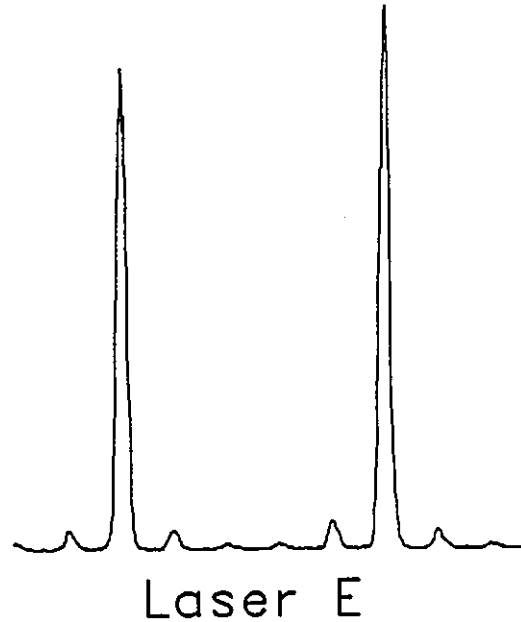


Fig. 6.10 Measured spectrum of laser E, at mid point between shifting from longer wavelength to shorter wavelength with increasing current or temperature.

To quantify shifts in frequency between the two lasing modes, a parameter (Ψ) was created such that if I_1 is the intensity of one mode and I_2 is the intensity of the other, then

$$\Psi = \frac{I_1 - I_2}{I_1 + I_2} . \quad (6.7)$$

This parameter Ψ is positive if $I_1 > I_2$, and negative if $I_1 < I_2$, and varies continuously from -1 to 1. Figure 6.11 shows two graphs of Ψ plotted as a function of the laser cooler current for the same laser. The cooler current is assumed to be proportional to the energy being absorbed by the laser, and also proportional to the

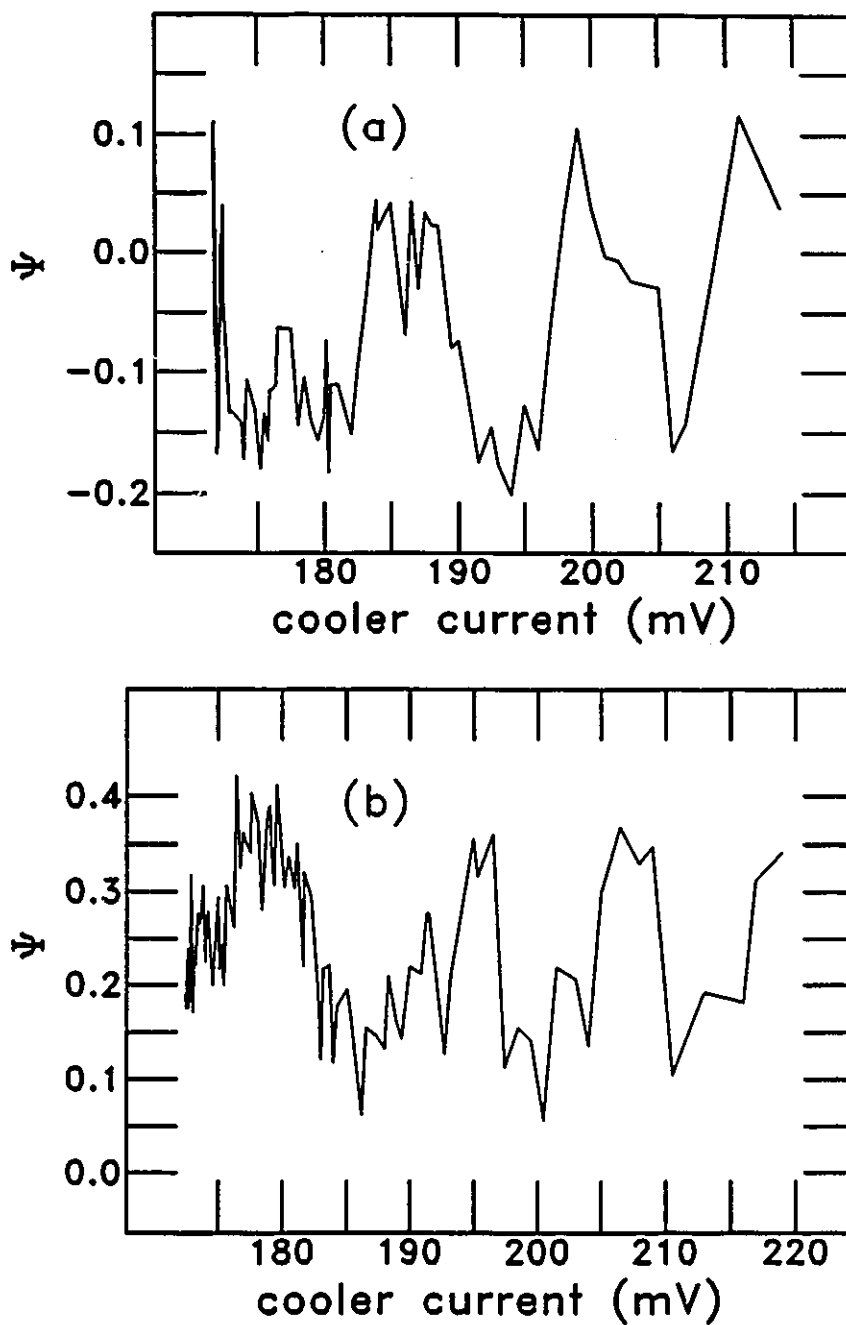


Fig. 6.11 Plots of changes in Ψ with the temperature gradient through device which is represented by the cooler current. Notice the oscillations of Ψ with respect to the temperature gradient.

applied current gradient. One can see from the results that oscillation do indeed occur in frequency with respect to the applied temperature gradient. This gives an indication that the phenomenon described in this section is a reasonable explanation into the negative tuning behaviour of diode lasers.

6.5 Summary

A model has been developed which can be used to model complex laser structures. The model has demonstrated possible effects of many scattering centres on the spectral properties of lasers. Also a possible explanation has been given as to why lasers may tune to shorter wavelength with increasing temperature and current. This phenomenon is thought to be caused by the combined effect of a localized absorber and multiple scattering centres.

Chapter 7 Conclusion

7.1 Introduction

This concluding chapter is divided into two parts. Section 7.2 elaborates on further research which is recommended and Section 7.3 provides a summary of the work.

7.2 Recommended Additional Research

The degree of polarization (ρ) measurements outlined in this thesis were used to derive information on the stress and scattering distributions in diode lasers. Only ρ measurements away from the facet were used for this purpose. That is because large changes exist in ρ with applied current near the facets, changes which have not yet been explained. In Chapter 2 it was mentioned that above threshold stimulated TE light will scatter off the heat sink and couple into P1 light increasing the value of ρ . However below threshold ρ becomes highly negative near the facets. A possible explanation is based on the fact that the reflectance for TE light is higher than for TM light due to the shape of the guided mode. This means that more TM light will be transmitted. It is possible that the small amount of light transmitted through the facet at large angles of transmission may be scattered at the facet so as

to couple into the P1 and P2 light, decreasing ρ , since more TM light is transmitted. An understanding of the facet effects could be useful so that strain and scattering information near the facets may be obtained.

In Chapters 3-5 the scattering properties of diode lasers were measured and used to explain spectral properties of diode lasers, however the scattering mechanism is not yet known. It is recommended that further research be taken into understanding the scattering mechanism, and isolating the physical process responsible for the scattering.

The lasers studied should be examined with spatially resolved and polarization resolved photoluminescence (PL). The strain information should be identical to that obtained with EL. Also it would be interesting to find out whether there are non uniformities in the PL distributions that correspond to the non uniformities of the EL distributions.

Spatially resolved and polarization resolved EL and PL may be used to study the facets of lasers. The EL measurements would provide highly resolved near field measurements which could be taken far below threshold. Ideally these measurements would provide information about the current flow in the devices, and the development of the lasing modes.

In Chapter 6 graphs were shown of the theoretical effective reflectances of diode lasers with scattering centres. An experimental verification would be very useful to test the theory. If scattering centres could be made inside devices, subsequent measurements of their spectral and scattering properties might be very enlightening.

Also in Chapter 6, an explanation into the negative tuning behaviour of diode lasers was given. This was by no means a rigorous proof. Therefore further

work into understanding this phenomenon should lead to a better understanding of the operation of diode lasers.

Preliminary accelerated aging tests have been performed on diode lasers and stress relaxation is observed in previously unaged lasers. More research is needed to discover the nature of this process.

7.3 Summary

An instrument has been developed to measure the spatially resolved and polarization resolved electroluminescence (EL) of 1.3 μm semiconductor diode lasers. Using this device it is shown that the material properties of diode lasers are not uniform along the length of the active regions of the devices.

The stress distribution along the active region of diode lasers was measured. It was found that gain guided lasers have lower internal stresses than index guided lasers, and that the stress distributions for both devices are non uniform.

The scattering of stimulated emission has been measured in diode lasers. It is found that the scattering comes from sources distributed along the active region of the lasers. The amount of scattering varies between lasers, with gain guided devices scattering less light than index guided devices.

The scattering and spontaneous emission properties of diode lasers have been correlated with the spectral properties of diode lasers. It is observed that devices which scatter large amounts of light are more likely to operate single moded or multilongitudinal moded with highly modulated mode envelopes, than are devices which scatter small amounts of light. Also, the effect of the scattering on the spectral

properties of diode lasers is found to be masked by the amount of spontaneous emission produced by the laser; that is, a laser which produces a large amount of spontaneous emission is less affected by internal scattering than a laser which produces a smaller amount of spontaneous emission.

This correlation between the scattering, spontaneous emission and spectral properties has been explained theoretically using an appropriate model. The model was developed to consider the effect of scattering centres on the spectral properties of diode lasers. The results of the modelling have led to an understanding of the experimentally observed spectral properties of diode lasers, and have provided an explanation into the tuning characteristics of diode lasers. A reason for negative tuning has been given based on the results of a theoretical study of the effect of multiple scattering centres and localized absorbers.

Non uniformities of strain and scattering have been measured in $1.3 \mu\text{m}$ InGaAsP semiconductor diode lasers. These non uniformities have been modelled and provide an explanation for experimentally measured spectral properties of diode lasers.

Appendix Circuit Diagrams

This appendix contains diagrams of the circuits used to control the spatially resolved and polarization resolved electroluminescence apparatus. Not all decoupling capacitors have been marked on the circuit diagrams, e.g., in most of the circuits $0.1 \mu\text{F}$ capacitors are connected between the inputs of the power supply to the card and ground.

The following circuits are shown:

- (1) Laser Driver Circuit.
- (2) Laser Cooler Circuit.
- (3) Motor Driver Circuit.
- (4) Wien Bridge Oscillator Circuit.
- (5) Position Sensor Circuit.
- (6) 9-Pin Connector Diagram.

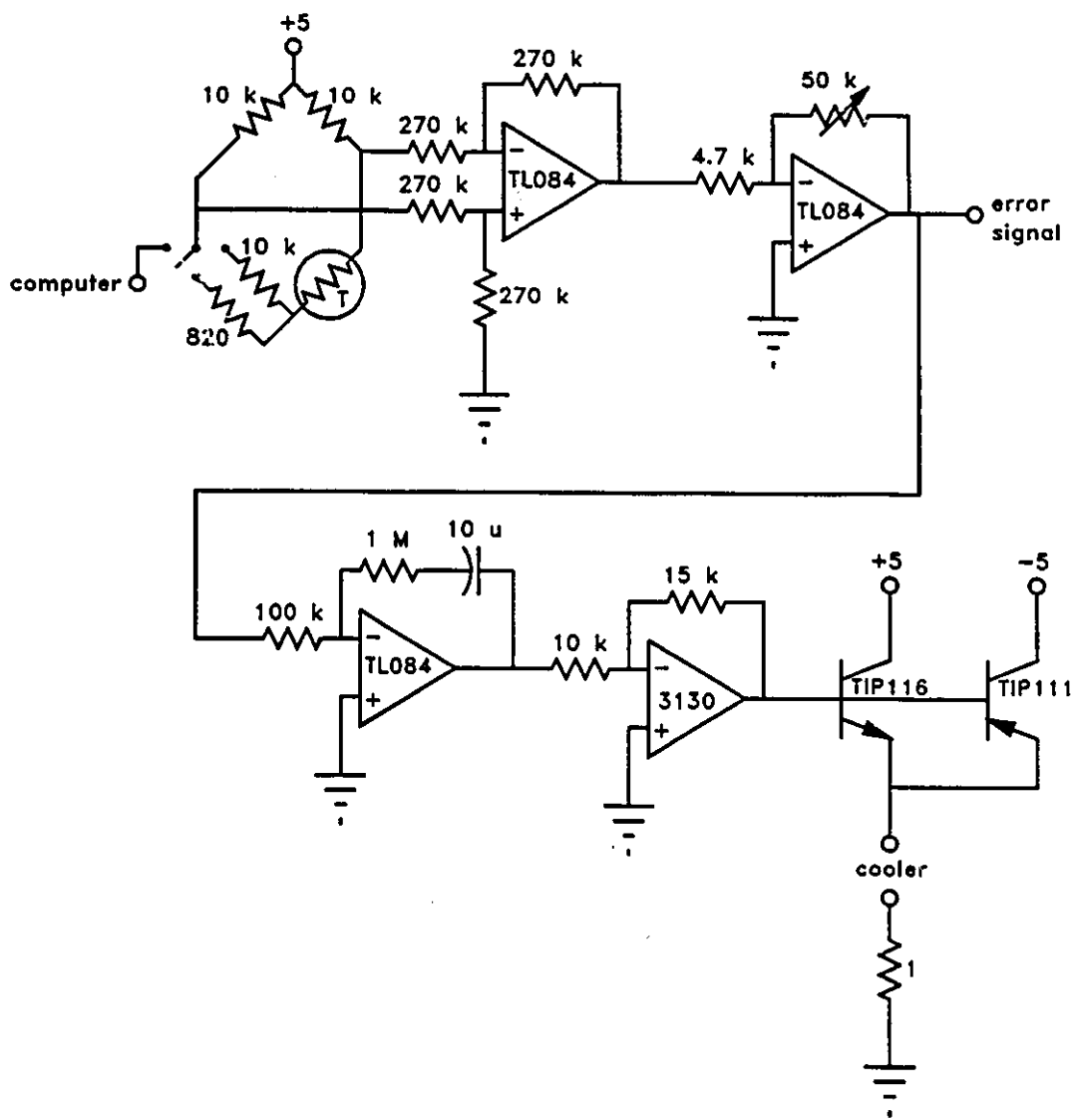


Fig. A.2 Laser Cooler Circuit.

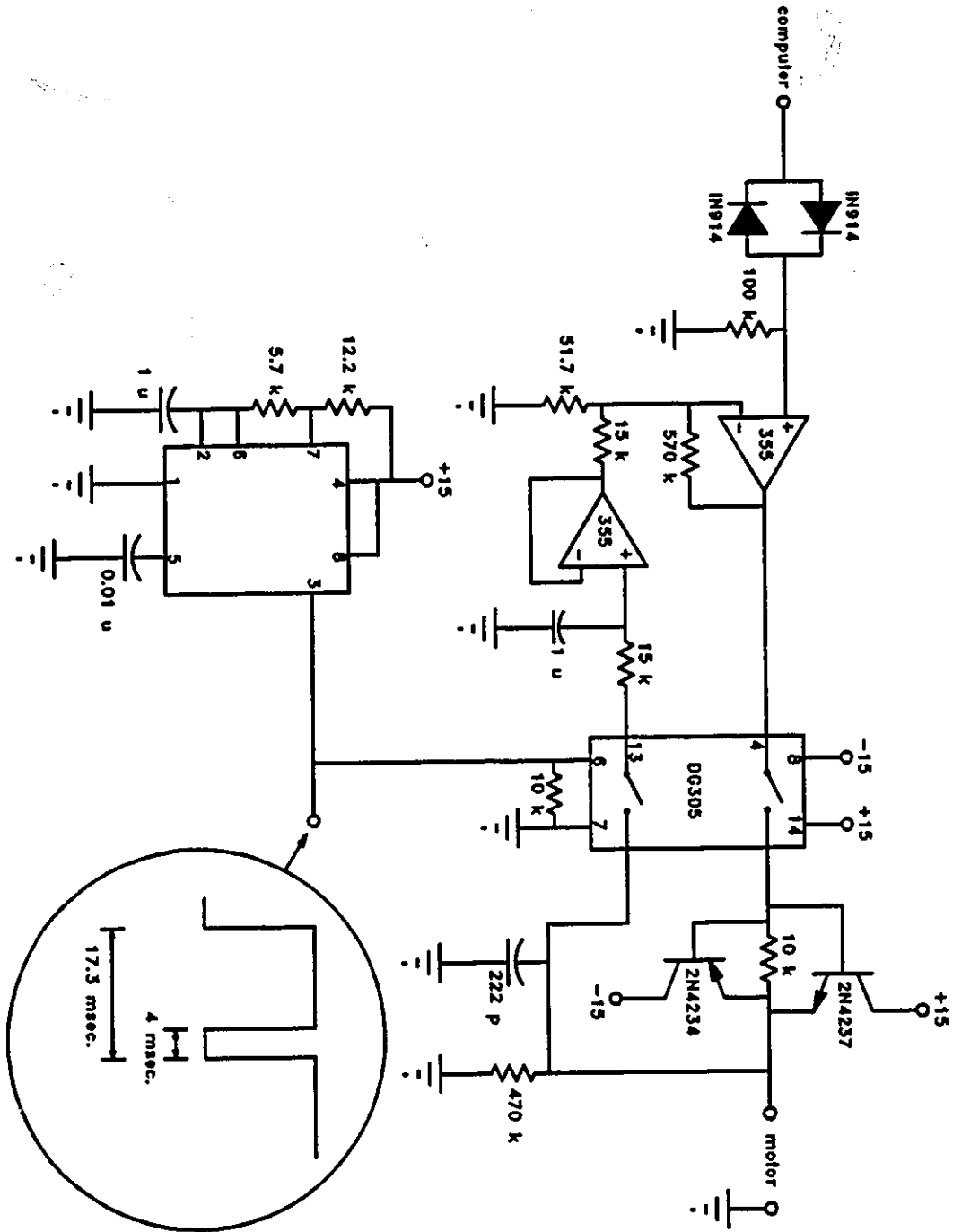


Fig. A.3 Motor Driver Circuit.

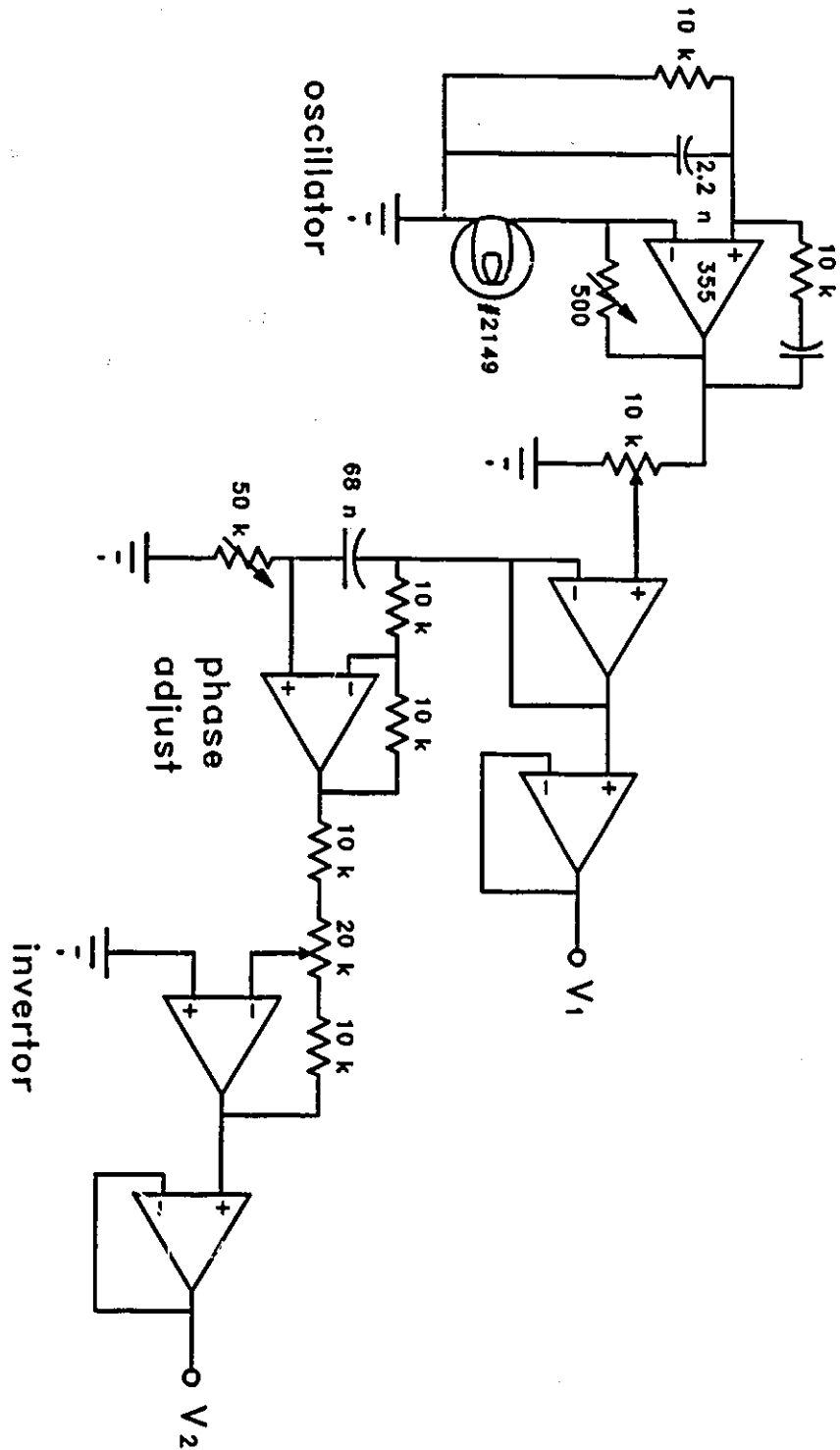
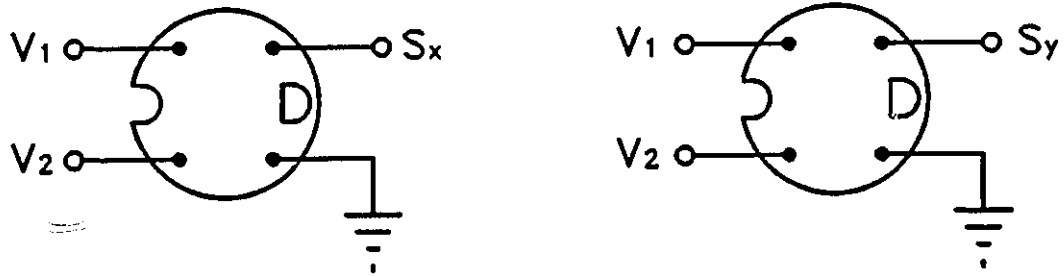
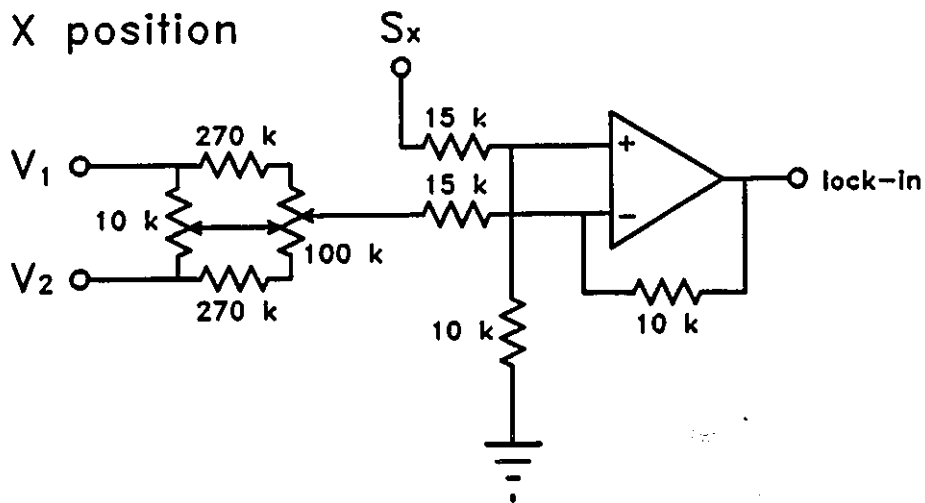


Fig. A.4 Wien Bridge Oscillator Circuit.



X position



Y position

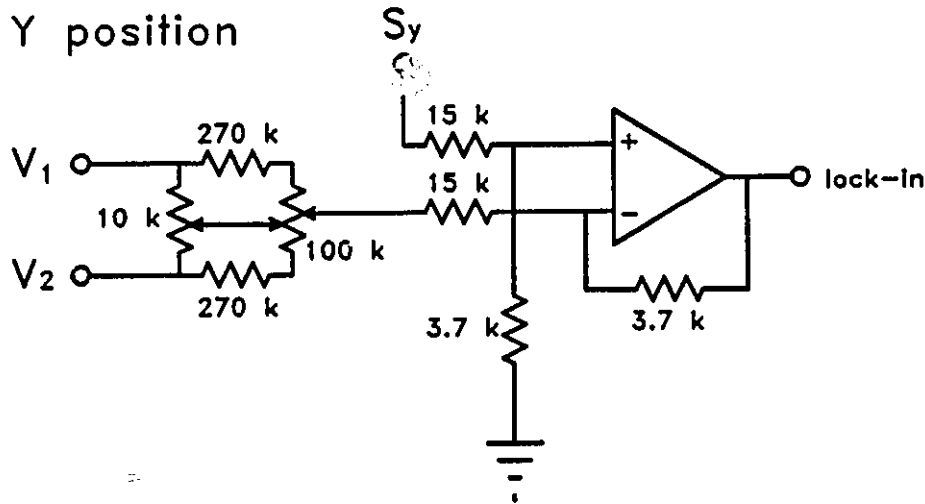


Fig. A.5 Position Sensor Circuit.

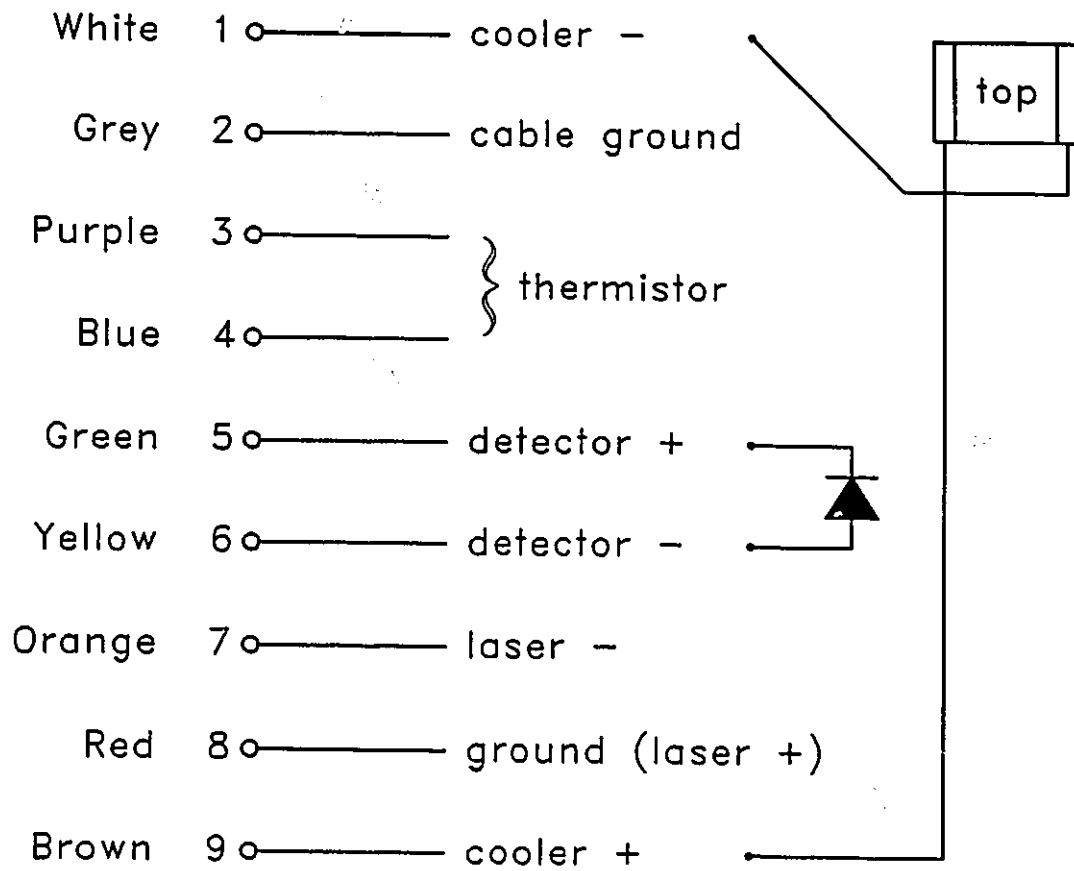


Fig. A.6 9-Pin Connector Diagram.

References

1. N. K. Dutta and A. B. Piccirilli, "Observation of anomalous far-field intensity distributions in semiconductor lasers and their explanation," *J. Appl. Phys.* **66**, 4621-4624, 1989.
2. F. H. Peters and D. T. Cassidy, "Spectral Output of $1.3\mu\text{m}$ InGaAsP Semiconductor Diode Lasers", *IEE Pt. J* **138**, 195-198, 1991.
3. F. H. Peters and D. T. Cassidy, "Strain and Scattering Related Spectral Output of $1.3\mu\text{m}$ InGaAsP Semiconductor Diode Lasers", *Appl. Opt.* **30**, 1036-1041, 1991.
4. F. H. Peters and D. T. Cassidy, "A Model of the Spectral Output of Gain-guided and Index-guided Semiconductor Diode Lasers", *J. Opt. Soc. Am. B.* **8**, 99-105, 1991.
5. F. H. Peters and D. T. Cassidy, "The Effect of Scattering on the Longitudinal Mode Spectrum of $1.3\mu\text{m}$ InGaAsP Semiconductor Diode Lasers", *Appl. Phys. Lett.* **57**, 330-332, 1990.
6. F. H. Peters and D. T. Cassidy, "Spatially and Polarization-Resolved Electroluminescence of $1.3\mu\text{m}$ InGaAsP Semiconductor Diode Lasers", *Appl. Opt.* **28**, 3744-3750, 1989.
7. D. T. Cassidy and F. H. Peters, "Spontaneous emission, scattering and the spectral properties of diode lasers," submitted to *IEEE J. Quantum Electron.* 1991.
8. F. H. Peters and D. T. Cassidy, "The Effect of Scattering in InGaAsP Semiconductor Diode Lasers", in *International Conference on Quantum Electronics Technical Digest Series 1990*, Vol. 8, (Optical Society of America, Washington, DC 1990), 206-208.
9. F. H. Peters and D. T. Cassidy, "Spatially-resolved and polarization-resolved electroluminescence of $1.3\mu\text{m}$ InGaAsP semiconductor diode lasers" *Conference on Lasers and ElectroOptics, 1989 Technical Digest Series*, Vol. 11 (Optical Society of America, Washington, DC 1989), 298-299.

10. P. L. Gourley, R. M. Biefeld, and L. R. Dawson, "Elimination of dark line defects in lattice matched epilayers through use of strained-layer superlattices," *Appl. Phys. Lett.* **47**, 482-484, 1985.
11. W. Wettling and J. Windschief, "Direct and fast comparison of near-infrared absorption and photoluminescence topography of semiinsulating GaAs wafers," *Appl. Phys. A* **40**, 191-195, 1986.
12. E. K. Riemer, T. G. Stoebe, and A. A. Khan, "Scanning photoluminescence," *SPIE 794 Modern Optical Characterization Techniques for Semiconductors and Semiconductor Devices*, 1987.
13. B. Wakefield, "Strain-enhanced luminescence degradation in GaAs/GaAlAs double-heterostructure lasers revealed by photoluminescence," *J. Appl. Phys.* **50**, 7914-7916, 1979.
14. T. Kobayashi, T. Kawakami, and Y. Furukawa, "Thermal diagnosis of dark lines in degraded GaAs-AlGaAs double-heterostructure lasers," *Jap. J. Appl. Phys.* **14**, 508-515, 1975.
15. K. Kazmierski, P. Hirtz, J. Ricciardi, M. Razeghi, and B. De Cremoux, "Validation of MOCVD GaInAsP/InP laser fabrication technology steps by photoluminescence imaging method," *Defect Recognition and Image Processing in III-V Compounds*, J. P. Fillard Ed. Amsterdam, 279-285, 1985.
16. R. L. Hartman and L. A. Koszi, "Characterization of (Al,Ga)As injection lasers using the luminescence emitted from the substrate," *J. Appl. Phys.* **49**, 5731-5744, 1978.
17. S. N. G. Chu, S. Nakahara, M. E. Twigg, L. A. Koszi, E. J. Flynn, A. K. Chin, B. P. Segner, and W. D. Johnston, Jr., "Defect mechanisms in degradation of 1.3- μ m wavelength channeled-substrate buried heterostructure lasers," *J. Appl. Phys.* **63**, 631-623, 1988.
18. S. Todoroki, M. Sawai, and K. Aiki, "Temperature distribution along the striped active region in high-power GaAlAs visible lasers," *J. Appl. Phys.* **58**, 1124-1128, 1985.
19. A. Rosiewicz, C. A. Park, B. R. Butler, C. J. Jones, and M. G. Palin, "Improvement of high reliability inverted rib-waveguide lasers by the observation of degradation mechanisms," *IEE Proc.* **132**, Pt. J, 319-324, 1985.

20. P. L. Gourley, M. Longerbone, S. L. Zhang and H. Morkoc, "Photoluminescence microscopy of epitaxial GaAs on Si", *Appl. Phys. Lett.* **51**, 599-601, 1987.
21. C. S. Adams and D. T. Cassidy, "Effects of stress on threshold, wavelength and polarization of the output of InGaAsP semiconductor diode lasers", *J. Appl. Phys.* **64**, 6631-6638, 1988.
22. D. T. Cassidy and C. S. Adams, "Polarization of the output of InGaAsP Semiconductor diode lasers," *IEEE J. Quantum Electron.* **QE-25**, 1156-1160, 1989.
23. J. C. Dymont, "Hermite-Gaussian mode patterns in GaAs junction lasers," *Appl. Phys. Lett.* **10**, 84-86, 1967.
24. I. Mito, M. Kitamura, K. Kobayashi, S. Murata, M. Seki, Y. Odagiri, H. Nishimoto, M. Yamaguchi and K. Kobayashi, "InGaAsP double-channel-planar-buried heterostructure laser diode (DC-PBH LD) with effective current confinement," *IEEE/OSA J. Lightwave Technol.*, **LT-1**, 195-201, 1983.
25. E. Oomura, H. Higuchi, Y. Sakakibara, R. Hirano, H. Namizaki, W. Suzaki, K. Ikeda and K. Fujikawa, "InGaAsP/InP buried crescent laser diode emitting at 1.3 μm wavelength," *IEEE J. Quantum Electron.* **QE-20**, 866-873, 1984.
26. H. Ishikawa, H. Imai, T. Tanahashi, K. I. Hori, and K. Takahei, "V-grooved substrate buried heterostructure InGaAsP/InP laser emitting at 1.3 μm wavelength," *IEEE J. Quantum Electron.* **QE-18**, 1704-1711, 1982.
27. H. Naito, N. Nagai, M. Yuri, K. Tateoka, M. Kume, K. Hamada, and H. Shimizu, "a new composite-cavity lasers with two different wavelength cores for stable longitudinal mode operation," *J. Appl. Phys.* **66**, 5726-5730, 1989.
28. L. F. DeChiaro, "Damage Induced Spectral Perturbations In Multi Longitudinal-Mode Semiconductor Lasers," *J. Lightwave Tech.* **8**, 1659-1669, 1990.
29. M. Yamada and Y. Suematsu, "Theory of Single Mode Injection Lasers Taking Account of Electronic Intra-band Relaxation," *Proc. of the 10th Conference on Solid State Devices, Tokyo*, 347-354, 1978.

30. R. F. Kazarinov, C. H. Henry, and R. A. Logan, "Longitudinal mode self-stabilization in semiconductor lasers," *J. Appl. Phys.* **53**, 4631-4644, 1982.
31. K. Petermann, "Calculated Spontaneous Emission Factor for Double-Heterostructure Injection Lasers with Gain-Induced Waveguiding," *IEEE J. Quantum Electron.* **QE-15**, 566-570, 1979.
32. D. T. Cassidy, "Comparison of rate-equation and Fabry-Perot approaches to modelling a diode laser," *Appl. Opt.* **22**, 3321-3326, 1983.
33. D. T. Cassidy, "Analytic description of a homogeneously broadened injection laser," *IEEE J. Quantum Electron.* **QE-20**, 913-918, 1984.
34. L. A. Coldren and T. L. Koch, "Analysis and Design of Coupled-Cavity Lasers-Part 1: Threshold Gain Analysis and Design Guidelines," *IEEE J. Quantum Electron.* **QE-20**, 659-670, 1984.
35. T. P. Lee, C. A. Burrus, D. Marcuse, A. G. Dentai and R. J. Nelson, "Measurement of beam parameters of index-guided and gain-guided single-frequency InGaAsP injection lasers," *Electron. Lett.* **18**, 902-904, 1982.
36. G. Agrawal, "Heuristic approach to spontaneous emission factor of gain-guided lasers," *J. Opt. Soc. Am. B* **1**, 406-408, 1984.
37. D. T. Cassidy, "Spontaneous-emission factor of semiconductor diode lasers," *J. Opt. Soc. Am. B*, **6**, 747-752, 1991.
38. M. Born and E. Wolfe, Principles of Optics, 4th Ed., Pergamon Press, New York, 652, 1970.
39. R. G. Plumb and J. P. Curtis, "Channelled substrate narrow stripe GaAs/(GaAl)As lasers with quarter-wavelength facet coatings", *Electron. Lett.* **16** 706-707, 1980.
40. M. Ettenberg, D. Botez, D. B. Gilbert, J. C. Connolly, and H. V. Kowger, "The Effect of Facet Mirror Reflectivity on the Spectrum of Single-Mode CW Constricted Double-Heterojunction Diode Lasers", *IEEE J. Quantum Electron.* **QE-17**, 2211-2214, 1981.
41. C. H. Henry, "Theory of Spontaneous Emission Noise in Open Resonators and its Application to Lasers and Optical Amplifiers", *J. Lightwave Technol.* **LT-4**, 288-297, 1986.

42. D. T. Cassidy, "Explanation of the influence on the oscillation spectrum of diode lasers for a change of facet reflectivity", *J. Appl. Phys.* **57**, 987-989, 1985.
43. D. T. Cassidy, "Consequences of a lower level population on the modelling of a homogeneously broadened injection laser", *Appl. Phys. Lett.* **44**, 489-491, 1984.
44. K. J. Ebeling and L. A. Coldren, "Analysis of multielement semiconductor lasers", *J. Appl. Phys.* **54** (6) pp. 2962-2969, 1983.
45. G. Bjork and O. Nilsson, "A New Exact and Efficient Numerical Matrix Theory of Complicated Laser Structures: Properties of Asymmetric Phase-Shifted DFB Lasers", *I.E.E.E J. Light. Tech* **LT-5** (1) pp. 140-146, 1987.
46. B. F. Ventrudo and D. T. Cassidy, "Operating characteristics of a tunable diode laser absorption spectrometer using short-external-cavity and DFB laser diodes," *Appl. Opt.* **29**, 5007-5013, 1990.